Coordination Chemistry Reviews 469 (2022) 214655

Contents lists available at ScienceDirect

Coordination Chemistry Reviews

journal homepage: www.elsevier.com/locate/ccr

Review

Metal-Tyrosine Kinase Inhibitors: Targeted metal-drug conjugates

Darren F. Beirne [a], Martina Dalla Via [a,b], Trinidad Velasco-Torrijos [a,c,*], Diego Montagner [a,c,*]

[a] Department of Chemistry, Maynooth University, Maynooth, Co. Kildare, Ireland
[b] Department of Pharmaceutical Science, University of Padua, Padua, Italy
[c] Kathleen Lonsdale Institute for Human Health Research, Maynooth University, Maynooth, Co. Kildare, Ireland

ARTICLE INFO

Article history:
Received 1 October 2021
Accepted 6 June 2022
Available online 23 June 2022

Keywords:
Tyrosine Kinases
Inhibitors
Metal Complexes
EFGR
BCR-ABL
PDGFR
VEGFR

ABSTRACT

Tyrosine Kinases are enzymes that catalyse the phosphorylation of the tyrosine residues of their substrates and activate downstream pathways involved in cellular proliferation. Their overexpression/hyper-activity is implicated in numerous different cancerous cell lines. Small molecule Tyrosine Kinase Inhibitors (TKi's), such as Imatinib, Erlotinib and Sunitinib have been developed as targeted anti-cancer therapeutics but, at the moment, their clinical usage is hindered due to acquired and innate resistance and/or dose limiting side effects. Recently, Metal-Tyrosine Kinase Inhibitor conjugates have become a promising field to overtake these drawbacks since the TKi's show potential to improve selectivity and pharmacological properties of metal-based drugs, overcoming the resistance associated with current TKi's. Metal-Tyrosine Kinase Inhibitor conjugates further find applications in several biological fields as dual-modal activity drugs, pro-drug systems and selective metal theragnostics. In this review, advancements over the past decade in the field of metal based-TKi conjugates are discussed and insights are provided to successfully develop metal – TKi conjugates. Four main TK targets are discussed here: EGFR (Epidermal Growth Factor Receptor), BCR-ABL (Breakpoint Cluster Region – Abelson Kinase), PDGFR (Platelet Derived Growth Factor Receptor) and VEGFR (Vascular Endothelial Growth Factor Receptor). Future perspectives and applications of this promising research area are also outlined.

© 2022 Elsevier B.V. All rights reserved.

Contents

* Corresponding authors at: Department of Chemistry, Maynooth University, Maynooth, Co. Kildare, Ireland.
E-mail addresses: trinidad.velascotorrijos@mu.ie (T. Velasco-Torrijos), diego.montagner@mu.ie (D. Montagner).

https://doi.org/10.1016/j.ccr.2022.214655
0010-8545/© 2022 Elsevier B.V. All rights reserved.

Nomenclature

List of abbreviations

AML	Acute Myeloid Leukaemia
ATP	Adenosine Triphosphate
BCR-ABL	Breakpoint Cluster Region-*Abelson* Kinase
BGM	Buffalo Green Monkey cells
CDK-2	Cyclin-dependent kinase 2
c-FES	Tyrosine-protein Kinase Fes
c-KIT	Mast/stem Cell Growth Factor Receptor
CML	Chronic Myeloid Leukemia
CT	Computerized Tomography
CV	Cyclic Voltammetry
DMEM	Dulbecoo's Modified Eagle Medium
DMSO	Dimethyl Sulfoxide
DNA	Deoxyribonucleic Acid
DOTA	Dodecane Tetraacetic Acid
DTPA	Diethylenetriamine Penta-acetic acid Dianhydride
DYRK	Dual-specificity Tyrosine-regulated Kinases
EDTA	Ethylenediaminetetraacetic Acid
EGFR	Epidermal Growth Factor Receptor
ELISA	Enzyme-linked Immunoassay
EtBr	Ethidium Bromide
FGFR	Fibroblast Growth Factor Receptor
FLT3	FMS-related Tyrosine Kinase 3
FMT	Fluorescence Molecular Tomography
FRET	Fluorescence resonance energy transfer
HBED-CC	*N,N'*-bis-[2-hydroxy-5-(carboxyethyl)benzyl]ethylene-diamine-*N,N'*-diacetic acid
HELF	Human Lung Fibroblast
HER	Human Epidermal Receptor
HIPK4	Homeodomain-interacting protein kinase 1
HK-2	Human Kidney 2 Cells
HPLC	High Performance Liquid Chromatography
HRMS	High Resolution Mass Spectrometry
ICP-MS	Inductively Coupled Plasma Mass Spectrometry
LCK	Lymphocyte-specific Protein Tyrosine Kinase
MAPKAPK3	Mitogen-activated Protein Kinase-activated-3
MS	Mass Spectrometry
MTT	3-(4,5-dimethylthiazol-2-yl)-2,5-diphenyl-2H-tetrazolium bromide
NADH	reduced Nicotinamide Adenine Dinucleotide
NODAGA	1,4,7-triazacyclononane-1-glutaric acid-4,7- diacetic acid
NOTA	1,4,7Triazacyclononane-1,4,7-triacetic Acid
NSCLC	Non-small Cell Lung Cancer
PAK1	p21-activated kinase-1
PBS	Phosphate Buffer Saline
PDGFR	Platelet Derived Growth Factor Receptor
PDT	Photodynamic Therapy
PET	Positron Emission Topography
PI3K	Phos-phoinositol-3-kinase
QLMPFGCL	Glutamine-Leucine-Methionine-Proline-Phenylalanine-Glycine-Cysteine-Leucine
RASA1	Ras p21 Protein Activator
ROS	Reactive Oxygen Species
SPECT	Single-Photon Emission Tomography
TEG	Triethyleneglycol
TGFβR	Transforming Growth Factor β Receptor
TIE2	Angiopoietin-1 receptor
TK	Tyrosine Kinase
TKi	Tyrosine Kinase Inhibitor
ToF-SIMS	Time-of-Flight Secondary Ion Mass Spectrometry
ULS	Universal Linkage System
UV-vis	Ultraviolet light-Visible Light
VEGFR	Vascular Endothelial Growth Factor Receptor
WHO	World Health Organisation

1. Introduction

The use of metals in medicine has grown drastically in the modern era, with its history dating back to as early as 1500 BCE in Egypt – according to the "Ebers Papyrus" which states that copper was used as an anti-septic[1]. To date, 38 metal containing medicines reside on the World Health Organisation List of Essential Medicines (out of a total of 450 medicines, including vaccines and combination of medicines)[2]. These include salts and complexes containing Pt, Cu, As, Sb, Ag, Zn, Ba, Co, Se, Na, Mg, Ca, Li, and K. In addition, a further 24 medicines may be administered as a sodium, potassium, or calcium salt, depending on the means of administration. A wide variety of metal containing FDA approved drugs are used today to aid treatment against various ailments, for example, arthritis (Auranofin based on gold) and fungal infections (Silver Sulfadiazine). Cancer is defined as the growth of abnormal cells which have the capacity to divide at an uncontrollable rate and have the ability to invade surrounding tissues – either locally or systemically *via* metastasis. It is estimated that 40% of males and ~38% of females (of all ethnicities in the USA) will develop cancer in any location of the body during their lifetime[3]. On average, one third of patients diagnosed with cancer will not survive past 5 years (depending greatly on the stage and type of cancer, and the age of the patient at diagnosis).

Arguably, the most important anti-cancer chemo-therapeutic drug on the WHO List of Essential Medicines is *cis*-platin (Fig. 1). One example of the success of *cis*-platin chemotherapy is observed in the survival rate of patients diagnosed with testicular cancer – increased from just 10% to 85%[4]. While *cis*-platin chemotherapy remains the success story of bio-inorganic medicinal chemistry, it shows several drawbacks and side-effects: (i) development of resistance (acquired or intrinsic), (ii) dose limiting toxicity, including but not limited to ototoxicity, nephrotoxicity, neurotoxicity and fatigue, (iii) poor oral bioavailability which results in the necessity to administer *cis*-platin intravenously[5].

The inadequacy of platinum(II) containing complexes has led to main shifts in direction into the research of other metal complexes as anti-cancer agents. Firstly, various metals are now being studied with the desire that the resulting complexes are less toxic towards healthy cells with respect to platinum, due to differing pharmaco-

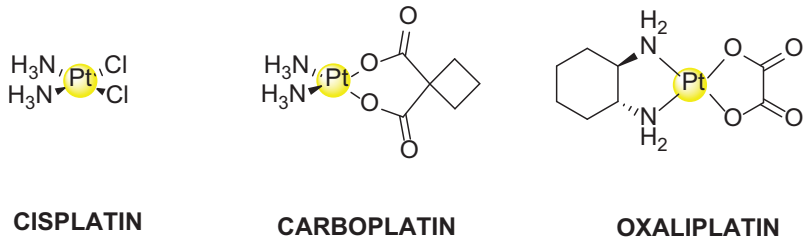

Fig. 1. Structures of world-wide approved Pt(II) based anticancer drugs, *cis*-platin, carboplatin and oxaliplatin.

logical properties (e.g. bioavailability, mechanism of action, drug elimination half-life etc.). Primary examples include copper chemical endonucleases, which cleave the DNA *via* Fenton chemistry[6] and ruthenium complexes which have entered clinical trials such as NAMI-A (discontinued after phase II trial)[7], KP1019[8]/KP1339 (undergoing phase 1 clinical trials)[9,10] and TLD1433 (undergoing phase I clinical trials)[11] (Fig. 2).

Secondly but equivocally, research has shifted towards metal anti-cancer agents that are targeted against tumours. This is typically done *via* two main strategies: (i) modifying the metal complex with a tumour targeting ligand – in the form of ancillary ligands (e.g. carbohydrates[12,13] and peptides[14,15]) or antibodies[16]; (ii) encapsulation of a metal drug in liposomes/Metal-Organic-Frameworks or immobilising of the metal on a nanoparticle scaffold, with selective delivery to cancerous cell lines[17]. This review, in the context of (i), will focus on the recent development of selective metal-based anticancer drugs conjugated with Tyrosine Kinases inhibitors.

Tyrosine Kinases (TK's) are enzymes that catalyse the transfer of a phosphate group from Adenosine Triphosphate (ATP) specifically to tyrosine residues of cellular targets. TK's are often implicated in tumoral tissues formation as their overexpression and/or mutation, resulting in constitutional activity, is connected with increased cellular proliferation[18]. Tyrosine Kinase inhibitors (TKi's) are drugs that supress signal transduction pathways by inhibiting the activity of TK's. Naturally, TKi's are used as selective anti-cancer therapeutics against cell lines that overexpress TK's.

The first FDA approved TKi was Imatinib (Imatinib Mesylate, or Gleevec®, CAS: 220127-57-1), approved in 2001 (Fig. 3), which is used primarily against Chronic Myeloid Leukaemia (CML). Its inhibitory activity involves binding to the inactive conformation of BCR-ABL (Breakpoint Cluster Region – Abelson Kinase), which is a constitutionally active mutated Tyrosine Kinase, expressed by the fusion of BCR and ABL genes. This is caused by the translocation of a section of chromosome 9 (containing ABL gene) with a section of chromosome 22 (containing BCR gene) forming the Philadelphia chromosome[19]. Imatinib has revolutionised the treatment of CML, with the life expectancy of patients treated with Imatinib not differing significantly from the general population[20]. Due to this success, further generations of BCR-ABL inhibitors have been developed to circumvent resistance and/or side effects acquired with imatinib cancer therapy (such as dasatinib)[21]. Presently, four drug TKi's (imatinib, nilotinib, dasatinib and erlotinib) feature on the WHO List of Essential Medicines, under "targeted therapies" (Fig. 3)[2].

The primary purpose of this review is to highlight and summarise the recent developments of this emerging field, related to metal complexes tethered to TKi's. The rationale of these conjugates is that the resulting complexes may have greater selectivity towards cancerous cell lines, due to the intrinsic selectivity of the TKi ligands which may result in less toxic side effects and improved selectivity *versus* tumoral tissues. Additionally, the complexes may have greater anti-cancer activity due increased cellular uptake/bioavailability and the possibility of bi/multi-modal activity (compound dependant) which could aid the circumvention of drug resistance. The scope of the review narrows down to metal complexes conjugated directly to a TKi derivative, or indirectly *via* a linker. To the best of our knowledge, no current literature is covering this field with a comprehensive library exclusively on this class of compounds. Kaur *et al.* in 2020, published a review with a small section discussing solely one target, Epidermal Growth Factor Receptor (EGFR), and omitting key EGFR complexes, including erlotinib conjugates and the role of metal-TKi drugs in radio theragnostics[22]. As such, this review will act as a pivotal and the primary reference for design of efficient future metal – TKi conjugates, by discussing the following aspects: cellular targets of metal based-TKi's, appropriate/inappropriate sites for TKi-metal conjugation, metal-TKi kinetic lability, pharmacological and biological results, multi-modal activity and important applications of this class of metal conjugates (e.g. radio-theragnostics).

Some areas are omitted and not considered for purpose in this review, such as nanoparticle-TKi conjugates[23–25], metal complexes that act as TKi's on their own (no TKi-conjugates, i.e. complexes originating from Staurosporine derivates designed and covered extensively by Eric Meggers *et al.*[26]) and metal complexes with possible tyrosine kinase inhibitory interactions (for example, by Haleel A. *et al.*[27]). Finally, combinatorial cancer therapy of metal complexes with TKi's does not feature in this review

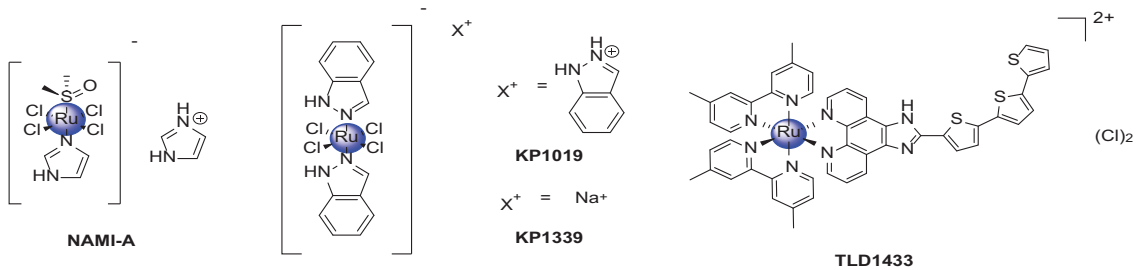

Fig. 2. Structures of ruthenium based anticancer drugs NAMI-A, KP1019/KP1334 and TLD1433.

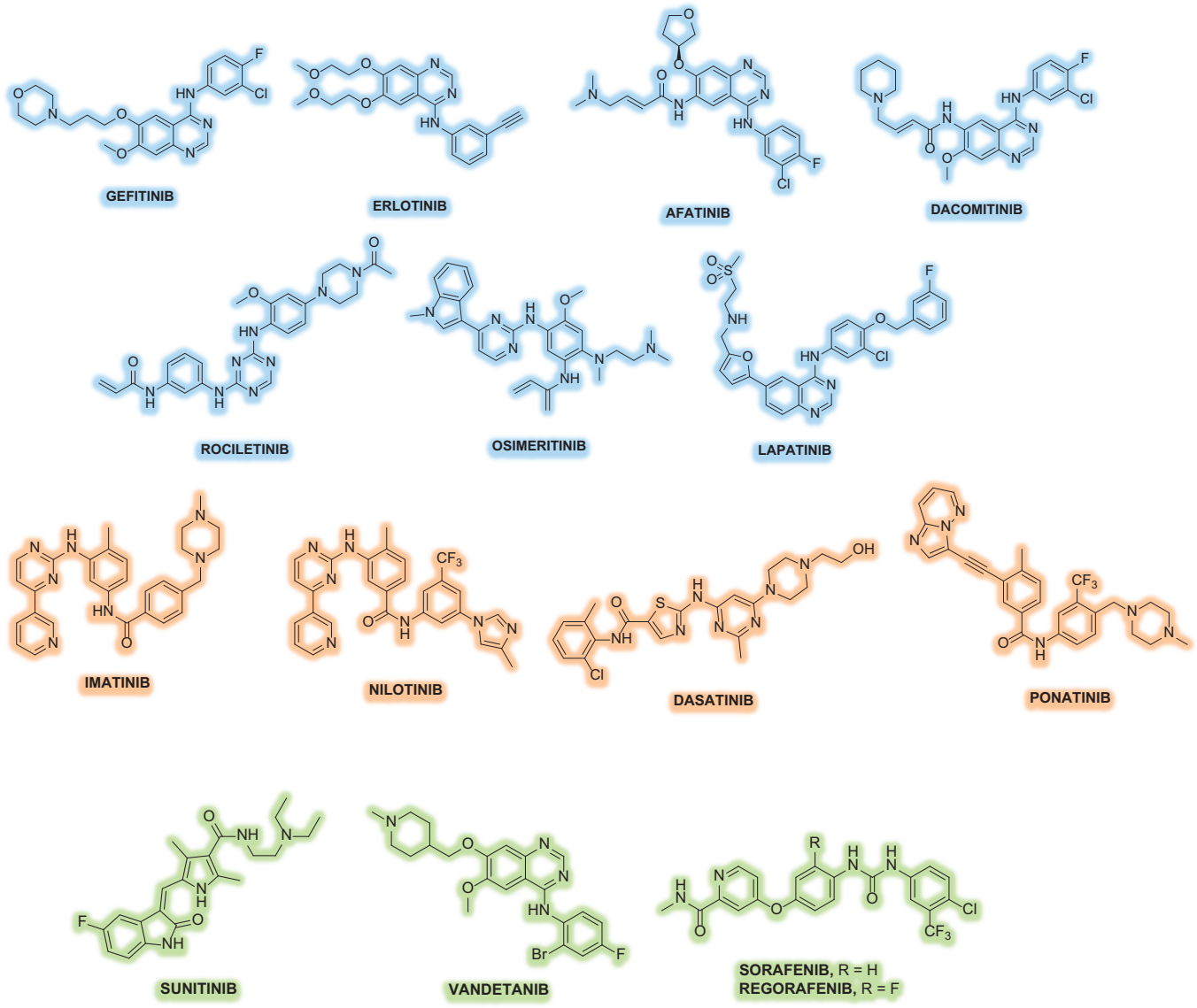

Fig. 3. Structures of Tyrosine Kinase inhibitors. EGFR Inhibitors (blue): Gefitinib, Erlotinib, Afatinib, Dacotinib, Rociletinib, Osimertinib and Lapatinib; BCR-ABL and PDFGR inhibitors (orange): Imatinib, Nilotinib, Dasatinib and Ponatinib; VEGFR inhibitors (green): Sunitinib, Vandetinib, Sarafenib and Regorafenib. It should be noted that some of them can inhibit more than one target. (For interpretation of the references to colour in this figure legend, the reader is referred to the web version of this article.)

but will be referred to demonstrate the superiority of linked metal-drug conjugates over conventional combination.

For convenience, this review is divided into three sections, each covering a different TK target: section 2 regards EGFR (Epidermal Growth Factor Receptor) target, section 3 BCR-ABL and PDGFR (Platelet Derived Growth Factor Receptor) targets and section 4 VEGFR (Vascular Endothelial Growth Factor Receptor) target. Each section has been further separated based on the nature of the metal centre.

2. Complexes targeting EGFR (Epidermal Growth Factor Receptor)

Epidermal Growth Factor Receptor (EGFR), a.k.a. ErbB1 and HER1 (Human Epidermal Growth Factor Receptor 1) is a tyrosine kinase receptor that is a member of the ErbB family (alongside ErbB2 a.k.a HER2/neu, ErbB3 and ErbB4). However, colloquially, EGFR is often also used to refer to the ErbB family as a whole – which this review will refrain from adopting. This family of receptors contains the same structural features: an extracellular domain for ligand binding (e.g. Epidermal Growth Factor, EGF), one hydrophobic transmembrane domain and an intracellular tyrosine kinase domain (Fig. 4)[28]. Upon ligand binding, homo- or hetero-dimerization of receptors occurs, in which one receptor acts as an activator, while the remaining receptor is activated. Hetero-dimerization is possible due to the similarities in the ErbB family of receptors. ErbB2 has no biological ligand capable of binding to its active site and remains constitutively active. ErbB3, due to a mutation in its kinase domain, is incapable of kinase activity. However hetero-dimerization of ErbB3 to ErbB1, ErbB3, ErbB4 can allow them to act as an activator[28]. Transauto-phosphorylation occurs between the N-terminus of one receptor, and the C terminus of another and phosphorylated tyrosine residues act as anchoring sites for substrates of ErbB family receptors[29]. For a comprehensive review on EGFR structure, role, mutations, over-expression and signal transduction pathways, see Ping Wee and Zhixiang Wang, [29].

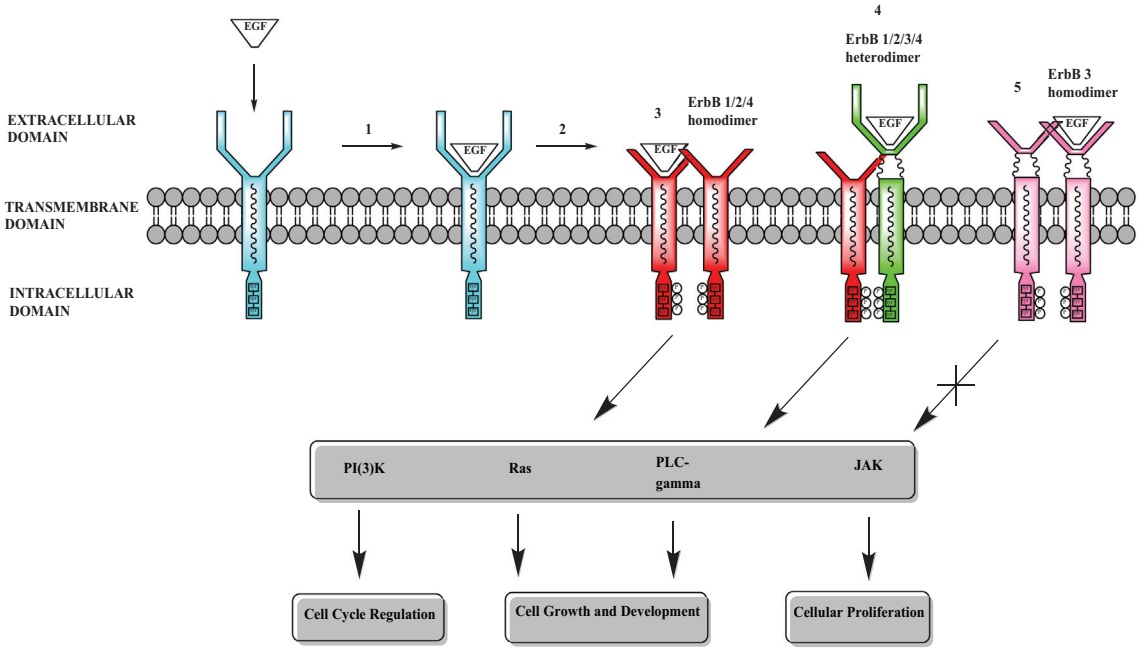

Fig. 4. Extracellular, Transmembrane and Kinase domains of HER family receptors alongside some important signal transduction pathway outcomes: (1) ligand binding, (2) dimerization, (3) homo-dimerization, (4) hetero-dimerization, (5) ErbB3 homo-dimerization results in no kinase activity.

The importance of EGFR resides in its implications in numerous cancers, namely non-small cell lung cancer (NSCLC), glioblastomas and colorectal cancer. For example, EGFR is over-expressed in 40–80% of NSCLC and 50% of colorectal cancers[29]. Ping Wee and Zhixiang Wang indicate that healthy cells typically exhibit 40,000–100,000 EGFR receptors per cell – in stark contrast to the reported 10^6 observed in cancerous cells. Similarly, ErbB2 (a.k.a. HER2) is implicated in many forms of breast and colorectal cancers; it is estimated that ~25% of breast cancer incidences are associated with an overexpression of HER2[30]. It is this oncological relevance and the over-expression of both EGFR and ErbB2 that has led to various targeted therapies against ErbB family receptors. Currently, two ErbB targeted therapies reside on the WHO List of Essential Medicines[2]: erlotinib (TKi which targets ErbB1) and trastuzumab (a mono-clonal antibody which targets ErbB2). Erlotinib, alongside gefitinib (Fig. 3), are known as the first-generation therapies against EGFR: It is solely used in patients with an EGFR activating mutation[31,32]. They operate *via* an ATP-competitive inhibitory mechanism. However, their downsides include both side effects (e.g. nausea and loss of appetite) and both acquired and innate resistance (for example, due to the T790M mutation in the kinase domain of EGFR[22] and upregulating of downstream pathways). This led to the development of second-generation inhibitors (such as afatinib and dacomitinib) which can somehow overcome this resistance, *via* irreversible binding (Fig. 3). Third generation of inhibitors (such as rociletinib and osimertinib) specifically target EGFR receptors containing either L858R or T790M mutations and do not target wild-type EGFR (Fig. 3). The clinical development of rociletinib was ceased in 2016, due to its lower efficacy than osimertinib, side effects such as high-grade hyperglycemia and the ambiguity of the starting dose[33]. Osimertinib itself is a successful TKi, which has shown to provide longer progression-free survival in patients with EGFR-mutated advanced NSCLC when compared to gefitinib and erlotinib[34,35]. However, even with the clinical success of Osimertinib, incidents of acquired resistance have still emerged[36]. As such, it is clear that further development of ErbB-TKi's is required to overcome both resistance and toxic side-effects during cancer therapy. It has been highlighted that metal complex/ErbB-TKi combinational cancer therapy (for example, combination of RAPTA-C and erlotinib[37]) may have a synergistic anti-tumour effect. In recent years, research has shifted towards the development of metal ErbB-TKi complexes, in order to overcome the posed problems of resistance and toxic side effects.

This section of the review covers metal complexes containing the EGFR inhibitors erlotinib and gefitinib, (Fig. 3), which can be generally categorized as anilino-quinazoline derivatives. To the best of our knowledge no metal complexes with the other EGFR inhibitors in Fig. 3 are reported.

2.1. Indium, technetium and rhenium

The first coordination complex containing an ErbB targeting TKi was synthesised in 2004 by N. Marjolijn, *et al*[38]. This complex contained a diethylenetriamine penta-acetic acid dianhydride (DTPA) trastuzumab conjugate chelator that allowed for radiolabelling with ^{111}In. The aim of this study was to provide a theragnostic approach against HER2-overexpressing breast cancer, as this complex could have applications in Positron Emission Topography (PET). This coordination complex was synthesised in reportedly high labelling yields (92.37 ± 2.3%) and radiochemical purity (97.07 ± 1.5%) and it was determined to have high stability in PBS buffer and retention of its immunoreactivity and biodistribution properties. The first transition metal – ErbB targeting TKi complexes were synthesised by Fernandes *et al.* in February 2008[39]. These complexes contained quinazoline derivatives conjugated to ^{99m}Technetium metal centres (**1** and **2**), resulting in complexes suitable for EGFR inhibition and simultaneous imaging *via* single-photon emission tomography (SPECT) (Fig. 5). These complexes could act as alternatives to the aforementioned PET acting ^{111}In complexes and other analogous radiolabelled TKi's (examples including ^{11}C[40,41], ^{18}F[42] and ^{124}I[43] radiolabelled EGFR-

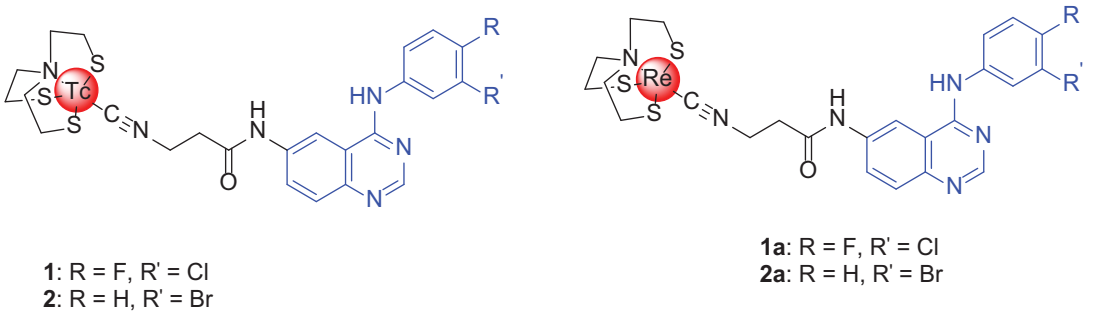

Fig. 5. Structures of Tc and Re – anilino-quinazoline complexes.

TKi's). The authors envisioned the properties of these ^{99m}Tc complexes would allow them to be applied in the prognosis of patient's tumour during cancer therapy. Their rhenium homologues (**1a** and **2a**) were also synthesised, to characterise and conduct biological assays with these complexes (due to the similar properties of Re and Tc elements).

Fernandes *et al.* sought to investigate the effect of the metal centre on the biological properties of the quinazoline kinase inhibitor. Tridentate chelates (N,N,O coordination donor atoms) were used to chelate to a *fac*-$[M(CO_3)]^+$ moiety (M = Tc and Re). One chelate ligand featured a pyrazolyl group while the other one featured a pyridine group (Fig. 6). The pyrazolyl-Tc or Re derivative **3** and its anilino-quinazoline analogue **4** were shown to be stable against cysteine and histidine challenge and in PBS buffer, like their pyridine counterparts **5** and **6**.

Each ligand and their respective complexes were tested for their EGFR inhibitory activity against A431 cell line. It was determined that ligands and complexes featuring the isocyanide group (**1** and **2**) were more potent inhibitors than the tridentate series of compounds (**3**–**6**). This decreased activity for **3**–**6** was due to the presence of the COOH acid group of the tridentate series: ionisation of this group could lead to decreased cellular uptake due to lower penetration of the cell membrane. Complex **2** was the most potent cell growth inhibitor complex (IC_{50} 2.9 ± 1.6 μM) and had a corresponding autophosphorylation inhibitory IC_{50} value of 108 nM. However, due to the similar results observed for the free ligands, it was concluded that the $[M(NS_3)]$ and fac-$[M(CO)_3]$ moieties did not enhance the activity of the compounds. While the indication of good cellular stability towards oxidation, hydrolysis and *trans*-chelation remained, unfortunately, no cellular uptake/radiolabelling studies were untaken.

In 2009, Bourkoula *et al.*, continued the investigation into Tc/Re-quinazoline complexes as EGFR biomarkers by again utilising a fac-$[M(CO)_3]$ moiety[44]. These Re and Tc complexes **7** and **8** exhibited functionalisation at the same position of the anilino-quinazoline core however using different functional groups; these complexes exhibited bidentate coordination via *N,N* donors derived from pyridine and imine nitrogens (Fig. 7). The Rhenium complex **8** exhibited excellent stability against cysteine and histidine coordination, with over 90% of the complex remaining intact after 24 h in a 1000 M excess of either. This further supported the presence of a chlorine in place of a water molecule in the precursor – as due to electrostatic reasons, the presence of a H_2O ligand would have lead to higher exchange with histidine and cysteine[45]. Biodistribution assays of the Tc complex **7** concluded that excretion occurred almost exclusively via the hepatobiliary system, due to decreasing radioactivity observed in the liver, in accordance with increasing in the intestines. Little radioactivity was observed in the stomach, which indicated minimal reoxidation of the complex to $^{99m}TcO_4^-$.

Kinase inhibitory assays were conducted against EGFR in the A431 cell line. Coordination of **L8** to Re, did not have any significant effect on the kinase inhibitory activity of the anilinoquinazoline derivative, as is observed by comparing the obtained IC_{50} values: 17 nM for the ligand to 114 nM for the complex (**8**). In fact, greater inhibition of cell growth (against A431) was observed upon coordination: 2.0 μM as opposed 5.2 μM. Complex **8** shows higher activity than both the fac-$[M(CO)_3]$ complexes and the $[M(NS_3)(CN\text{-}R)]$ complexes previously developed by Fernandes *et al.* MTT assays were utilised to further investigate inhibition of cell growth. Again, the Rhenium complex was more potent than the un-coordinated ligand, with an IC_{50} value of 2.0 μM and 4.8 μM, respectively.

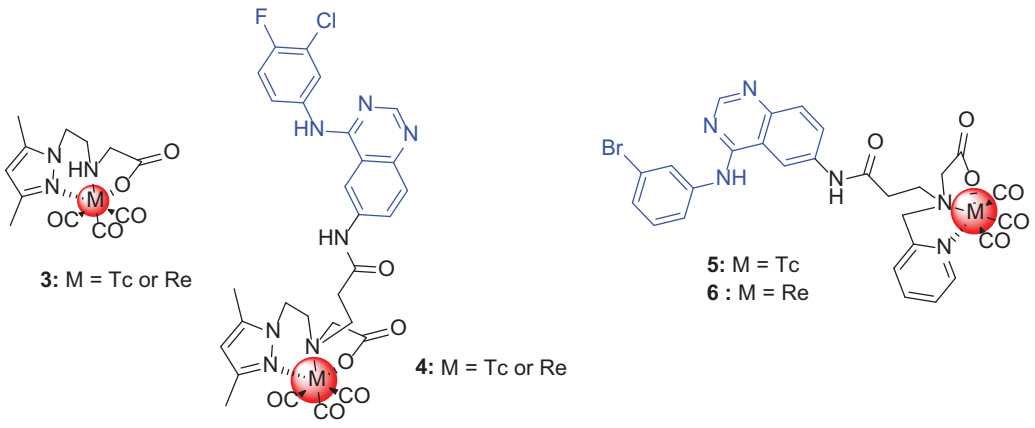

Fig. 6. Structure of pyrazolyl and pyridine anilinoquinazoline derivatives.

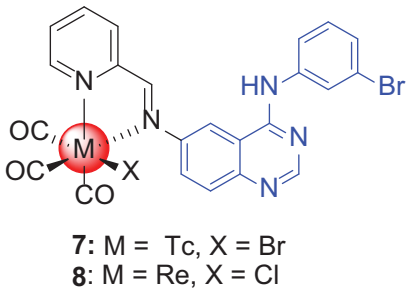

Fig. 7. Structure of fac Re/Tc 6-(pyridine-2-methylimine)-4-[(3-bromophenyl) amino]quinazoline derivatives.

Unfortunately, both previous studies limit their investigations to just A431 cell lines. It is important to discern if complexation and/or derivatisation of the quinazoline scaffolds results in loss of kinase inhibition specificity and/or increased healthy cell toxicity by testing against healthy cell lines, different kinases and EGFR negative cell lines. As previously mentioned, second generation inhibitors (such as afatinib) irreversibly bind to EGFR, *via* conjugate addition where the thiol group of cysteine 773 which acts as a nucleophile. Bourkoula *et al*., decided to investigate if the rhenium complex was an irreversible or reversible binder, postulating that cysteine could attack the imine of the quinazoline derivative. It was found that phosphorylation levels return to control level after 8 h indicating the ligand/complex is a reversible binder.

2.2. Zinc

In 2013, Zhang *et al*., released a communication detailing the development of novel Zinc(II) phthalocyanine based erlotinib conjugates (**9** and **10**, Fig. 8) for use as sensitising agents in targeted photodynamic therapy[46]. In photodynamic therapy, sensitisers, molecular oxygen and light are used to produce Reactive Oxygen Species (ROS) for use in cancer therapy. The aim was to utilise the intrinsic selectivity of erlotinib against EGFR-over expressing cell line to yield cancer cell selective photo-sensitizers. The erlotinib moiety was conjugated to the zinc(II)- phthalocyanine scaffold *via* a oligoethylene glycol linker of length n = 3 or n = 5. It is important to note that modification of the alkyne moiety is not ideal, as it can impact the interactions of erlotinib with EGFR. Appropriate conjugation strategies are discussed further in this review.

Due to the large, conjugated structure of phthalocyanine derivatives, they are prone to aggregation, resulting in no photocytotoxicity. To evaluate their photosensitizing ability, MTT assays against HepG2 cells (overexpress EGFR) were conducted in the presence and absence of light. Complexes **9** and **10**, and reference compounds zinc(II)-phthalocyanine and free erlotinib exhibited no obvious cytotoxicity up to 50 μM concentration. However, in the presence of light (670 nm, light dose: 1.5 J·cm^{-2}) complexes **9** & **10** exhibited IC_{50} values of 0.04 and 0.01 μM respectively, which were comparable to the zinc(II)-phthalocyanine reference (0.03 μM). Subcellular localisation assays of these complexes indicated no cellular localisation i.e. the complexes were distributed ubiquitously in the cytoplasm. To determine if the zinc(II)-phthalocyanine erlotinib conjugates could successfully target EGFR over-expressing cells (i.e. some cancerous cell lines), the conjugates and phthalocyanine control were administered to an equal mixture of HELF (Human Embryonic Lung Fibroblast: low EGFR expression) and HepG2 (EGFR overexpression) cell lines. These two cell-lines exhibit great morphological differences, allowing them to be distinguished *via* confocal laser scanning microscopy. The fluorescence observed was three times greater in HepG2 cells than HELF for both complexes, indicating a targeting effect of the erlotinib complexes towards EGFR over-expressing cell lines. For contrast, the zinc(II)-phthalocyanine reference showed no such targeting effect. To confirm this observation, *in vivo* fluorescence molecular tomography (FMT) was conducted with mice bearing a A431 (EGFR+) tumour using complex **9** and zinc-phthalocyanine control. Again, concrete evidence for EGFR targeting was indicated: after 2.5 h, accumulation of complex **9** was easily observed in the tumour prior to gradual decrease. In contrast, the control had no obvious tumour accumulation. The tumour/skin accumulation of complex **9** was found to be five times greater than its control.

In 2015, Zhang *et al* continued their study into zinc(II)-phthalocyanine erlotinib conjugates and decided to further investigate the effect of linker length and substitution pattern (α, also known as "non-peripheral" substitution or β, also known as "peripheral" substitution) on ROS production efficiency (**11a-e**, Fig. 8)[47]. Various zinc(II)-phthalocyanine erlotinib conjugates were synthesised with n = 0, 2, 3, or 4 and the substitution pattern was α or β. It was observed that varying the linker length did not affect the photo-chemical/physical properties of the complexes and, similarly with the previous study, use of confocal laser scanning microscopy confirmed the selectivity of the drugs towards EGFR over-expressing cell lines. To further assess this aspect, quantitative cellular uptake studies were conducted using fluorescence spectrometry. As expected, it was clear the conjugates had a higher affinity for HepG2 cells than HELF. Importantly, it was observed that linker length may influence cellular uptake; complexes with n = 3 had the highest uptake in HepG2 cells and consequently a higher ratio of HepG2/HELF uptake. It is clear that linker length is an important aspect to consider in the design of metal-tyrosine kinase inhibitor conjugates.

Similar to the previous study, the complexes showed retention of their photosensitising ability – i.e. high cytotoxicity in the presence of light, and low toxicity in the dark. This study indicated that α complexes had a slightly higher IC_{50} value against HepG2 cells (9.61– 44.50 nM) than the β complexes (33.97–91.77 nM) while the control zinc-phthalocyanine displayed an IC_{50} value of

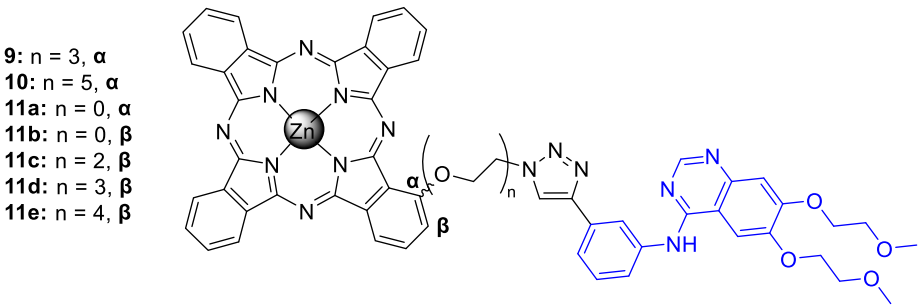

Fig. 8. Structure of Zinc(II) phthalocyanine-erlotinib based targeted photodynamic agents, linked via the α or β position.

43.30 nM. Subcellular localisation assays of the previous study indicated no cellular localisation i.e. the complexes were distributed ubiquitously in the cytoplasm. In contrast, this study indicated that the complexes localised in the lysosomes, with partial localisation in the mitochondria (while the control complex localised in both).

2.3. Gallium

In 2009, Garcia *et al.* developed the first Ga-TKi conjugate complex (**12**, Fig. 9).[48] This ^{67}Ga complex featured a DOTA chelator conjugated to a modified gefitinib derivative, with the aim of producing a targeting Ga complex for single photon emission scintigraphy detection. For gallium complexes to become successful radiopharmaceuticals, they must fulfil three main requirements:

- Resistance to hydrolysis forming species such as [Ga(OH)$_3$];
- Reversible binding to blood plasma proteins (most predominately transferrin);
- Kinetically inert towards *trans*-chelation.

With these requirements in mind, it was found that the complex **12** was stable in PBS buffer at 37 °C for up to 5 days, and stable over 5 days in the presence of DTPA (1000-fold excess). DPTA is a chelator with a stronger formation constant with Ga(III) than transferrin (log K = 25.1 and log K = 20.3 respectively)[49]. Finally, incubation of the complex in blood serum (6-day stability) and analysis of the proteic fraction (post-precipitation) showed a time dependent concentration of the complex, indicating a reversible binding of the complex to blood proteins. The total *in vitro* stability data infers that the complex fulfils all three requirements. While all attributes prior appear to demonstrate a promising radiolabelled TKi conjugate for EGFR-imaging, the complex falls short in its pharmacokinetic properties. Cellular uptake studies indicated essentially zero (<0.2%) cell internalisation, which is backed up by the complex's poor cell growth inhibition: **12** displayed no growth inhibition in the range 1 nM to 100 μM against A431 cells (MTT assay). Biodistribution studies indicated that no release of free Ga (III) occurs, as localisation did not occur in the lungs nor the liver (Ga(III) is known to localise as such due to strong binding to transferrin). Overall, this source emphasises the importance of a utilising a suitable linker (a.k.a. spacer) in metal-TKi conjugates, as observed by Zhang *et al.* with the zinc phthalocyanine-erlotinib conjugates previously discussed. Inclusion of a linker in the Ga quinazoline conjugate may have improved its cellular uptake (and therefore its cellular growth inhibitory activity) drastically, with minimal impact on complex stability and specific activity.

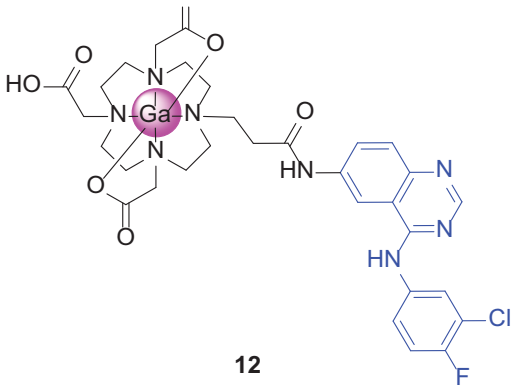

Fig. 9. Structure of Ga-DOTA-gefitinib complex **12** based EGFR targeting agents.

In 2017, Jain *et al.* developed a ^{68}Ga erlotinib conjugate **13** utilising a NOTA chelator (1,4,7-Triazacyclononane-1,4,7-triacetic acid (Fig. 10)[50]. This isotope of gallium was used for its application in PET, which the authors reason is superior to SPECT for EGFR imaging due to higher sensitivity and resolution.

The log $P_{o/w}$ (lipophilicity index) value of **13** was determined to be – 0.6 ± 0.1, indicating it is more lipophilic than the previous Ga complex (**12**). Here, complex **12** exhibits a higher hydrophilicity relative to **13** due to the presence of the free carboxylate group not observed in **13**. Nevertheless, this is an early indicator that the cellular uptake problems associated with **12** have been lessened and/or rectified. Overall, complex **13** is more hydrophilic than free erlotinib and it exhibited high stability in EDTA solution and human serum solution separately for 2 h. Cell viability studies were conducted against A431 cells: a 1 μM NOTA-Erlotinib solution resulted in 12.5 % viability after 72 h. A lack of these studies is that they were not conducted against cell lines with low or normal EGFR expression. However, cellular uptake studies did indicate preferential uptake of **13** by A431 cells over A549 (low EGFR) cells – 9.8 % vs no uptake. Additionally, the NOTA-erlotinib ligand was observed to be more active than free erlotinib. Finally, the *in vivo* stability of the complex was assessed *via* Swiss mice urine analysis via HPLC. A single peak assigned to the complex was observed, indicating complex stability *in vivo*. Due to the improved cellular uptake in respect to the previous complex, this was a positive step in the development of a Ga(III)-TKi conjugate.

In 2018, Jain *et al.* synthesised a ^{68}Ga labelled NODAGA-erlotinib complex (**14**, Fig. 11) utilising the previous conjugation strategy (NODAGA = 1,4,7-triazacyclononane,1-glutaric acid-4,7-acetic acid). However, the activity of this complex was overall reduced in contrast to the previous erlotinib conjugate **13**, postulated due to the higher hydrophilicity of complex **14** (log $P_{o/w}$ = – 1.21 ± 0.2) resulting in lower cellular uptake (7.8 %) on A431 cells. However, one important positive from the study indicated that the complex had an improved tumour/non-specific cell uptake ratio than its predecessor, indicating its promise in improving signal/noise ratio in PET EGFR imaging[51].

In 2020, Liolios *et al.*, synthesised two ^{68}Ga labelled complexes (**17** and **18**), starting from the corresponding Fe(III) complexes **15**

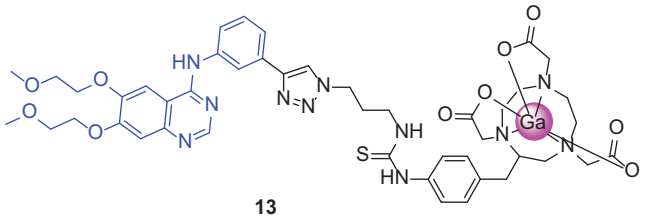

Fig. 10. Structure of ^{68}Ga-NOTA-erlotinib complex **13** based PET agent.

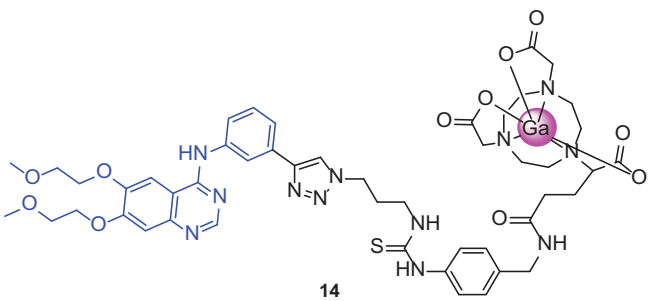

Fig. 11. Structure of ^{68}Ga-NODAGA-erlotinib complex **14** based PET agent.

and **16**), with applications in PET/EGFR imaging[52]. The complexes featured a *N,N′*-bis[2-hydroxy-5-(carboxyethyl)benzyl]ethylenediamine-*N,N′*-diacetic acid (HBED-CC) ligand, with either one or two quinazoline derivatives conjugated to the chelator (Fig. 12).

Radiolabelling of these complexes was achieved in high yields (98%), with a specific activity of 7 and 20 MBq/μg for **17** and **18,** respectively. The complexes remained intact after two hours in saline buffer at 37 °C. Complex **17** was shown to be more hydrophilic than complex **18**, possibly due to the presence of the free carboxylate group and only one EGFR moiety (log Do/w = − 1.60 vs 1.32). Using a MTT assay against A431 cell lines, the anti-proliferation activity of the mono/dimeric complexes were found to be similar – IC_{50}: 62.8 μM for **17** and 68.8 μM for **18**. However, they were less effective than the original free amine quinazoline moiety (IC_{50}: 16.3 μM), indicating that the HBED-CC moiety has negatively affected the potency of the compounds. No MTT assay was conducted on cell lines with normal/low EGFR expression. Using biodistribution studies for these compounds, the monomeric complex exhibited slightly higher tumour/blood and tumour/muscle ratios, but not enough to warrant preferential synthesis of monomeric EGFR imagers over multi-valent imagers in general.

2.4. Platinum

Aside from radiochemistry, the first metal-TKi conjugate was developed by Temming *et al.*, in 2008[53] who synthesised a gefitinib-trastuzumab drug-antibody conjugate linked *via* a Pt(II) universal linkage system (ULS) (**19**, Fig. 13). The aim of this system was that both gefitinib and trastuzumab would be intracellularly released *via* displacement by various biological nucleophilic species such as glutathione. Unfortunately, the source is limited by its lack of relevant biological studies.

In 2016, Yuming *et al.*, developed Pt(II)-erlotinib conjugates[54]. These Pt(II) complexes were based on *cis*platin (**20**), *trans*platin (**21**) and oxaliplatin (**22**) allowing for evaluation of the effect of stereochemistry on the pharmacological properties (Fig. 14).

Interestingly, while the oxaliplatin (**22**) and cisplatin (**20**) derivatives were stable in saline and phosphate buffer over 24 h at physiological temperature, the transplatin derivative (**21**) showed gradual degradation/release of erlotinib. The selectivity of the complexes towards EGFR was not affected by the presence of the platinum moiety and were found to be more effective against HCC827 cell lines (containing ΔE746-A750 mutation) than H292 cell line (wild-type), while they showed minimal cytotoxicity towards LLC-PK1 (normal kidney cell line). This is advantageous as in contrast, platinum(II) drugs such as cisplatin are known to be highly nephrotoxic[5]. However, most importantly, the overall activity of complexes **20** and **22** against HCC827 cell lines was reduced drastically when compared to the erlotinib control (IC_{50}′s against HCC827: Complex **20** = 0.16 ± 0.03 μM, Complex **22** = 0.12 ± 0.07 μM, erlotinib = 0.0010 ± 0.0005 μM). This 100-fold decrease in activity relative to erlotinib demonstrates that functionalisation at the quinazoline moiety is a poor conjugation strategy that can negatively impact the interactions of such conjugates with EGFR. As previously mentioned, appropriate conjugation strategies are further discussed at a later point. The transplatin conjugate **21** also utilised the same poor conjugate strategy as **20** & **22** but in contrast, exhibited similar activity (IC_{50} = 0.006 ± 0.002 μM) to the erlotinib control against HCC827 cell line. This may be explained by the aforementioned observation that complex **21** was unstable in PBS resulting in the release of free-erlotinib. Further studies were conducted towards the complexes higher ratio of activity against mutated EGFR vs wild-type in contrast to erlotinib. Docking studies confirmed interactions with EGFR L858R/T790M mutant kinase differed using erlotinib vs Pt(II)-

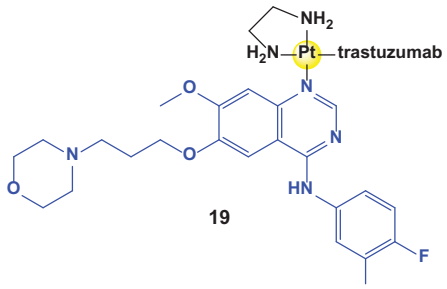

Fig. 13. Structure of Pt(II)-gefitinib trastuzumab ULS conjugate.

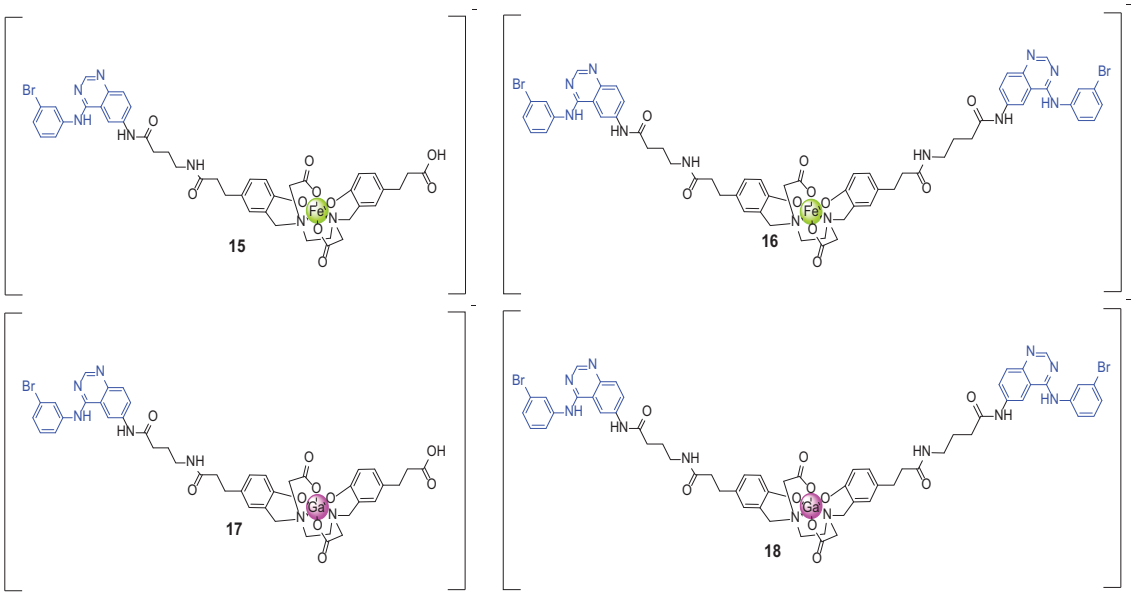

Fig. 12. Structure of mono- (**15**, **17**) and dimeric (**16**, **18**) Fe(III) and ^{68}Ga(III)-HBED-CC quinazoline derivatives.

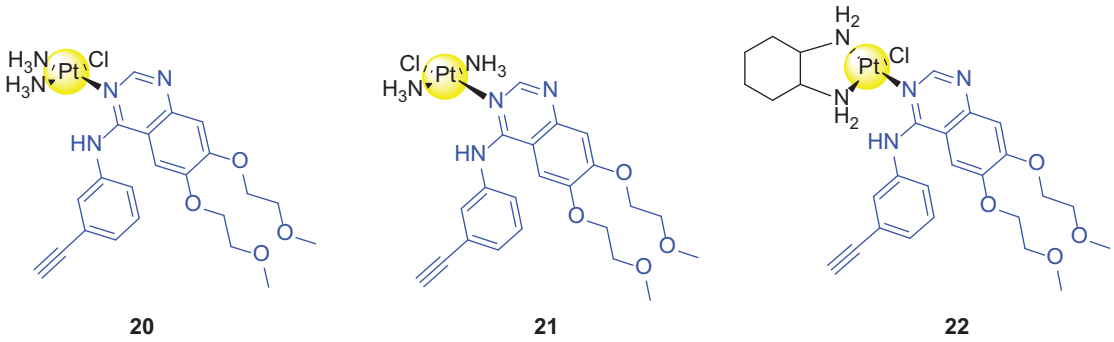

Fig. 14. Structure of Pt(II)-erlotinib conjugates **20**–**22**.

erlotinib, as the Pt(II) moiety created an additional site for amino acid residue interaction.

In 2017, Zhang *et al.* synthesised and assayed four cyclometallated Pt(II) anilino-quinazoline complexes for their utility as luminescent DNA/EGFR dual-modal probes (**23**–**26**, Fig. 15)[55]. The complexes were expected to have dual-modal activity due to reversible binding to EGFR receptors which could allow for later DNA interaction (similar to earlier synthesised ruthenium complexes, discussed later in section 2.5). Notably, these complexes were weakly fluorescent – however fluorescence emission could be greatly promoted upon DNA binding, providing potential as fluorogenic probes for DNA. Binding constants of **23** (5.26×10^4 M^{-1}) and its Pt(II) precursor (1.82×10^4 M^{-1}) demonstrated that substitution of the chlorido ligand enhanced DNA binding. As expected, based upon previous results, an increasing linker length led to higher DNA binding. Additionally, the complexes demonstrated higher affinity towards G-quadruplex (G4) DNA, with a binding constant of 1.06×10^6 M^{-1} to the G-rich sequence Pu27 – approx. 20 times higher than ctDNA. Both molecular docking studies and circular dichroism inferred DNA interaction at the minor groove and *via* intercalation. EGFR inhibition assays demonstrated that the complexes have a similar inhibition activity to gefitinib, while again displaying the importance of linker length on inhibition. The choice of tridentate ligand was found to have little impact on EGFR inhibition. Molecular docking confirmed the importance of linker length on the activity of these complexes and it was found that docking of complex **23** resulted in the breaking of a hydrogen bond interaction between the fluorine of the anilino-quinazoline moiety and the NH_3 of Lys721, slightly reducing its EGFR inhibition. In contrast, the complex utilising a longer linker (**24**) retained the hydrogen bonding interaction.

Both ToF-SIMS and confocal microscopy verified the dual-modal activity of these complexes in similar fashion as seen previously. Additionally, ICP-MS indicated their higher cellular uptake due to observed increased membrane bond protein and DNA interactions. The antiproliferative activity of **25** and **26** was higher than **23** and **24**. This was consistent with their docking scores. All complexes were observed to be more active than their Pt(II) pre-cursors, with **23** and **24** displaying greater activity than both cisplatin and gefitinib *via* EGF-dependent inhibition, against the MCF-7 cell line. The complexes were observed to be 30 times more active against MCF-7 than healthy cells, indicating their high degree of selectivity. Finally, the IC_{50} values of complexes **23** and **24** against MCF-7 cells in the presence of EGF (3.68 μM and 1.92 μM) and absence of EGF (7.30 μM and 4.9 μM) demonstrated that they were more effective than an equimolar mixture of gefitinib and cisplatin (16.3 μM in presence and 16.3 μM in absence of EGF).

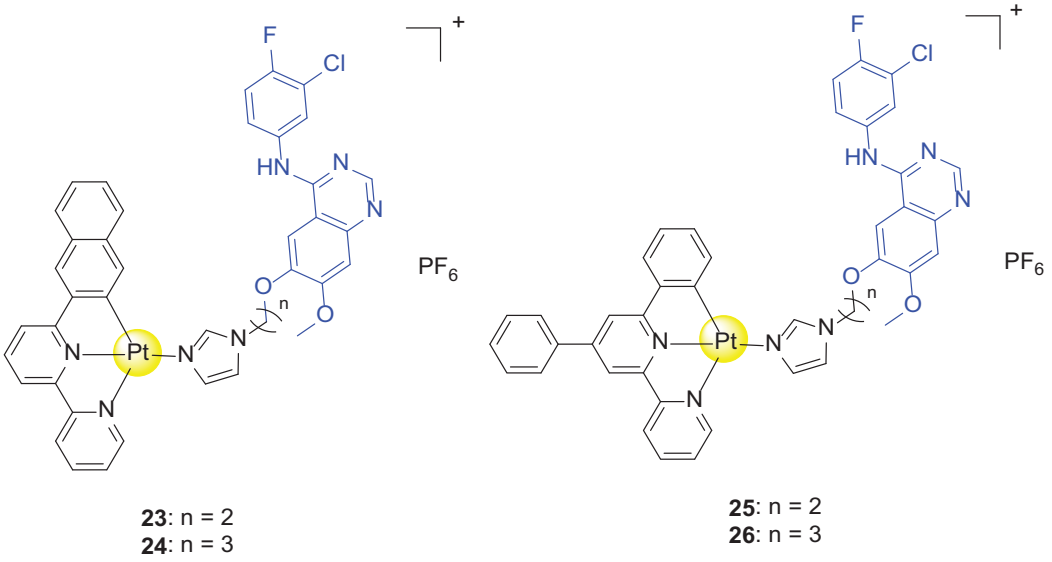

Fig. 15. Structure of platinum(II) cyclometallated anilinoquinazoline conjugates.

In 2020, Li *et al.* continued the research on Pt(II) anilinoquinazoline derivatives by utilising R-substituted terpyridine moieties analogous to the cyclometallated entities above (**27**–**30**, Fig. 16)[56].

Largely, replacing the cyclometallated derivatives with a terpyridine moiety had little effect – no hydrolysis, DNA intercalative interactions and minor groove binding and improved EGFR inhibition upon complexation of the anilinoquinazoline inhibitor to the Pt(II) moiety were observed. Most importantly, little difference was seen between complexes bearing a Br or a CH_3 substituent in relation to DNA intercalation and EGFR inhibition. Interestingly, an increased linker length did not correlate with increasing EGFR inhibition, in direct contrast to previously discussed studies. This may be due to the fact that shorter linker lengths are utilised in this study (1 or 2 in contrast to 2 or 3). Finally, the complexes studied exhibited lower resistance factor (lower than 3) than cisplatin (~3), indicating their dual-modal activity may aid towards overcoming resistance.

In 2018, Yang *et al.* synthesised anilinoquinazoline derivatives containing a Pt(II) moiety, that could act as a metallo-electrophile towards cys797, inducing irreversible EGFR inhibition[57].

Yang *et al.* improved upon their previous Au(I) thiol-reactive study (complexes **69**–**71**, see Section 2.6) by ensuring that these Pt(II)-conjugates retained a chloride ligand leaving group that play important role in the DNA binding resembling cisplatin structure (**31**–**34**, Fig. 17).[58].

ATP-independent EGFR inhibition assays determined the dissociation constants of **31** and **32** to be 1 and 3.4 nM respectively (gefitinib: 0.9 nM), suggesting platination of the quinazoline derivatives did not affect the first reversible binding of the inhibitors to EGFR. In agreement with this suggestion, **31** showed a similar selectivity to gefitinib against a panel of 145 kinases containing domains with "targetable" cysteine residues: High activity was retained against ErbB family kinases (except ErbB3), FMS-related tyrosine kinase (FLT3) and lymphocyte-specific protein tyrosine kinase (LCK). However, it is important to note that this similarity in EGFR dissociation constant may be a result of dissociation of the ligands from the complexes themselves: at a nM concentration, due to the labile nature of the metal centre, complexes **31** and **32** may have released free anilinoquinazoline derivatives with comparable EGFR dissociation constants to the gefitinib control. As above (previously aforementioned complex **21** & complexes **31**/**32**), the kinetic lability of certain transition metal-complexes is an important consideration that is often overlooked, as what is often perceived as activity of an intact complex may be in fact activity of undesirable ligand release.

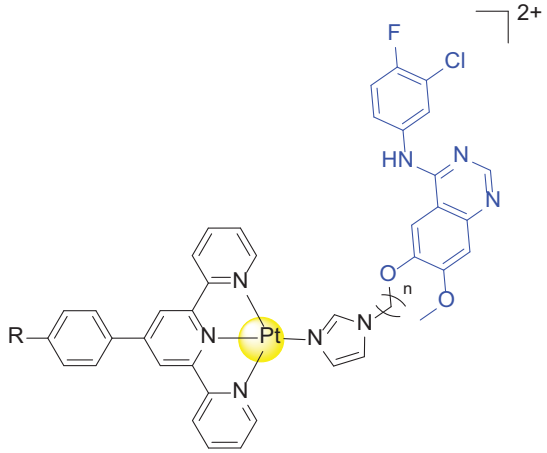

27: n = 1, R = CH_3
28: n = 2, R = CH_3
29: n = 1, R = Br
30: n = 2, R = Br

Fig. 16. Structure of platinum(II) terpyridine anilino-quinazoline conjugates.

Reactions of representative complexes **33** and **34** with QLMPFGCL peptide, resulted in the desired cysteine residue platination due to chloride ligand loss. However, a second ligand exchange reaction was observed depending on the nature of the ancillary amine ligands. With complex **33**, an amino ligand is replaced by a deprotonated amido ligand forming a S,N chelate (Fig. 18), where the anilinoquinazoline conjugates remains bound. In complex **34**, where the ancillary ligand is a bidentate chelator, it is the quinazoline conjugate that is lost to form an analogous chelating peptide-platinum(II) moiety (Fig. 18), making **34** a non-ideal TKi candidate. Additionally, it was found that both the mono- and bi-dentate adducts were observed by HR-MS upon reaction of **34** with a truncated (88 kDa) intracellular domain of recombinant EGFR while no adducts were observed upon reaction with **33**. Finally, no adducts, were observed with any methionine residues (peptide or truncated kinase), supporting the selectivity of these complexes.

There is current development towards a gefitinib based light induced Pt(IV) pro-drug (Fig. 19); even if preliminary biological results are available[59], the work is not published yet.

2.5. Ruthenium

In 2013, Zhang *et al.* released a communication detailing the development of organometallic ruthenium(II) complexes containing different chelating ethylenediamine quinazoline moieties (**35**–**40**, Fig. 20)[60].

IC_{50} values of complexes **35**–**40** against EGFR were at a nanomolar level, lower in C_2 linked complexes vs C_3 and lower when the arene substituent was smaller. Sulforhodamine B assay was employed to investigate their cellular growth inhibitory activity against MCF-7 (overexpresses EGFR). Comparison against a literature quinazoline EGFR derivative, "L0"[61], as the positive control showed that the complexes had higher inhibition of EGF-induced cellular growth. However, as the complexes were found to be worse inhibitors of EGFR than L0, they may have another mechanism of action (DNA-Ru adducts etc) other than EGFR inhibition. IC_{50} values against normal human bronchial epithelial cells were >100 μM for most complexes, showcasing their retention of high selectivity.

In 2015, Zhang *et al.* of the same lab furthered the research into ruthenium(II) "piano-stool" anilinoquinazoline conjugates with eight new conjugates (**41**–**48,** Fig. 21)[62].

Circular dichroism indicated that these complexes could bind to calf thymus DNA *via* both groove binding and coordination. Hoechst binding assays verified their groove binding ability, with K_{sv} constants between 8.8×10^4 μM^{-1} and 9.2×10^4 μM^{-1}. Using enzyme-linked immunosorbent assay, the complexes **44** and **47** were identified as better inhibitors of EGFR than gefitinib. Advancing previous results, MTT assays showed that the complexes displayed inhibitory activity against HeLa cells in the absence of EGF, indicating inhibition *via* other mechanisms – further evidence supporting their dual-targeting behaviour. Finally, molecular docking studies demonstrated that hydrolysis of the complexes (chloride ligand substitution) was favourable for DNA binding, due to increased potential hydrogen-bonding interactions and the complexes exhibited DNA binding abilities (energy between – 133 to −95 kcal/mol) like cisplatin (-128 kcal/mol).

In 2014, Yi, Liyun *et al.* developed Ru(II)/(III) anilinoquinazoline conjugates featuring ancillary monodentate dimethyl sulfoxide

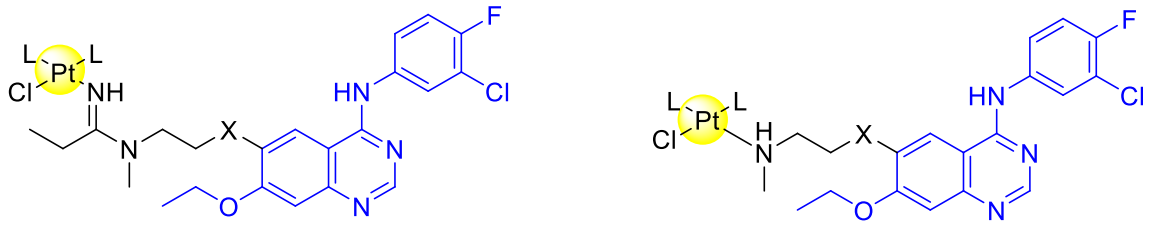

31: L = NH_3, X = NH
32: L = tmeda, X = NH
33: L = NH_3, X = O

34: L = pn, X = O

Fig. 17. Thiophilic Pt(II) anilinoquinazoline derivatives.

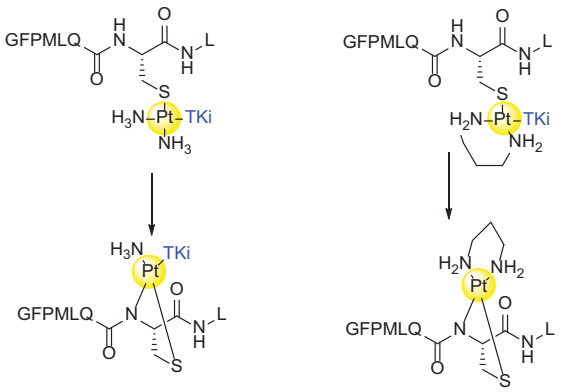

Fig. 18. Reactions of complexes **33** and **34** (representing mono- and bi-dentate ancillary ligands) with QLMPFGCL peptide.

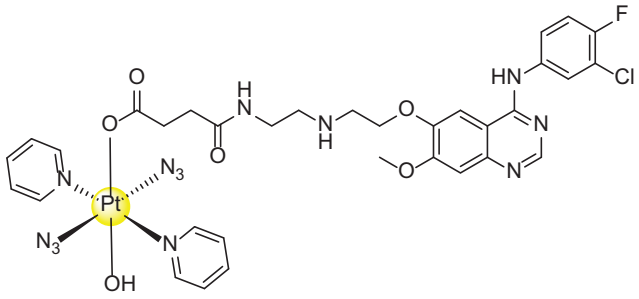

Fig. 19. Structure of gefitinib based light induced Pt(IV) pro-drug.

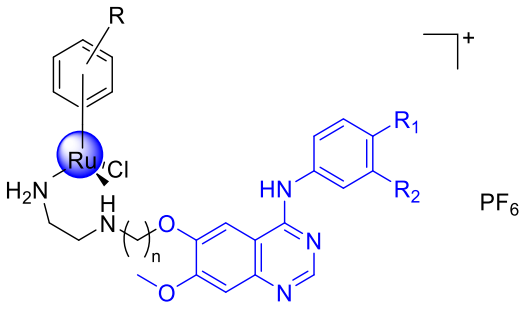

41: R_1 = F, R_2 = Cl, n = 2, R = 2-phenylethanol
42: R_1 = F, R_2 = Cl, n = 2, R = indane
43: R_1 = F, R_2 = Cl, n = 3, R = 2-phenylethanol
44: R_1 = F, R_2 = Cl, n = 3, R = indane
45: R_1 = H, R_2 = CN, n = 2, R = benzene
46: R_1 = H, R_2 = CN, n = 2, R = p-cymene
47: R_1 = H, R_2 = OCH_3, n = 2, R = benzene
48: R_1 = H, R_2 = OCH_3, n = 2, R = indane

Fig. 21. Ruthenium(II) piano-stool anilinoquinazoline derivatives.

(DMSO) ligands (**49**–**53**, Fig. 22).[63] ELISA against EGFR identified the outcome of poor conjugation strategies to synthesise complexes **51** and **53**. It was indicated that the anilino-quinazoline ligands ("L"), **L49/50** and **L52** retained relative EGFR inhibitory activity (100% relative to a known quinazoline derivative) due to correct modification at the methoxy substituent, whereas incorrect modification of the anilino moiety in **L51** and **L53** leads to reduced inhibition (77 and 58% respectively). This effect was maintained upon complexation: **49**, **50** and **52** retained their EGFR inhibitory activity while the others were reduced again upon complexation

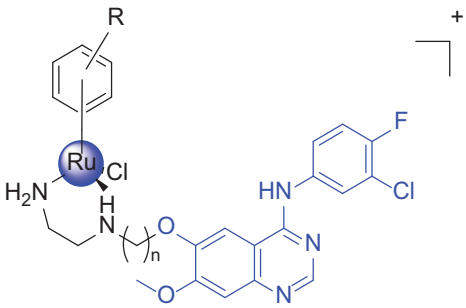

35: n = 2, arene = benzene
36: n = 2, arene = p-cymene
37: n = 2, arene = bi-phenyl
38: n = 3, arene = benzene
39: n = 3, arene = p-cymene
40: n = 3, arene = bi-phenyl

Fig. 20. Structure of ruthenium(II) anilinoquinazoline derivatives.

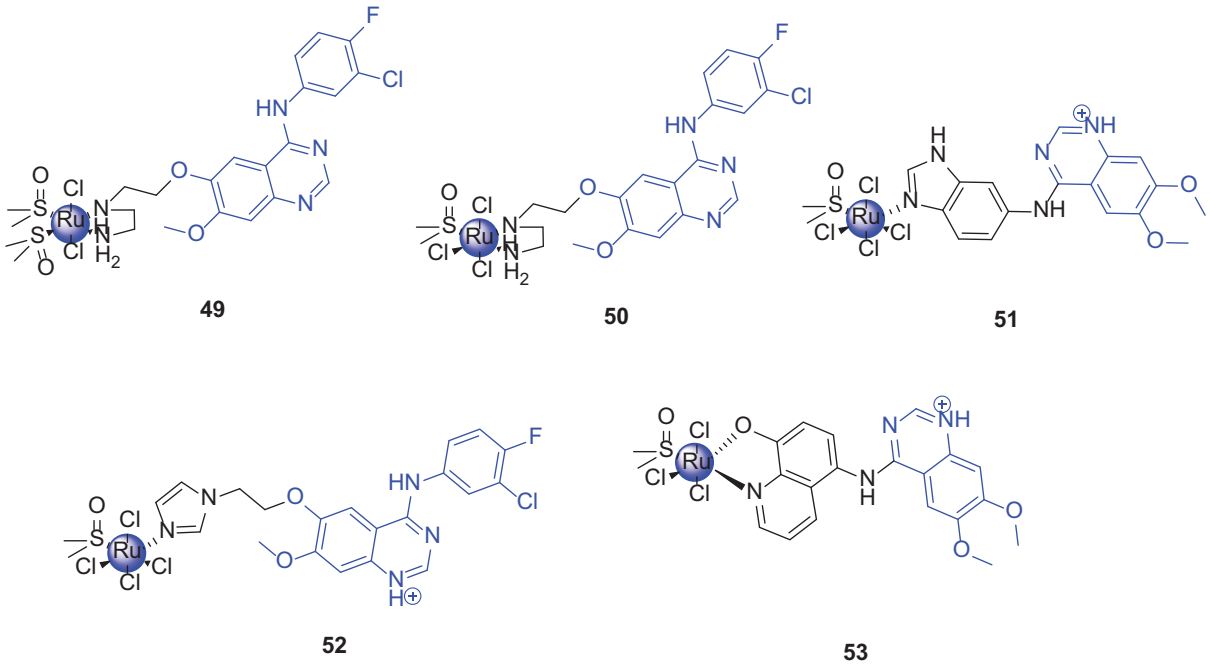

Fig. 22. Structure of ruthenium(II) (**49, 50**) and Ru(III) (**51**–**53**) DMSO quinazoline complexes.

(**51**: 23.8% and **53**: 51%). This is one piece of strong experimental evidence that improper conjugation at the aniline moiety in the synthesis of EGFR targeting metal-TKi's can have a negative impact in the inhibition performance. IC_{50} values against EGFR revealed that **49** and **50** had reduced inhibitory activity with respect to their ligands (while still at sub-micromolar level). Molecular docking studies of the complexes were conducted using intact models of the complexes, due to their slow hydrolysis rate. Interestingly, docking of **49** revealed an additional H-bond formation between a methoxy O and the amide N of Asp776, while **50** had H-bonds between N—H of the ethylenediamine linker and the COO^- of Asp 776 and N—H of the ethylenediamine linker and the C-O of Leu694, reducing the inhibitory capacity of both. No such additional H-bonds were observed with **52**, leading to its retention of EGFR inhibition. Finally, anti-proliferation examinations of **52** revealed its high cell selectivity, while it retained potency like that of RM116 (RM116 = [(η^6-*p*-cymene)Ru(en)Cl]PF_6, a ruthenium(II) arene complex with anti-tumour activity[64]). Like previous sources, it was postulated that **52** may operate in various means such as forming Ru-DNA adducts.

In 2015, Du *et al.* synthesised ruthenium(II) quinazoline complexes featuring elements of both previous studies: further research into use of imidazole functionalised quinazoline conjugates alongside new 2-aminomethyl pyridine derivatives.[65] These complexes **54**–**58** (Fig. 23) were synthesised using analogous synthetic strategies as before. The hydrolysis of **56** was the quickest ($t_{1/2}$ = 3.3 min) and involved hydrolysis of both chlorido ligands essentially simultaneously. As above, DNA minor groove binding was confirmed using Hoechst displacement assays, with K_{sv} values of 10.3×10^4 and 4.3×10^4 μM^{-1} for complexes **54** and **56** respectively. Enhancing previous studies, a DNA replication inhibition assay demonstrated the ability of such complexes to bind Homo Sapiens High Mobility Group Box 1 sequence DNA and inhibit replication – important evidence for their dual-modal activity. ELISA identified **56** as the most promising complex towards EGFR inhibition (IC_{50} = 66.1 nM), with its inhibitory activity being the greatest of all complexes tested, similar to the free ligand and more active than gefitinib control (94.0 nM). Interestingly, *in vitro* anti-proliferation assays indicated that only **55** and **56** had EGF-dependent activity. Complex **56** had the highest activity of all complexes, attributed to the possible hydrolysis of two chlorido ligands; in contrast **52** had similar EGFR inhibitory activity, but lower anti-proliferation activity than **56** against MCF-7. Additionally, the authors hypothesise that the bulkier ligand moieties in complexes **54**, **55**, **57** and **58** in contrast to **56,** lead to their weaker EGFR affinity and consequently, lower EGFR inhibition.

Through molecular docking studies, **56** was confirmed to have better affinity for EGFR than gefitinib (docking score 8.6>8.4), as hydrolysis of the chlorido ligands provides an additional H-bond between the H-O–H ligand and the carbonyl group of Asp831. Finally, cell localisation studies presented further evidence supporting dual-modal activity: **56** was found bound to membrane protein with EGFR binding moieties, while some was internalised into A549 cells and exert both enzyme inhibition and form DNA adducts.

In 2016, Du *et al.* synthesised a series of Ru(II) bisphenanthroline or bi-pyridine complexes featuring one or two previously seen imidazole-quinazoline ligands **59**–**63** (Fig. 24)[66]. ELISA against EGFR indicated again that a longer linker leads to increased EGFR inhibition. Additionally, the di-quinazoline complex showed the highest activity, while the type of ruthenium moiety had little influence on inhibition (phen vs bipyridine). Unfortunately, only **63** showed increased anti-proliferation activity upon complexation with ruthenium(II). However, it did display higher cytotoxicity than *cis*-[Ru(phen)$_2$Cl$_2$], than cisplatin in absence of EGF and than gefitinib in the presence of EGF. In correlation to the EGFR-inhibition, an increasing linker length gave increasing anti-proliferation activity. No correlation between the rate of hydrolysis and anti-proliferation activity was observed for this series of complexes. The di-quinazoline complex **61** exhibited moderate activity in the absence of EGF. This activity increased by a substantial amount in the presence of EGF, indicating it operated primarily *via* an EGF-dependent mechanisms. Comparison between fluorescence quenching Ethidium Bromide and Hoechst

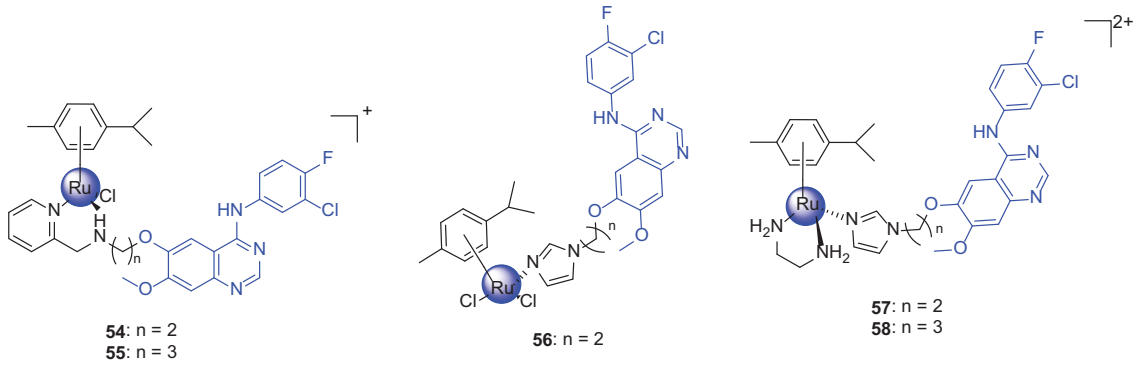

Fig. 23. Ruthenium(II) imidazole and 2-aminomethyl pyridine quinazoline piano-stool complexes.

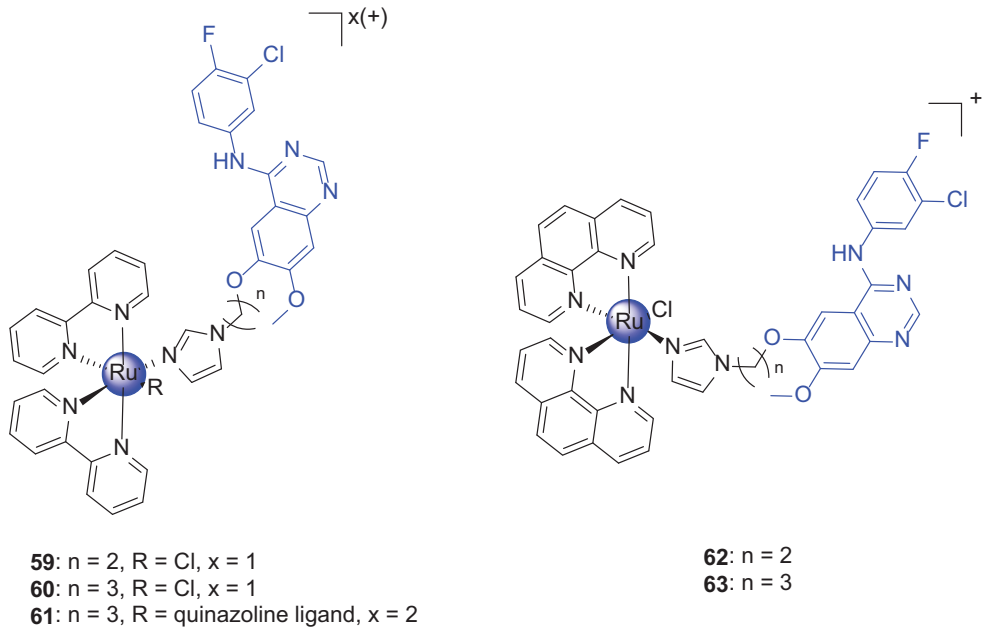

Fig. 24. Ruthenium(II) bis-phen/bipyridine quinazoline complexes.

assays identified **61** and **63** to bind to DNA *via* minor-groove binding. K_{sv} values obtained identified **63** as having a stronger interaction with DNA than **61** (example K_{sv} EtBr of **63** is 3.8×10^4 μM^{-1}, while for **61** it is 1.6×10^4 μM^{-1}). ICP-MS of **61** identified the levels of the complex in DNA and membrane proteins to be 36.7 ng Ru/mg DNA and 618 ng Ru/mg of membrane protein – further evidence of the dual-modal activity of ruthenium-quinazoline complexes.

In 2019, Ilmi *et al.*, developed an independent study featuring Ru(II)-polypyridyl-quinazoline theragnostic probes (**64** and **65**, Fig. 25) for use in imaging of cells in the Red/Near-IR region[67]. These complexes were designed to localise into the mitochondria, to inhibit/image translocated ErbB1 by coupling the quinazoline derivative to a Ru(II)-bipyridine moiety *via* a triethyleneglycol (TEG) linker containing terminal amino groups. Prior to complex-TKi functionalisation, it was decided to test whether combination of a quinazoline derivative and the $[Ru(bipyridine)_2(COOH\text{-}bipyridine)]^{2+}$ precursor would have a negative or synergistic affect in the presence and absence of EGF. Cell viability was not impacted by the presence of precursor complex; the mono (**64**) and bis-adduct (**65**) complexes were tested using an MTT assay against U87MG cells, alongside the TKi precursor without the PEG linker and $[Ru(bipyridine)_2(COOH\text{-}bipyridine)]^{2+}$. The IC_{50} values of the free amine quinazoline derivative and **64** were very similar (IC_{50} = ~ 0.06 μM) indicating incorporation of the PEG-polypyridyl-Ru (II) moiety has not impacted the EGFR inhibitory activity of the complex. A statistically significant higher efficacy was observed for the bis conjugate **65** over the mono conjugate **64**, possibly due to a higher cellular uptake due to the presence of a second lipophilic TKi structure. Fluorescence imaging showed that a mitochondria-specific biomarker (MitoTracker FM) and **65** appeared to co-localise in organelles – indicating mitochondrial localisation of the complex. A fluorescence resonance energy transfer (FRET) efficiency of 24.44% was calculated between the mitochondria-specific biomarker (acceptor) and the complex (donor). This could be due to the fact that the mitochondria-specific biomarker and the complex are on average physically apart by 7–8 nm, further independently demonstrating co-localisation in the mitochondria. In addition, the mitochondrial specificity for **65** was found to be comparable to Mitotracker Green (90.91% vs

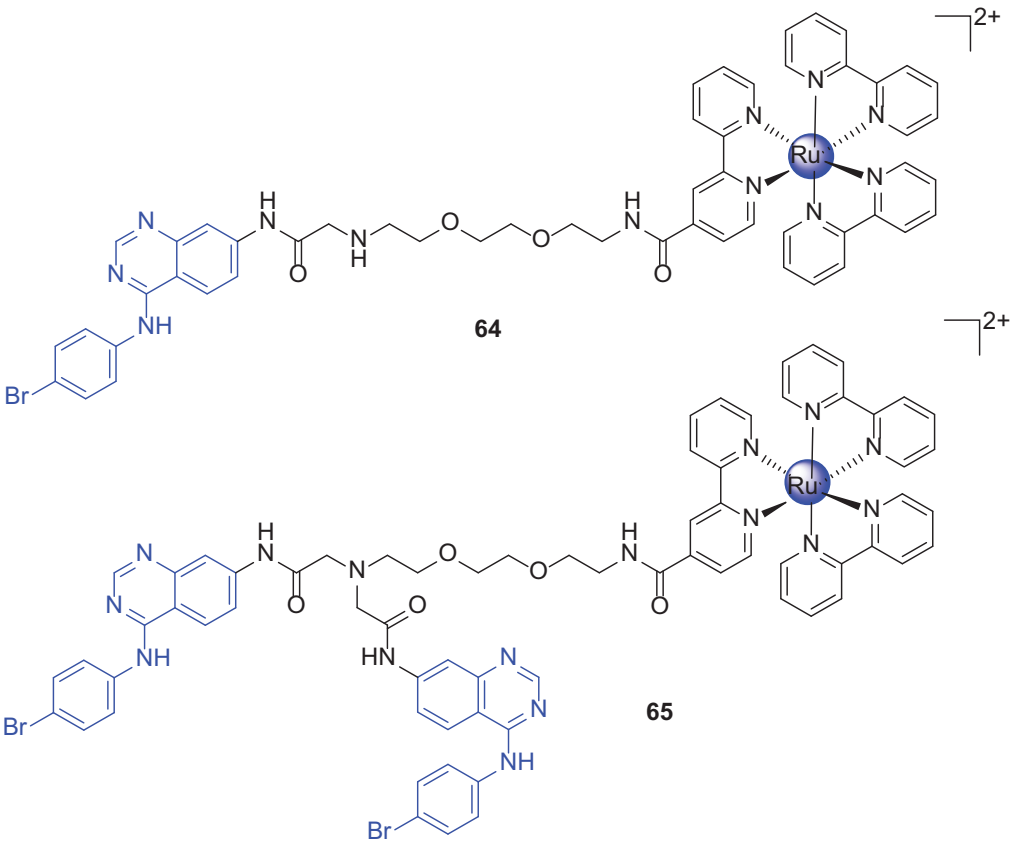

Fig. 25. Structure of the monomeric (**64**) and dimeric Ru(II)-polypyridyl-PEG-quin (**65**) complexes.

92.80% respectively). Unfortunately, unlike the previous study, no research was conducted to investigate the possible DNA binding activity of the Ru(II)-polypyridyl moiety.

2.6. Iron and gold

In 2013, Amin *et al.*, synthesised ferrocene containing bioisosteres and derivatives of anilinoquinazoline EGFR inhibitors (**66**–**68**, Fig. 26) in order to determine if incorporating a ferrocene structure leads to enhanced or weakened biological effects[68]. EGFR inhibition assays concluded that, while **67** exhibited submicromolar inhibition and was the most potent of all the complexes tested, they were observed to be much weaker inhibitors than un-derived anilino-quinazoline controls. The substitution of/at the aniline moiety has yet again proven to be a poor conjugation strategy for metal-TKi conjugates. Incorporation of the ferrocene else-where in the molecule (at the ether functional group) *via* a linker may have led to more desirable results. Anti-proliferative assays of the complexes against K562 cells showed little activity (IC_{50}: < 20 μM). However, as K562 cell lines do not express EGFR, it shows no correlation between the EGFR inhibition and cytotoxicity of these complexes. Finally, docking studies confirmed that only complex **67** was of suitable size and conformation for EGFR docking, consistent with its higher EGFR inhibitory activity.

In 2015, Yang *et al.* synthesised Gold(I) complexes featuring thiourea-modified quinazoline derivatives[69]. These complexes (**69**–**71**, Fig. 27) were designed to act as irreversible EGFR inhibitors in a similar fashion to afatinib (Fig. 3), which acts as a Michael

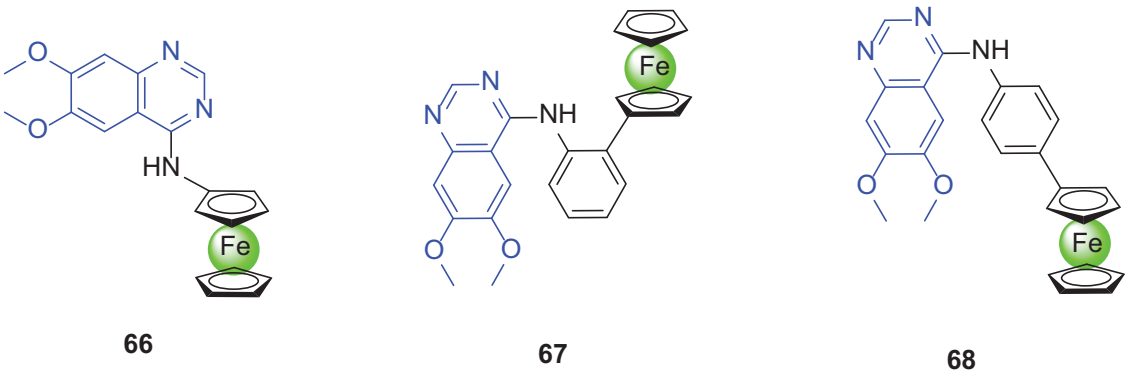

Fig. 26. Ferrocene anilinoquinazoline bioisosteres and derivatives.

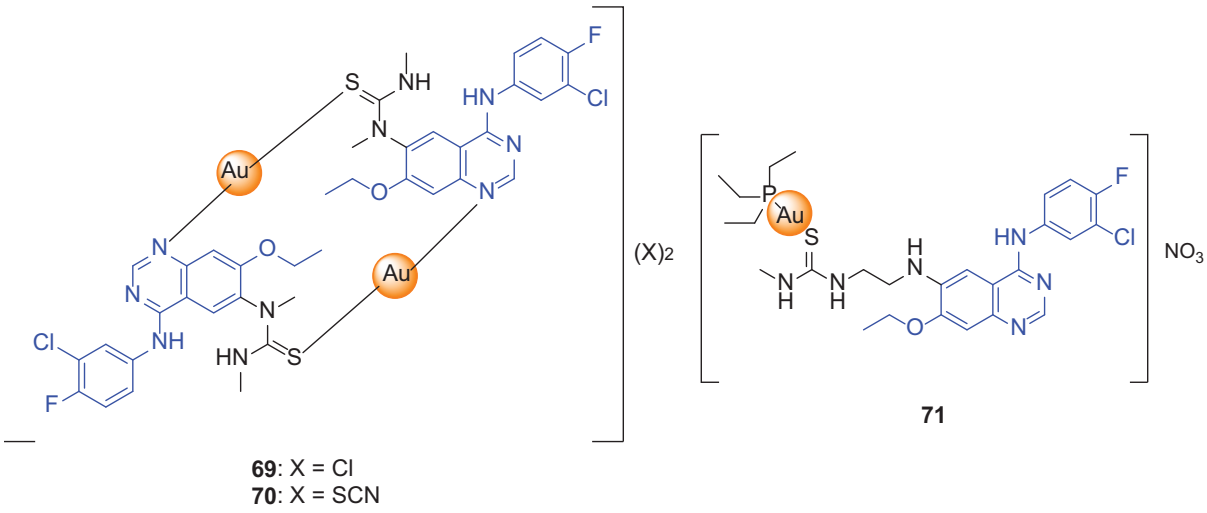

Fig. 27. Thiophilic Au(I) anilinoquinazoline derivatives.

addition acceptor towards the thiol group of cysteine797. Here, in place, the complexes would contain a thiophilic gold(I) metal centre mimicking this mechanism.

The dimeric complexes **69** and **70** showed slightly poorer activity against NCI-H460 (EGFR wild-type) and NCI-H1975 (EGFR L858R/T790M mutant) cell lines relative to gefitinib. Ligand **71L** displayed low micromolar IC_{50} values against NCI-H460 (4.2 μM) and NCI-H1975 (1.7 μM). Complexation of this ligand with Au(I), **71**, increased its potency against NCI-H460 but not NCI-H1975 – albeit similar IC_{50} values in both cases. The authors reasoned that the introduction of the $[Au(PEt_3)]^+$ moiety has not negatively impacted ligand active site binding, but has also not resulted in reaction with cys797, or that the Au species, resulting from early intracellular cleavage, has negligible cellular killing activity in both cell lines tested. Indeed, reaction of **71** with QLMPFGCL peptide (mimicking hinge region residues) results in production of [Au(PEt_3)]-peptide, as a consequence of the high *trans* effect of the phosphine ligand resulting in Au-S bond cleavage. Corresponding results were obtained when reacted with glutathione, indicating premature cleavage. Finally, EGFR inhibitory assays proved underwhelming, demonstrating their inability to act as irreversible Michael acceptor mimetics yielding irreversible inhibition.

In 2020, Ortega *et al.*, synthesised a gold(I) erlotinib conjugate, **72**, *via* coordination to the terminal alkyne moiety[70] (Fig. 28). The authors hypothesised that this conjugate may retain its reactivity with ErbB1 while simultaneously leading to an increase in uptake of gold(I) – however, what resulted was a complete change in mechanism of action.

72 exhibited higher cytotoxicity than erlotinib against EGFR over-expressing cell line MDA-MB-231 (IC_{50}: 1.64 μM vs 68.11 μM respectively). However, the ability of **72** to kill EGFR negative cell lines (MCF-7, RC-124 and BGM cells) led to the consideration that **72** may operate *via* a different mechanism; a cell cycle analysis showed that **72** induced cell cycle arrest in S and G_2/M phases in contrast to G1/S by erlotinib. Also, it was found that the Au content bound to DNA was 3-fold higher than DNA platination by the positive control cisplatin indicating that the conjugate operates *via* a DNA damage mechanism in contrast to erlotinib. However it was observed that **72** did not bind covalently with DNA as determined by EtBr displacement assays and attempted reaction with 9-ethylguanine nucleobase. It would have been interesting to study the EGFR inhibitory activity assays with **72** to further support its loss of EGFR inhibitory activity. Finally, it was importantly shown that the complex may still retain cancer cell line selectivity over normal cell, even with the poor conjugation strategy: ~ 25% cell death in cancer cells vs 5% in normal renal cells.

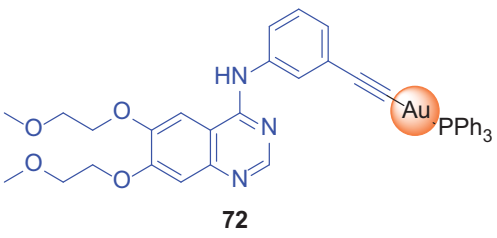

Fig. 28. Structure of gold(I) Erlotinib Conjugate (**72**).

2.7. Cobalt

In 2014, Karnthaler-Benbakka developed a Co(III) quinazoline pro-drug targeting EGFR, **73,** Fig. 29[71]. This was based on the idea that intracellularly, Co(III) complexes undergo reduction to Co(II), which may be re-oxidised to Co(III) in the presence of oxygen. However, in hypoxic tissue, little O_2 is present and the Co(II) species can undergo ligand substitution, releasing a bioactive ligand. It was hypothesised that the Co(III)-quinazoline complex would be too bulky for interaction with the active site of EGFR, while quinazoline TKi ligand release in hypoxic tissue after Co (III)/(II) reduction would lead to EGFR inhibition as the steric problems have been removed.

Ligand **73L** displayed improved activity against erlotinib-resistant H1975 cells (IC_{50} of 15 μM vs erlotinib: > 25 μM). Western blotting confirmed that the dose-dependent EGFR inhibitory activity of **73L** affected downstream targets such as ERK1/2 with a similar profile to erlotinib. **73L** was observed to be fluorescent with a maximum at 455 nm when irradiated with 370 nm light and this fluorescence was quenched upon coordination to Co(III) forming **73**, allowing for easy analysis of complex stability and pro-drug activity in hypoxic tissue. **73** was stable in Dulbecoo's Modified Eagle Medium over a 24 hr period (DMEM), while showed clear release of ligand in hypoxic conditions. Western-blotting analyses further confirmed reduced EGFR-inhibition in normoxic conditions, supporting that the intact complex reduces receptor binding *via* steric hinderance. Finally, **73** inhibited tumour

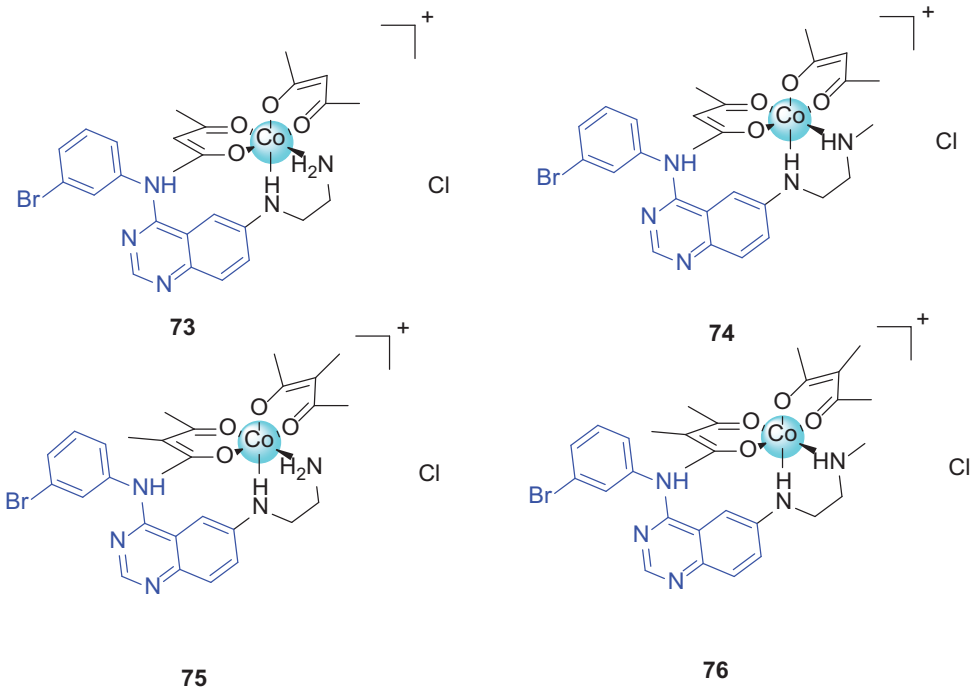

Fig. 29. Co(III)-ethylenediamine quinazoline conjugates **73**–**76**.

growth of A431 xenografts with similar efficacy to erlotinib – the first instance of *in vivo* proof of Co(III) hypoxic pro-drug activity.

In 2020, Mathuber *et al.* continued the development of Co(III)-quinazoline EGFR targeted pro-drugs[72]. After the previous article, further study indicated the moderate stability of the complexes towards blood serum. Analogues of **73** were synthesised in order to improve their stability, by methylating the terminal amino group of the ligand and/or methylation of the acetylacetone (acac) ancillary ligand (**74**–**76**, Fig. 29). Cyclic Voltammetry (CV) of the complexes indicated that methylation of the acac ligand led to a desired decrease in reduction potential (e.g. in **76**), while methylation of the ligand "en" moiety had the opposite effect (in **74**). The Co(III)/Co(II) reduction process was observed to be irreversible – however this is not uncommon in the literature for Co(III) pro-drugs in aqueous media. Potentiometric titrations of analogous MethylEn and PhenylEn control complexes strongly indicated near complete release of "en" ligand after Co(III)/(II) reduction process. Release of the quinazoline ligand was not observed upon interaction of the complex with common biological reducing agents (such as glutathione, ascorbic acid and NADH) indicating they are not responsible for the Co(III)/(II) reduction process and the complexes are stable with respect to them. Finally, MS was used to analyse the stability of the complexes in blood serum; in accordance with the CV reduction potential observations, the $Co(Meacac)_2MeL$ remained 85% intact, while $Co(acac)_2MeL$ and $Co(acac)_2L$ remained 50% and 43% intact respectively.

In this first section of the review, it has been demonstrated through a large variety experimental data; that several quinazoline conjugation strategies reported so far did not show the expected results in terms of EGFR inhibition activity. It is clear the extent of this problem as each aforementioned complex containing erlotinib has been conjugated or *via* CuAAC click chemistry utilising the terminal alkyne group, or *via* direct coordination to a quinazoline nitrogen or *via* coordination to the terminal alkyne – all of which resulted to be not an ideal design for tyrosine kinase inhibition activity (e.g. complexes **9**, **10**, **11a-e**, **13**, **14**, **20**, **21**, **22**, **72**). Functionalisation of the EGFR inhibitors such as erlotinib, gefitinib and lapatinib at the solvent exposed regions, as highlighted in Fig. 30**,** would be a better strategy; this strategy has been used to great success in numerous aforementioned studies (e.g. complexes **1**–**8**, **12**, **15**–**18, 23**–**65**, **71**, **73**–**76**).

The above regions (highlighted in red in Fig. 30) have no interaction with the active site of EGFR wild-type receptor and therefore the functionalisation of these areas should have minimal impact on EGFR inhibition (however, there are exceptions to the rule, generally due to steric implications as seen above – for example if the ethylenediamine moiety in **73L** is replaced with a bipyridine moiety[71]). This hypothesis found confirmation in the analyses of the EGFR – TKi crystal structures, where it is appreciable that the above regions extend out from the EGFR active site (Fig. 31).[73].

3. Complexes targeting BCR-ABL and PDGFR (Platelet Derived Growth Factor Receptor)

As previously briefly introduced, BCR-ABL is a tyrosine kinase receptor expressed as a fusion of two separate genes: breakpoint cluster region (BCR) and ABL1. This fusion is caused by a translocation of chromosome number 22 (which contains the BCR gene) with chromosome 9 (containing ABL gene), forming the Philadelphia chromosome[19]. BCR-ABL is clinically relevant as it is a constitutionally active mutant kinase that causes Chronic Myeloid Leukaemia (CML) – which accounts for ~20% of all adult affecting leukemias[74]. In actual fact, the BCR-ABL gene encodes for three proteins isoforms of molecular weight 210 kDa, 185/190 kDa and less commonly 230 kDa; the BCR-ABL p210 is the isoform used as the marker for CML[75]. Upon comparison of the BCR-ABL and ABL1 proteins, it is indicated that a lack of autoinhibitory N-terminal myristoylation leads to the constant activity of the mutant kinase[75]. Currently, three BCR-ABL targeted tyrosine kinase inhibitors reside on the WHO List of Essential Medicines [2]: imatinib, nilotinib and dasatinib. The three aforementioned TKi's are also FDA approved, alongside ponatinib (Fig. 3). As previ-

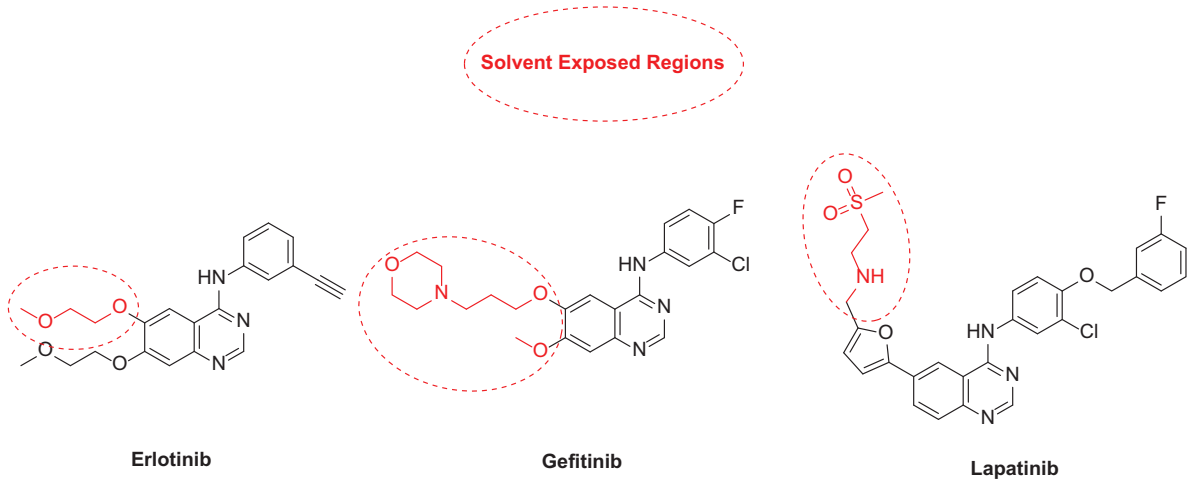

Fig. 30. Solvent exposed regions of three EFGR inhibitors erlotinib, gefitinib and lapatinib.

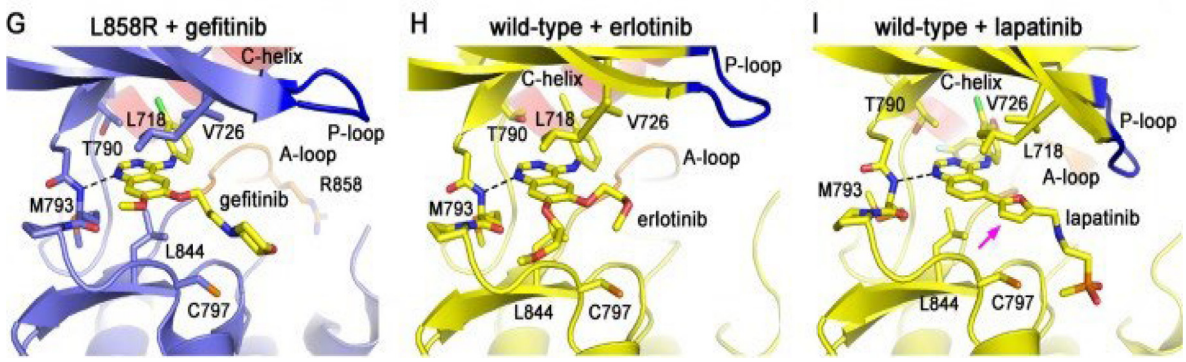

Fig. 31. Crystal Structures of L858R EGFR mutant + gefitinib, EGFR + erlotinib and EGFR + lapatinib[73]. Taken with permission from Zhu *et al.*, 2018.

ously mentioned, imatinib has revolutionised the treatment of CML, with the life expectancy of patients treated with imatinib not differing significantly from the general population[20]. Imatinib inhibits BCR-ABL *via* a reversible ATP-competitive mechanism. However, resistance to imatinib poses a challenge partially remedied by an analogous tyrosine kinase inhibitor, nilotinib. Nilotinib is approximately 30 times more potent than imatinib[76], with the addition of a trifluoromethyl substituents that allows for increased Van der Waal active site interactions. Nilotinib can circumvent 32 out of 33 clinically relevant imatinib resistant mutations, but importantly falls short in combating the T315I gatekeeper mutation[77,78]. This has lead to the synthesis of other TKi's including, but not limited to, dasatinib and ponatinib. Unfortunately, their usage is limited by adverse side effects such as severe arterial thrombotic events (in particular with ponatinib[79]). This hinderance on an otherwise huge success story leaves remaining research into combating BCR-ABL.

In recent times, imatinib has been shown to provide synergistic anti-tumour effects when used in combination with cobalt complexes[80] and cisplatin[81–84]. Due to this, one strategy that has been utilised to circumvent resistance and dose-limiting side effects is to conjugate the BCR-ABL TKi's to metallic moieties in a similar fashion used to target EGFR above.

As observed for the EFGR inhibition, BCR-ABL Tyrosine Kinase Inhibitors should be functionalised in the correct fashion to avoid reducing their BCR-ABL inhibitory activity upon conjugation to a metal moiety. In accordance with this, it is important and advised to functionalise BCR-ABL TKi's at the solvent exposed regions which are identified below (Fig. 32).

These solvent exposed regions extend out from the BCR-ABL active site, as observed in the BCR-ABL – TKi crystal structures (Fig. 33).

In addition, to circumvent BCR-ABL TKi resistance and side effects, research into BCR-ABL TKi- metal conjugates has stemmed for the fact that these TKi's are also known to inhibit other clinically relevant TKi's, notably Platelet Derived Growth Factor Receptor (PDGFR), Mast/stem cell growth factor receptor (c-KIT), Transforming Growth Factor β Receptor (TGFβR) and Fibroblast Growth Factor Receptor (FGFR)[86–88]. For example, 85% of gastro-intestinal tumours are associated to c-KIT overexpression while PDGFR is known to be overexpressed in 30% of colorectal cancers. BCR-ABL – metal TKi conjugates may also be utilised to combat aggressive cancers such as colorectal cancer as the solvent exposed regions upon interaction with BCR-ABL are analogues when interacting with c-KIT, TGFβR or PDGFR (no Imatinib-PDGFR co-crystal exists, however the interaction has been studied *via in silico* methods)[88,89].

In this section we will discuss all the examples of complexes reported in literature, containing the BCR-ABL and PDGFR inhibitors imatinib and ponatinib. To the best of our knowledge, no metal complexes with nilotinib or dasatinib are reported.

3.1. Platinum

The first coordination complex containing a BCR-ABL targeting TKi was based on a Pt(II) scaffold (**77**) and synthesised in 2011 by Dolman *et al.* (Fig. 34)[89]. This complex was designed to deliver imatinib to kidney proximal tubular cells *via* a imatinib-Pt(II) ULS-

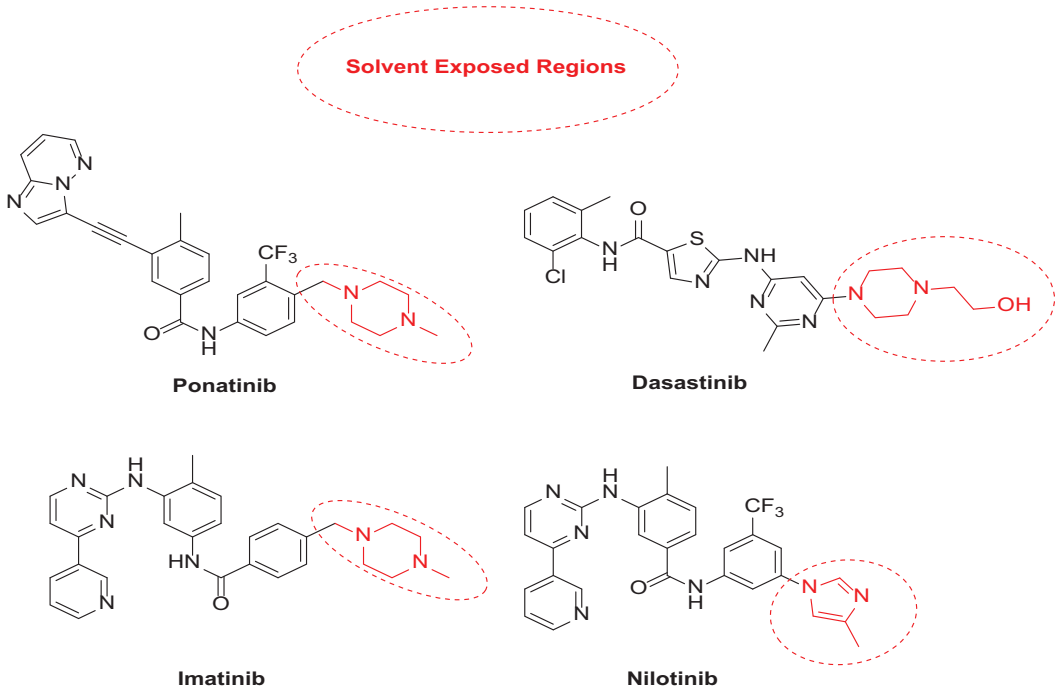

Fig. 32. Solvent exposed regions appropriate for functionalisation in common BCR-ABL TKi's.

Lysozyme carrier (**78**), to combat tubulointerstitial fibrosis *via* inhibition of both PDGFR and TGFβR.

The *in vitro* cytotoxicity effect of **77** was tested against human kidney 2 cells (HK-2), displaying no cytotoxicity after 24 hrs in a 2 – 38 μM range. Similar results were obtained upon testing **77** against NRK-52E rat tubular cells and healthy rats, indicating the complex is non-cytotoxic. Internalization into renal proximal tubular cells was observed to be rapid (within 10 min of administration) while degradation of the conjugate after 24 h was observed – for both intravenous and intraperitoneal administrations. The renal and plasma bioavailability of the complex **78** was 100% after intraperitoneal administration. The conjugate was rapidly absorbed into the bloodstream upon administration ($t_{1/2}$ absorption of 29 mins) and had retained a renal localisation half-life of over 2 days regardless of method of administration. The conjugate was observed to be highly stable, with the complex only observed in the bloodstream and imatinib-conjugate observed in the kidneys. The authors acknowledged that conjugation *via* the pyridine nitrogen would interfere with kinase inhibition and realised that sufficient TKi release from the ULS system would be required for desired activity, in accordance with the conjugation strategy provided earlier. Unfortunately, only 1.3% of imatinib was released as desired. However, free imatinib mesylate control was observed to have rapid elimination from kidney cells, while **78** was retained as above. This sustained level of imatinib derived from **78** provided a $\geq$ 15 times renal exposure to active imatinib than imatinib mesylate. Unfortunately, poor *in vivo* activity was observed with **78** and the authors claim this may be the result of experimental conditions, citing the observed activity of other ULS linked systems.

In 2016, Yuming *et al*., developed Pt(II)-imatinib conjugates alongside the previously mentioned Pt(II)-erlotinib conjugates **20**–**22**[54]. These Pt(II) complexes were based on oxaliplatin and both *cis*platin and *trans*platin, allowing for evaluation of the effect of stereochemistry on pharmacological properties (**79**–**81**, Fig. 35).

In line with the erlotinib complexes **20**–**22**; the above imatinib-oxaliplatin (**81**) and cisplatin derivatives (**79**) were stable in saline and phosphate buffer over 24 h at physiological temperature, while the transplatin derivative (**80**) showed gradual degradation/release of imatinib. As aforementioned, release of imatinib is important as the current coordination of imatinib to Pt(II) *via* the pyrimidine nitrogen will interfere with BCR-ABL inhibition. As a result of the poor conjugation strategy, the activity of the complexes towards K562 cells (Bcr-Abl+) cells was reduced ten-fold or more, when compared to imatinib (IC_{50}'s against K562 cells: Complex **79** = 1.86 ± 0.29 μM, Complex **81** = 2.27 ± 0.33 μM, imatinib = 0.15 ± 0.02 μM). Interestingly here, in contrast to the previous erlotinib conjugate **21,** the unstable transplatin-imatinib conjugate **80** did not have comparable activity (which should release free imatinib) to the imatinib control (IC_{50}'s against K562 cells: Complex **80** = 1.04 ± 0.01 μM). Overall, the three conjugates did however, retain a kinase selectivity profile similar to imatinib; for example, the conjugates had higher potency towards the K562 cells than RPMI8226 cells (Bcr-Abl−). The conjugates also displayed minimal normal cell cytotoxicity (against normal porcine kidney epithelial cell line: LLC-PK1) and showed the ability to circumvent resistance; the IC_{50} value for inhibition of Bcr-Abl E255K mutant was only 5–10 times higher than that in the wild type Bcr-Abl, in contrast to Imatinib which was 364 times greater. This observation was supported by *in silico* molecular docking, which reported a slightly different binding to BCR-ABL E255K mutant with respect to Imatinib. DNA damage was also observed with the conjugates, which were able to form monodentate adducts with guanine base pairs.

3.2. Zinc, copper and iron

In 2018, Dalla Via's detailed the synthesis of hydroxamate functionalised imatinib ligands and their coordination to zinc, copper and iron, in order to assess modulation of redox balance (**82**–**87**, Fig. 36)[90]. The conjugates are ideally functionalised, replacing the n-methylpiperazine moiety with a hydroxamate group that allow coordination to the metal centres, resulting in bis adducts **82**–**85** (Cu(II), Zn(II)) and tris adducts **86**–**87** (Fe(III)).

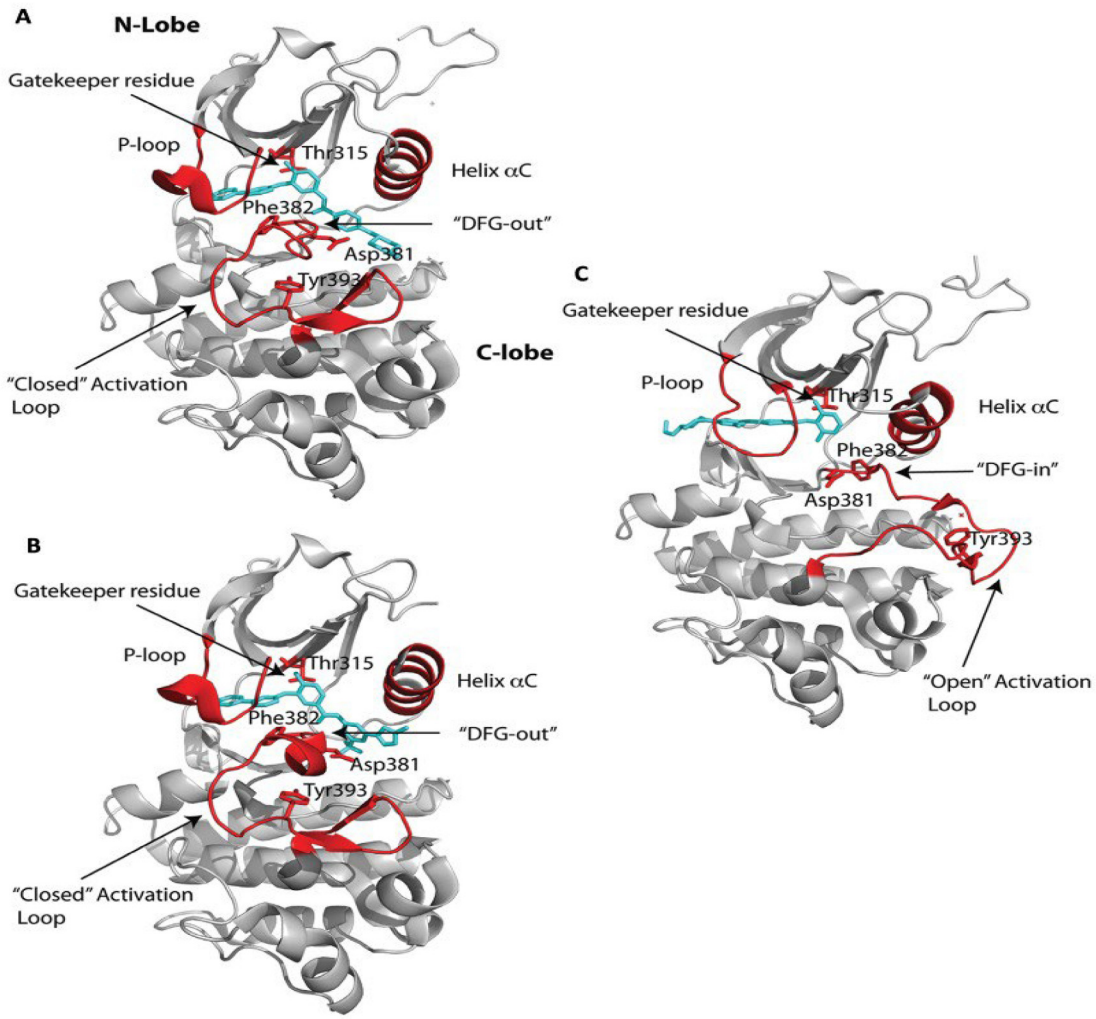

Fig. 33. Co-crystals of BCR-ABL with **A** Imatinib, **B** Nilotinib and **C** Dasatinib. Taken from Reddy *et al.*, 2012 with permission[85].

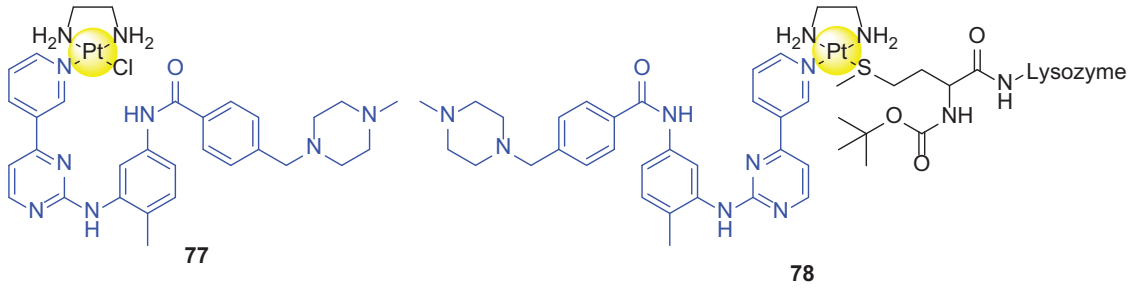

Fig. 34. Imatinib-Pt(II) ULS (**77**) and Imatinib-Pt(II) ULS-Lysozyme conjugates (**78**).

All the above complexes were shown to be stable by HPLC in 1:1 ACN/H_2O + 0.1% TFA for at least 5 days. Biological assays are currently underway for these novel complexes, as of which results will be compared to the metal-free ligands.

3.3. Ruthenium

In 2018, Rohrabaugh *et al.* synthesised Ru(II) polypyridyl imatinib conjugates designed for photochemical release of imatinib intracellularly (**88**–**92**, Fig. 37)[91]. The group envisioned that the Ru(II) moiety would impair interaction of the intact imatinib conjugate to BCR-ABL due to its binding *via* the pharmacologically important pyridine nitrogen, while upon irradiation, ligand exchange with a solvent molecule would occur and the released imatinib would as desired.

Irradiation of tested complexes **88**–**90** with red light resulted in the release of imatinib and corresponding formation of solvated Ru (II) analogue. Additionally, no such release of imatinib was observed in the absence of light as desired. **90** and its water solvated complex were both observed to be substrates for PDT. Analogous complexes **91** and **92** were synthesised containing a c-KIT antibody and were determined by UV-Vis to have an average of 3

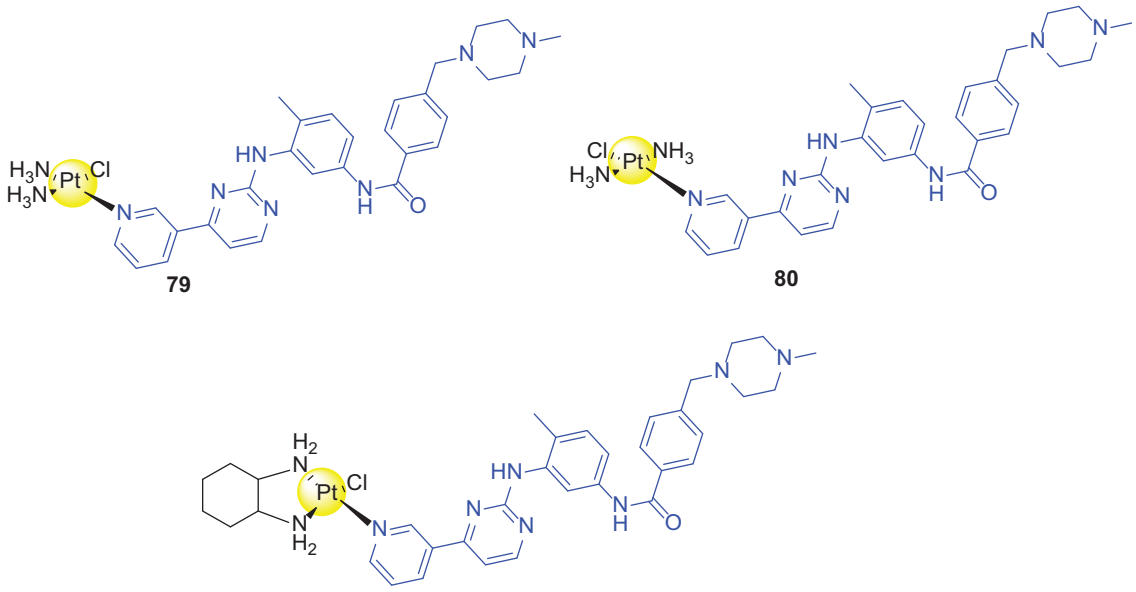

Fig. 35. Structure of Pt(II)-imatinib conjugates.

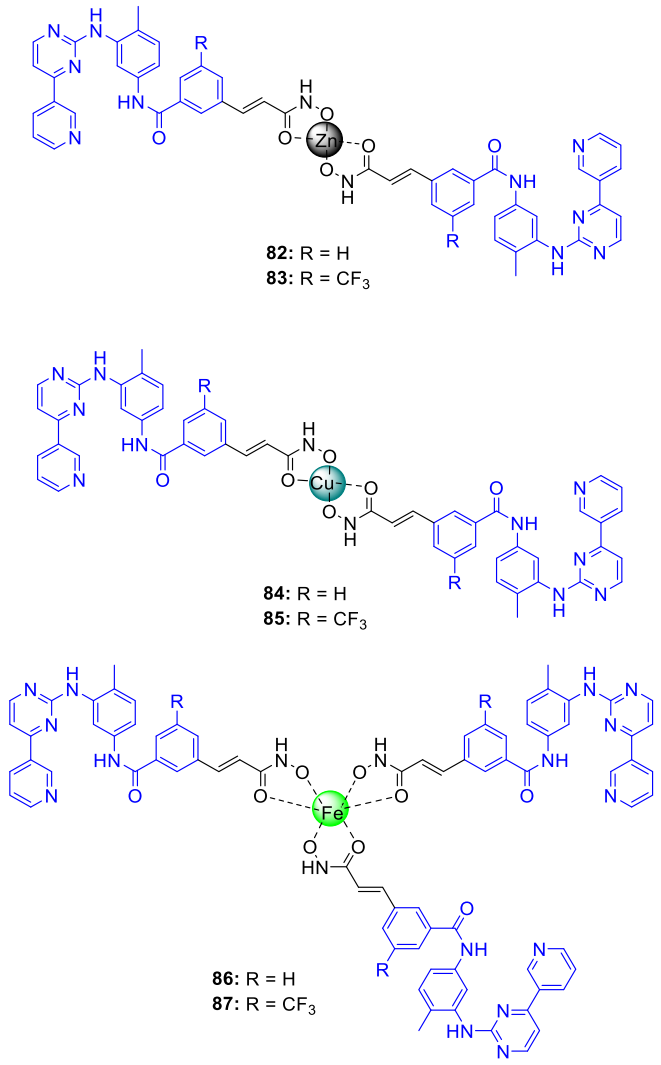

Fig. 36. Hydroxamate functionalised imatinib coordination complexes of Zn(II), Cu (II) and Fe(III).

and 10 complexes per antibody respectively. UV-Vis was used to demonstrate that the photochemical ability of the complexes to release Imatinib was un-impaired.

Overall, this study constitutes an important foundation for intracellular release using Ru(II) polypyridyl complexes. However, this study fails to demonstrate that binding of imatinib to the Ru (II) moiety would impair BCR-ABL inhibition in the absence of light (due to no release of imatinib). While this hypothesis is expected to be true by analysis of the literature above, it would be necessary confirm/deny *via* BCR-ABL inhibition assays. Additionally, it would be important to determine if the intact complex retains selective uptake towards cancerous cell lines *versus* normal cells.

3.4. Imatinib-mesylate metal derivatives

In 2019, Cipurkovic *et al.*, synthesised a series of imatinib-mesylate Co(II), Cu(II) and Ni(II) complexes (**93**–**95**, Fig. 38)[92]. They proposed a coordination *via* oxygen donors of mesylate ion to the metal centre through IR spectra analyses). The proposed structure is a 1:2 (metal centre: imatinib mesylate) square planar complex, or octahedral if axial water molecules were considered (Fig. 38). As expected, imatinib mesylate exhibited no anti-microbial activity when administered at 5.0 mg/ml. but the Co $(ImatinibM)_2$ complex **93** exhibited higher zones of inhibitions against C. albicans (15 mm), B. subtilis, L. monocytogenes,S. aureus (all three between 16 and 20 mm) and S. aureus P. aeruginosa (14 mm). However, the positive control Ciprofloxacin exhibited zones $\geq$ 30 mm when administered at 1 mg/ml, indicating **93** as a weak anti-microbial agent. This study has a number of shortcomings: (i) not identifying a clear objective for synthesis of these complexes; (ii) uncertainty over the structure of the complexes (square planar vs octahedral) and (iii) no kinase inhibition assays nor cytotoxicity assays were conducted. In similar fashion to the above study, BCR-ABL inhibition assays would have been important to confirm/deny either retention or loss of activity upon coordination. In any case, it is of our opinion that activity would have remained similar to a imatinib mesylate control, as no functionalisation toward the main imatinib moiety was made.

In 2020, Gundogdu *et al.*, developed a formulation consisting of a ^{99m}Tc imatinib mesylate conjugate (**96**) for use in SPECT[93]. The

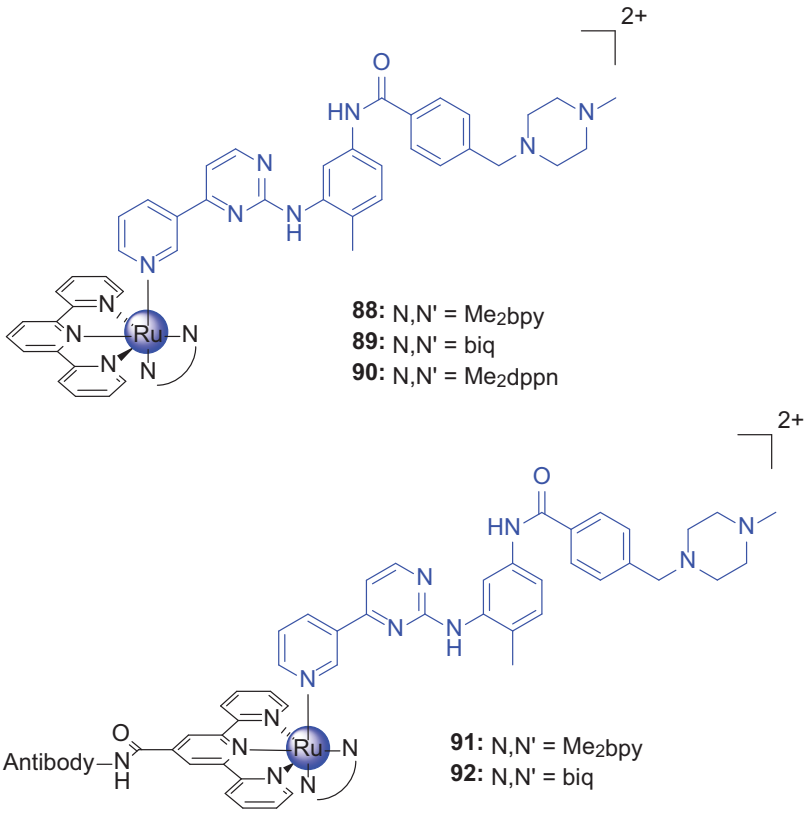

Fig. 37. Ru(II) polypyridyl imatinib conjugates and additional c-KIT antibody functionalised derivatives.

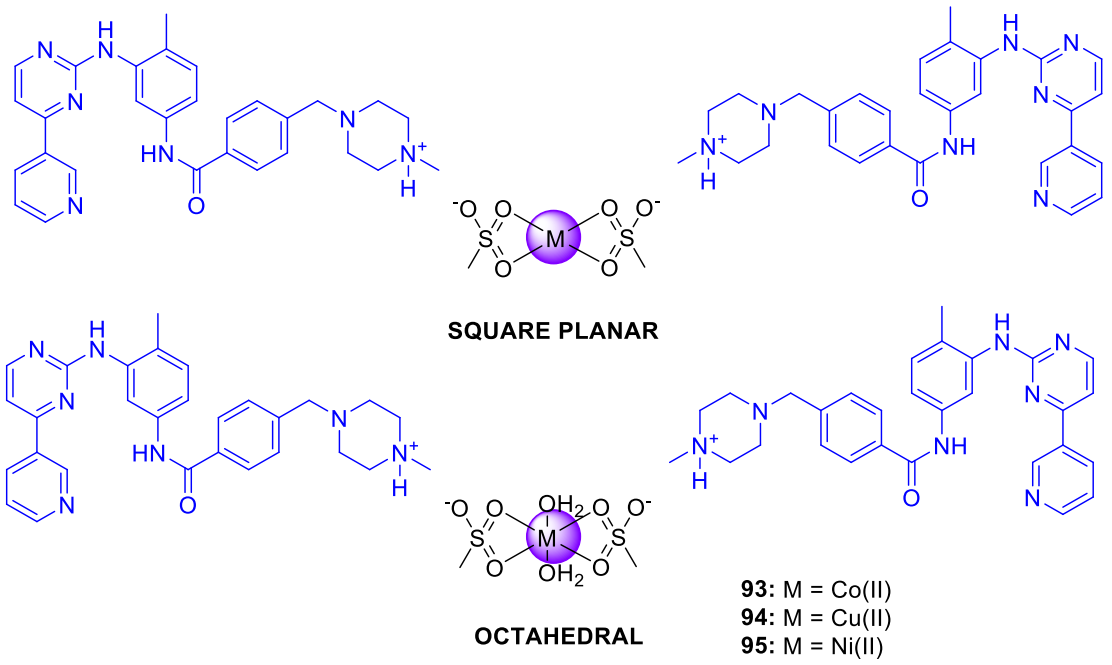

Fig. 38. Cu(II), Co(II) and Ni(II) Imatinib Mesylate coordination complexes.

authors hypothesised that this conjugate would provide a higher ratio of cellular uptake. The optimum formulation for radiolabelling within the scope of the Quality by Design principles was determined theoretically (Fig. 39).

Microbiological analyses indicated no anti-microbial activity, similar to what observed for the analogues Cu(II) **94** and Ni(II) **95** complexes above, while a gel clot test concluded that the formulation was pyrogen free. Finally, cell-binding studies indicated towards the higher on target cell uptake from Tc-imatinib: the cell binding ratio of a ^{99m}Tc solution was observed to be 15.77 %, while the ^{99m}Tc imatinib formulation had a much higher ratio of 88.90 % for MCF-7 cells. The authors stated that binding of imatinib to Tc

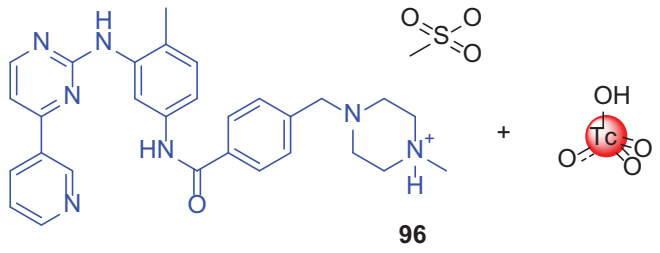

Fig. 39. ^{99m}Tc Imatinib Mesylate formulation.

most likely occurs by a nitrogen donor to an unknown reduced state of Tc. As in above studies, it is unclear as which nitrogen (pyridine vs pyrimidine) is involved in coordination. Additionally, the oxidation state of ^{99m}Tc is unknown – this may have been deduced *via* gel electrophoresis against standards of known charge, as conducted by Garcia *et al.*, 2009[48].

3.5. Cobalt

Most recently in 2021, Mathuber *et al.* developed two Co(III)-ponatinib pro-drugs (**97**–**98,** Fig. 40) to target cancers that overexpress either BCR-ABL and FGFR[94]. These Co(III)-ponatinib conjugates should release the TKi in hypoxic conditions due to a reduction from kinetically inert Co(III) to kinetically labile Co(II), which allows ligand substitution with H_2O. It is also hypothesised that in normoxic conditions, the intact Co(III)-ponatinib will render the TKi too sterically bulky to bind to BCR-ABL and/or FGFR, resulting in selective cancer therapy and reduced off-target adverse side effects. Molecular docking studies indicated that replacing the piperazine moiety did not affect the binding mode to either BCR-ABL or FGFR, and also demonstrated that the presence of the Co (III) moiety would interfere with kinase binding due to steric hinderance. As such, the modelled ligand was used to synthesise two Co(III) pro-drugs containing acetylacetone (acac, **97**) or methylacetylaceton (Meacac, **98**) ancillary ligands (Fig. 40).

The intrinsic fluorescence of the ponatinib derivative ligand in **97** and **98** (λ_{em} = 470 nm at λ_{ex} = 320 nm) was quenched upon

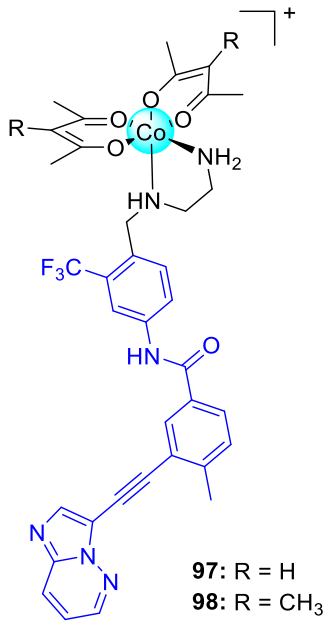

Fig. 40. Structure of Co(III) Ponatinib pro-drug systems.

coordination to Co(III). Cyclic Voltammetry indicated an irreversible Co(III)/Co(II) reduction at −314 mV and −442 mV for **97** and **98,** respectively, attributed to increased space (additional CH_2 group) between the Co(III) moiety and chelating TKi pharmacophore. Both **97** and **98** were stable in fetal calf serum (FCS) after 26 h (~90% intact) and after 72 hrs **98** was shown to be more stable than **97** (80% vs 70%), as expected due to the Meacac ancillary ligands. In cells, a 2 to 4 fold higher intensity was absorbed for **98** in normoxic and hypoxic conditions respectively, due to TKi release, while fluorescence indicated that **97** was 2.8 times less stable in hypoxic than normoxic conditions, accordingly. Kinase screening of ponatinib derivative ligand against ABL1 confirmed that it was essentially unaffected by functionalisation in comparison to ponatinib (IC_{50} = 1.93 nM vs 1.75 nM respectively), however, the functionalisation unfortunately led to a 5-fold decrease in FGFR1 inhibition relative to ponatinib (IC_{50} = 5.54 nM vs 25.9 nM respectively). Both complexes were shown to be considerably less active than the free ligand against K-562 cells (BCR-ABL+) in normoxic conditions, while hypoxic conditions (0.1% O_2 concentration) led to a huge increase in activity (**97** IC_{50} = 5 nM, **98** = 10 nM). Clonogenic assays showed that the complexes inhibited cell growth by only 50% in normoxic conditions (ponatinib = 90%) but achieved 80% in hypoxic conditions. Western blot analysis showed that **97** had a weaker impact on the phosphorylation on downstream targets (ERK1/2 and S6) than **97**. Finally, *in vivo* activity of **97** against BCR-ABL-driven K-562 cells and FGFR3-driven UM-UC-14 cells in xenograft mouse models was observed – significant reduction of tumour size with no weight loss. A less pronounced effect was observed with **98**, due to its slower ligand release.

Similar to what observed in the previous section, metal – BCR-ABL type targeting conjugates proved to be an effective strategy for circumventing resistance/dose-limiting side effects and/or providing greater on-target metal ion cellular uptake. This is a promising area that has the same premise as EGFR targeting metal conjugates (Section 1) but with an unfortunate limited number of sources at present. There is little indication of current investigations in the literature except from our group that is currently developing a series of Pt(IV)-imatinib/nilotinib pro-drugs (Fig. 41) with the intention to combat colorectal and gastrointestinal cancers by targeting PDGFR. Our synthetic strategy involves conjugates reminiscent of the work conducted by Dalla Via[90], utilising the carboxylic acid functional groups to conjugate the imatinib and nilotinib derivatives to a cisplatin scaffold. These will be the first examples in literature of metal conjugates to nilotinib. Upon intracellular reduction of the Pt(IV) prodrug, the inhibitor will be removed from the cisplatin scaffold and the two entities will cooperatively work to increase the anticancer activity with particular focus on colorectal cancers, where the current chemotherapeutic platinum based drugs are failing. (Fig. 41)[95].

4. Complexes targeting VEGFR (Vascular Endothelial Growth Factor Receptor)

Vascular Endothelial Growth Factor Receptor (VEGFR) is a family of receptors containing three main subtypes: VEGFR1, VEGFR2

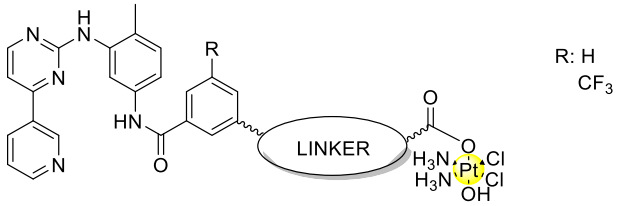

Fig. 41. Generic structure of Pt(IV)-Imatinib and Nilotinib prodrugs.

and VEGFR3. Each receptor shows the same structural features with an extra-cellular ligand binding region made of seven loop domains and a transmembrane helix which links the binding region to a cytoplasmic catalytic domain (Fig. 42)[96]. The VEGFR family is clinically relevant as it is involved in increased neighbouring vessel formation (angiogenesis) which facilitates cancer cell proliferation *via* delivery of essential nutrients and oxygen[97]. Over-expression, for example, of VEGFR2, has been observed in a multitude of cancers: breast, lung, gastrointestinal, ovarian and bladder cancer. Currently, no VEGFR inhibitors are present on the WHO List of Essential Medicines 2019[2], however, sunitinib, vandetanib, sorafenib and regorafenib (Fig. 3) are all FDA approved drugs for the treatment of various cancers. In particular, sunitinib is used for renal cell carcinoma and imatinib-resistant gastrointestinal stromal tumour, vandetanib for medullary thyroid cancer, sorafenib for primary kidney or liver cancer, FLT3-ITD positive AML (Acute Myeloid Leukemia) and radioactive iodine resistant advanced thyroid carcinoma and regorafenib for the treatment of metastatic colorectal cancer. For example, sunitinib has proven successful in the treatment of renal cell carcinoma where patients obtain a longer median progression-free survival than those on control treatment i.e., interferon α (11 vs 5 months; $P < 0.001$) [98]. Sunitinib treatment is unlikely to produce severe adverse side reactions in patients even if less serious side reactions are still common. Unfortunately, the other three aforenamed VEGFR kinase inhibitors – for example, regorafenib, are associated with severe and sometimes fatal hepatotoxicity, which was observed in clinical trials[98].

Truthfully, the aforementioned inhibitors are classed as multi-tyrosine kinase inhibitors, due to their ability to inhibit a multitude of kinases. For example, sunitinib is known to also inhibit PDGFR and vandetanib is also an EGFR inhibitor, which may be expected from its quinazoline based structure and analogy to previous EGFR inhibitors (Fig. 3). Sorafenib additionally inhibits PDGFR and RAS kinases, while regorafenib is a dual targeted VEGFR2-TIE2 tyrosine kinase inhibitor. As such, this section has overlapping bases to both previous sections. Research into VEGFR kinase inhibitor metal conjugates have two main objectives (i) to improve selective uptake of metal ions/complexes, circumventing resistance and adverse side effects and (ii) to develop new metal-based drugs to target other cancerous cell lines utilising their multi-kinase ability.

As already observed for the previous two classes of inhibitors, the conjugation of a metal centre should happen in the solvent exposed regions, in order to minimise the inhibition activity disruption (Fig. 43). Analysis of the sunitinib-VEGFR co-crystal allows for determination of the binding mode and therefore where functionalisation is appropriate (Fig. 44 [100]). The entirety of the sorafenib/regorafenib structure has pharmacological relevance (each part of the molecule either occupies the adenine, hydrophobic or allosteric pocket, Fig. 44) leading to difficult conjugation of a metal centre. Therefore, it is advised molecular docking studies are conducted prior to sorafenib/regorafenib functionalisation to determine how binding will be affected. Unfortunately, no co-crystal exists between VEGFR-vandetanib nor between EGFR-vandetanib – however, binding between EGFR and vandetanib is expected to be analogous to previous quinazoline scaffolds.

4.1. Metallocene of iron, ruthenium and cobalt

In 2008, Spencer *et al.* released a communication detailing the synthesis and biological examination of ferrocene-substituted 3-methylidene-1,3-dihydro-2H-indol-2-ones (**99** and **100**)[101]. In essence, they decided to replace the pyrrole and amide portions of sunitinib with ferrocene while investigating the effect stereochemistry on the double bond has on biological activity (Fig. 45). They hypothesised that incorporation of a ferrocene moiety may

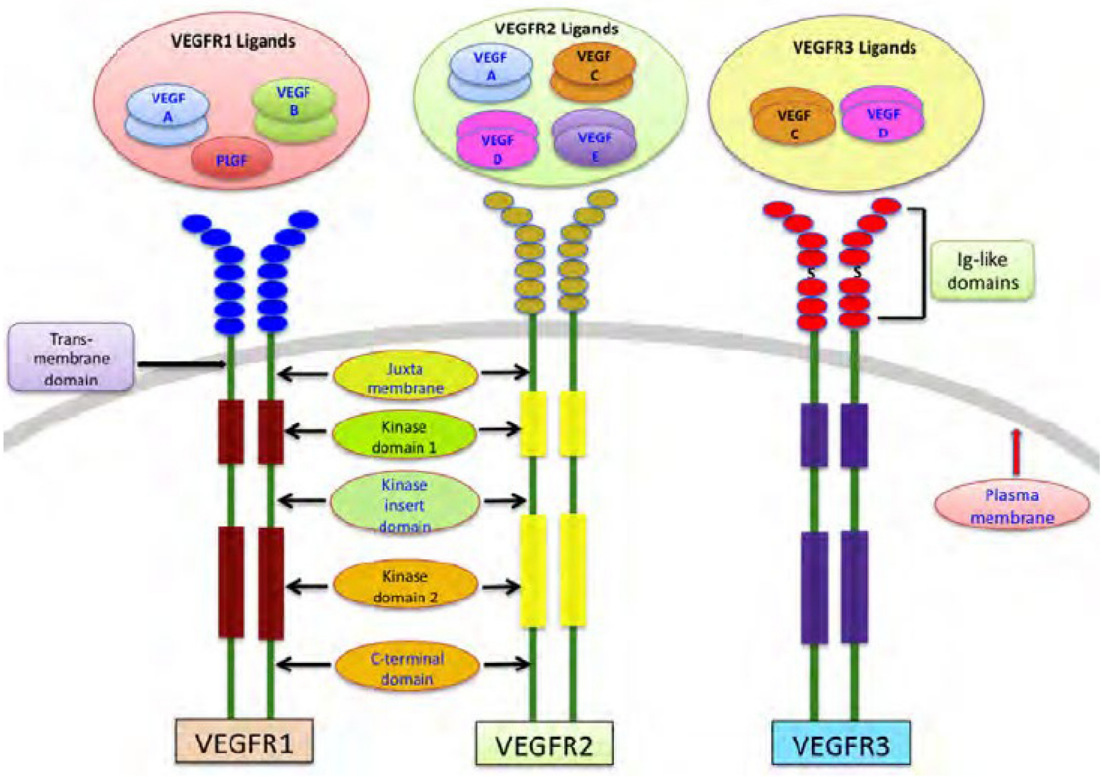

Fig. 42. Schematic structure of VEGFR1, VEGFR2 and VEGFR3. Taken with permission from Lawrence *et al.*, 2012[99].

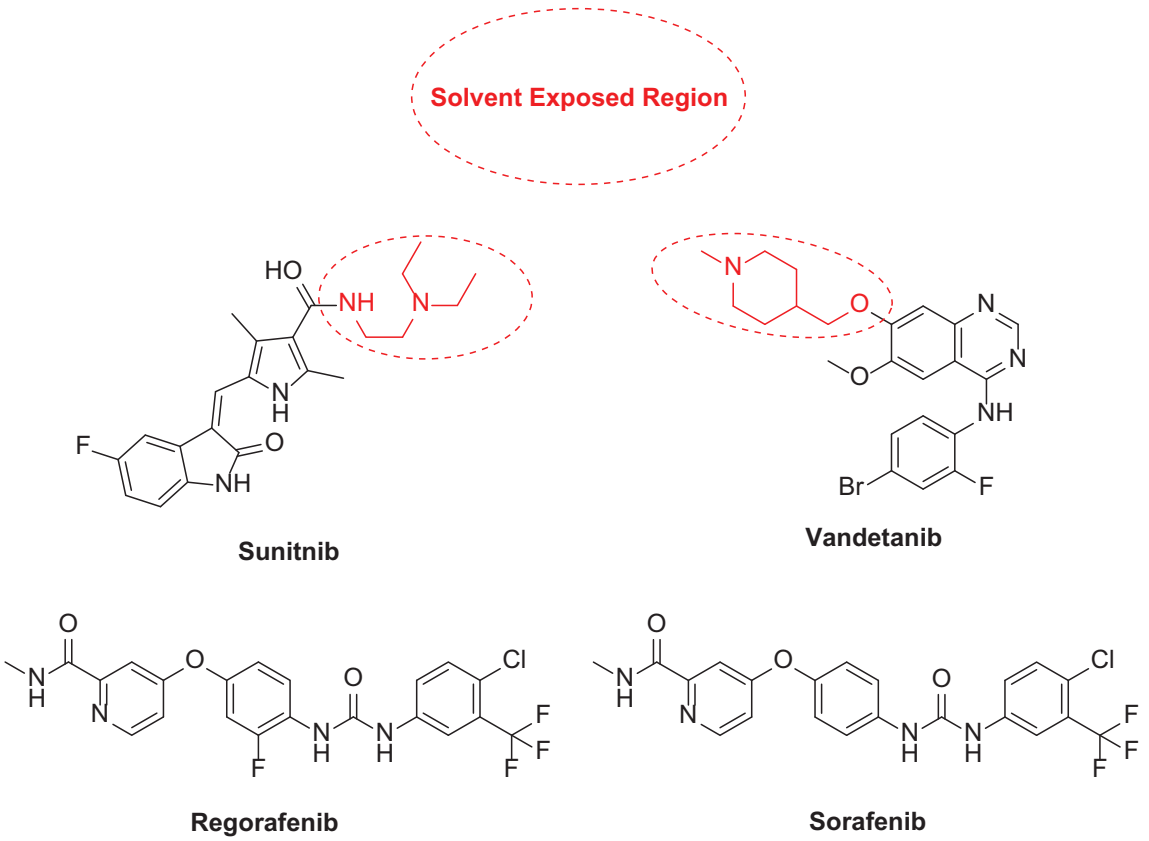

Fig. 43. Structures of VEGFR inhibitors sunitinib, sorafenib, regorafenib and vandetanib.

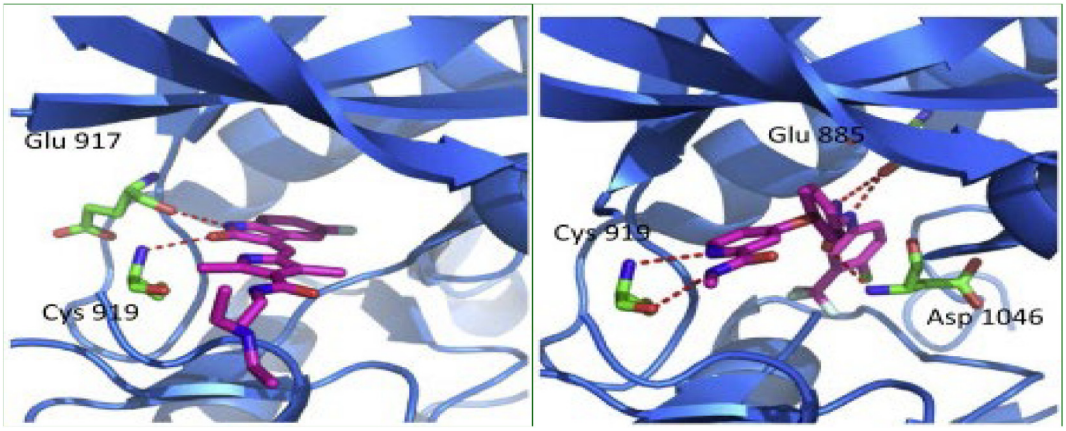

Fig. 44. Cocrystal of VEGFR2 with sunitinib (left) and sorafenib (right). Taken with permission from Peng *et al.*, 2015[100].

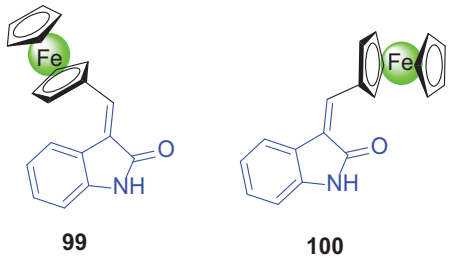

Fig. 45. Structure of ferrocenyl-oxindole derivatives; E isomer (left) **96** and Z isomer (right) **97.**

enhance lipophilicity and affect biological activity[102]. Additionally, in the same year, Silva *et al.*, 2008 independently released a library of homologous ferrocenyl oxindoles – again, without biological investigation[103].

Crystals of both isomers **E 99** and **Z 100** were obtained and both complexes were tested against B16 (Murine Melanoma) and Vero (African Green Monkey Kidney Epithelial) cell lines. The complexes were highly active against both cell lines with, unfortunately, no tumour cell line selectivity – **100** had an IC_{50} value of 0.7 μM against both cell lines. The activity of the Z isomer (**100**) was marginally higher than the E isomer (**99**), which had an IC_{50} of 0.9 μM against B16 cells. Kinase screening showed that both isomers

obtained a 90% VEGFR inhibition level at 10 μM, while the IC_{50} were nearly identical (**99:** 214 nM and **100**: 220 nM).

In 2011, Spencer *et al.* furthered the research into ferrocenyl oxindoles in order to optimize their biological activity *via* development of a structure activity relationship (**101**–**109,** Fig. 46)[104]. As such, they explored the effect the following aspects have on biological activity: (i) substituents on the oxindole moiety; (ii) hydrogenation of the double bond to introduce free rotation; (iii) *N*-methylation of the oxindole amide moiety and (iv) replacement of the ferrocene portion with ruthenocene (Fig. 46).

In addition to the previous results, the original Z isomer ferrocenyl oxindole (**100**) was found to inhibit dual-specificity tyrosine-regulated kinases (DYRK) with an IC_{50} value of 390 nM, while the E isomer (**99**) had negligible activity at 1 μM. All the complexes (**101**–**109**) were then tested against various DYRK isoforms for activity: no appreciable activity was shown against DYRK1 or DYRK2 isoforms, while **101** displayed the greatest activity against DYRK3 (IC_{50} = 110 nM). Unfortunately, the complexes showed a much lower activity against VEGFR compared to **99** and **100**, with the greatest activity due to **106** – IC_{50} = 8.5 μM. Utilising a Xenopus embryo *in vivo* model demonstrated that all complexes **101**–**109** (excluding **106**) displayed potent anti-angiogenesis ability *via* downregulation of VEGFR1.

In 2011, Spencer *et al.* developed sterically encumbering metallocene oxindole derivatives to investigate if larger metallocene moieties would impact their ability to bind various kinases[105] and 1,2,3,4,5-pentaphenyl-ferrocene (**110, 111**) and (η^4 -tetraphenyl-cyclobutadiene)-(η^5-cyclopentadienyl)cobalt (**112, 113**) were synthesised in analogous manners (Fig. 47).[105].

Sterically hindered complexes **110**–**113** were tested against a multitude of kinases: DYRK, Homeodomain-interacting protein kinase 1 (HIPK4), MAPKAPK3 (mitogen-activated protein kinase-activated-3) and VEGFR2. Against each kinase, no appreciable inhibition was observed (<10% inhibition at 10 μM). Unfortunately, no testing was conducted against PDGFR (but it may be safely assumed a similar outcome would result). However, further testing was conducted against PAK1 (p21-activated kinase-1), which is known to have a large ATP binding domain in order to assess the effect of the steric hinderance on kinase inhibition. No inhibition was observed between 10 and 30 μM. At first, it appears that steric hindrance prevents binding ability to the receptor and therefore inhibition, however, no inhibition was observed with the controls either (**99** and **100**). Finally, the Xenopus embryo *in vivo* model demonstrated that all sterically hindered complexes tested (**110**–**113**) did not display anti-angiogenesis ability in direct contrast to the original complexes **99** and **100.** This can be presumably

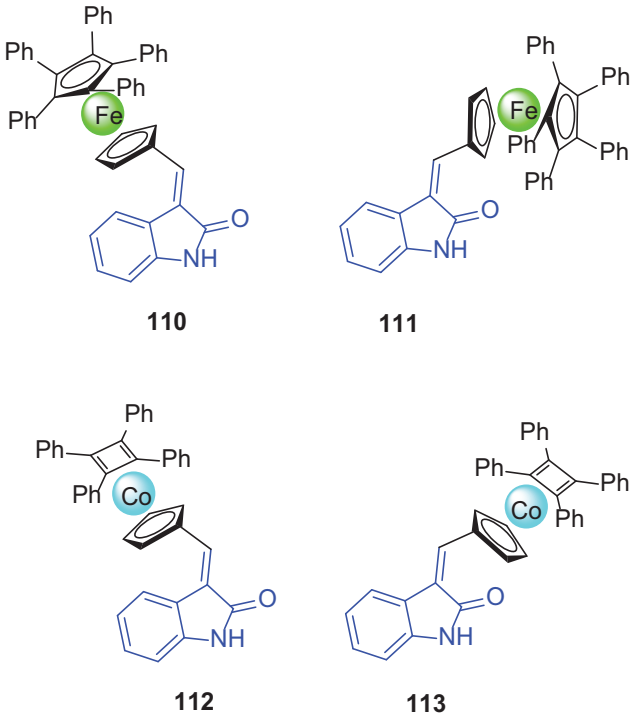

Fig. 47. Structure of sterically hindered Cobalt and Iron oxindole metallocenes.

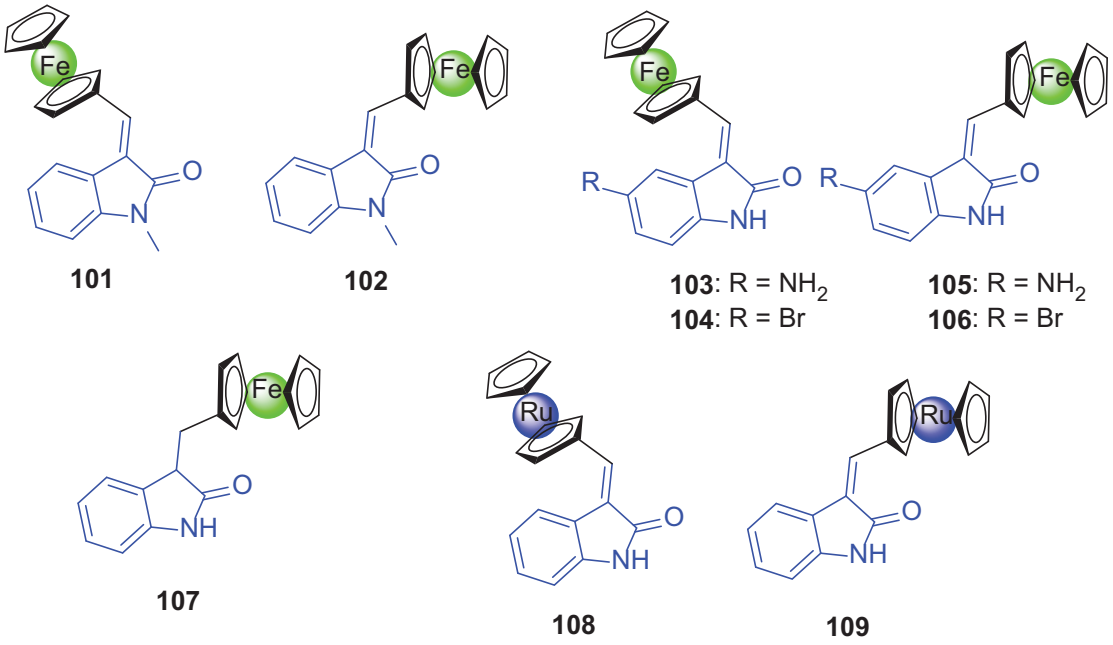

Fig. 46. Structure of E and Z ferrocenyl and ruthenocenyl oxindole derivatives.

explained by the total loss of kinase inhibition due to the introduction of steric factors.

In 2013, Amin *et al.* synthesised a larger series of ferrocene oxindole derivatives by introducing di-substituted and directly conjugated ferrocene oxindole derivatives (**114**–**124**, Fig. 48).[106] Initial biological assays indicated the importance of retention of the pyrrole in VEGFR kinase inhibitory structural design since **122** had moderate activity against VEGFR while **114** and **115,** which replaced the pyrrole group with a ferrocene moiety, had minimal activity. This experimental evidence emphasises the need to retain the pyrrole moiety when developing metal – oxindole TKi conjugates (something that had not been observed prior to this conjugate). Additionally, the furan derivative (**124**) showed weaker VEGFR2 inhibition, highlighting the importance of the pyrrole moiety. Molecular docking studies demonstrated that the low VEGFR2 inhibitory activity of **114**/**115**, as there was no suitable conformation for docking due to steric constraints. None of the complexes above showed important activity (IC_{50}'s >20 μM) against K562 (a CML cell line) and as such, further investigation was ceased. The authors speculated that this low *in vitro* activity was possibly due to low cellular uptake (however, introduction of ferrocene moieties would be expected to increase lipophilicity of the conjugates). Unfortunately, no conjugate that retains the oxindole-pyrrole pharmacophore, while only introducing a ferrocene moiety in the solvent exposed region, was developed. This conjugate may be expected to retain the benefits of both introduction of a ferrocene moiety and retention of the pyrrole moiety and as such may have closer inhibitory activity to a sunitinib control than before.

In 2017, Sansook *et al.* synthesised oxindole derivatives functionalised with a pentafluorosulfanyl moiety, containing one ferrocene-oxindole conjugate (**125** and **126**, Fig. 49)[107]. This oxindole TKi-metal conjugate contained a pentafluorosulfanyl (SF_5) substituent which has been shown to mimic the biologically relevant purpose of a trifluoromethyl (CF_3) group – increase lipophilicity and therefore cellular uptake. In this scenario, the

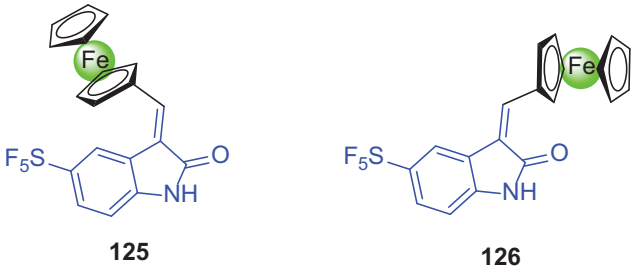

Fig. 49. Structure of pentafluorosulfanyl ferrocene-oxindole analogues.

SF_5 would be expected to occupy the hydrophobic pocket of VEGFR in similar fashion to the fluorine substituent of sunitinib. Unfortunately, a pyrrole moiety, which showed great importance in the previous study, was again removed from the core oxindole structure and as a result, poor inhibitory activity of the complexes was observed. Both complexes only inhibited DYRK3 in low micromolar concentrations and showed little activity against PDGFRα and VEGFR3 (insufficient activity to calculate an IC_{50} value). As such, no further testing was conducted on these ferrocene oxindole derivatives.

4.2. Platinum

In 2011, Harmsen *et al.* synthesised a Pt(II)-sunitinib and Pt(II)-ULS lysozyme-sunitinib derivative complexes (**127** and **128**) in order to target renal tubular cells to overcome dose-limiting side effects associated with sunitinib[108]. The authors anticipated, based on previous studies, that the Pt(II)-sunitinib bond may be stable intracellularly and decided to rational functionalise the sunitinib derivative at the solvent exposed region with a pyridine moiety (Fig. 50), expecting that coordination to the Pt(II) moiety

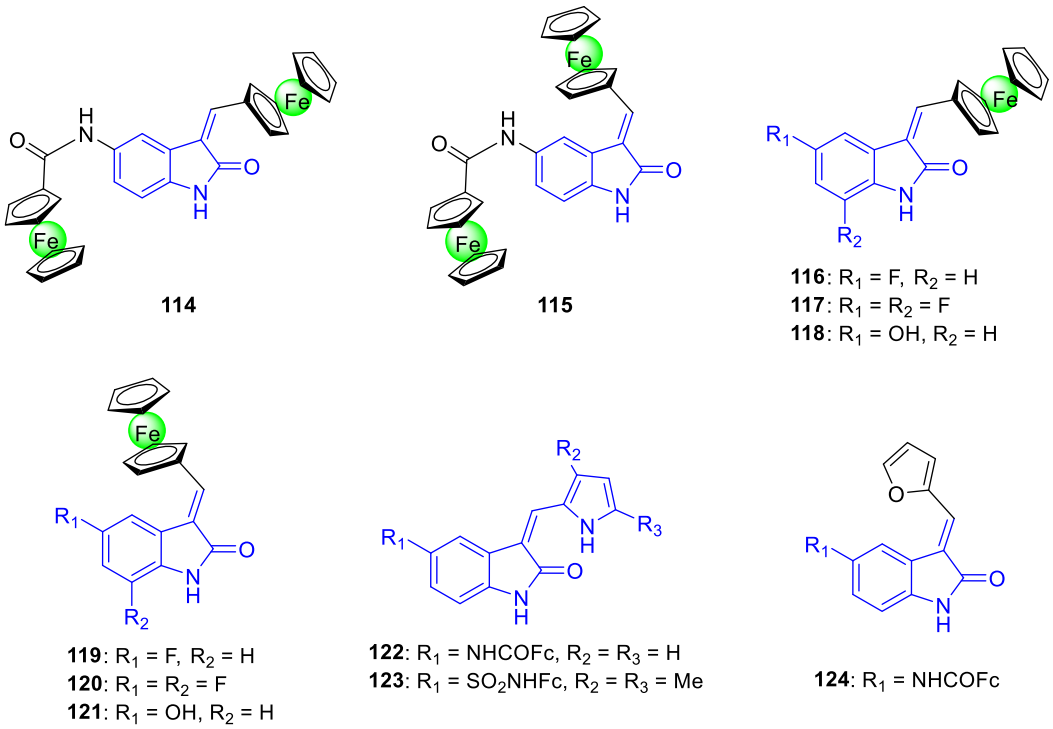

Fig. 48. Structure of di/tri-substituted ferrocene oxindole derivatives.

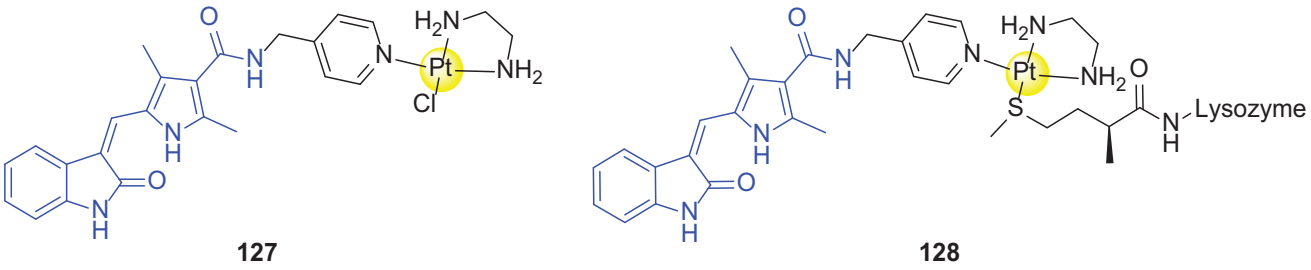

Fig. 50. Structure of Pt(II)-sunitinib (**127**) and Pt(II)-ULS-sunitinib-lysozyme conjugates (**128**).

would have minimal effect on the inhibitory properties of the sunitinib derivative.

Preliminary data indicated that complexation of the sunitinib derivative to Pt(II) did not affect its inhibitory activity; it was found that both **127** and **128** had greater total tyrosine phosphorylation inhibitory activity than the free ligand. Next, it was observed that drug uptake in immortalized human proximal tubular cells (HK-2) was 5 times higher for **128** than for the free ligand after 24 h. A flow-through tyrosine kinase peptide array assay determined the main intracellular targets to be VEGFR2, PDGFRβ and downstream receptors such as phos-phoinositol-3-kinase (PI3K), paxillin, Ras p21 protein activator (RASA1), cyclin-dependent kinase (CDK)-2, and c-FES. Kinase inhibition assays against c-KIT and PDGFR showed that conjugation of sunitinib derivative to Pt(II) did not affect PDGFR inhibition (IC_{50} of free ligand and **127** = 16 μM) while inhibition of c-KIT actually increased by 3-fold (IC_{50} of free ligand = 51 μM, IC_{50} of **127** = 17 μM). This activity is comparable to sunitinib itself (IC_{50} against PDGFR = 23 μM, IC_{50} against c-KIT = 14 μM). Unfortunately, introduction of the lysozyme portion (**128**) negatively affected kinase inhibition (due to increased steric hinderance) but the conjugate remained highly active with double-digit nM IC_{50} values. Finally, complex **128** was shown to have superior pharmacokinetics while retaining high inhibitory activity, by a pulse-chase experiment against HK-2 cells. The free ligand was shown to be rapidly cleared from the cells (<2 h) while the Pt(II)-sunitinib-lysozyme conjugate (**128**) was retained intracellularly past 48 h of testing. A level of >10% reduced total endogenous tyrosine phosphorylation was observed for up to 48 h after drug administration.

In 2012, Dolman *et al.* furthered the research into Pt(II) sunitinib-lysozyme ULS systems, **128**[109]. The conjugate did not result in reduced cell viability against HK-2 cells, in contrast with sunitinib malate which had an IC_{50} value of 12 μM. Distribution volumes of sunitinib malate and the conjugate were determined: sunitinib malate was shown to have a 15-fold larger distribution volume than the conjugate **128**, reflecting the ability of the small molecule to penetrate cells in contrast to the charged hydrophilic ULS conjugate. Additionally, no free sunitinib ligand could be detected in circulation after administration of the ULS conjugate, indicating the high stability of the complex. Again, the improved pharmaco-kinetic properties of the conjugate **128** were demonstrated: sunitinib had a renal elimination half-life of 66 min, in contrast to 28 h for the conjugate. Additionally, the renal drug exposure was 28-fold higher for the conjugate **128** than sunitinib control. Antifibrotic effects of the compounds were assessed in mice with UUO-induced tubulointerstitial fibrosis. Surprisingly, Western Blot analysis revealed that while daily treatment with a high dose of sunitinib resulted in lower p-PDGFRβ levels, treatment with the ULS conjugate **128** or low dose sunitinib did not result in decreased PDGFR level. The authors hypothesized that it may be that the conjugate requires a higher or preferably, more doses than tested (higher dose is unfeasible due to conjugate solubility). Otherwise, it may be due to the possible charged nature of ULS-conjugate metabolites in the lysozyme, which are unable to cross the organelles membrane and enter the cytoplasm in order to inhibit membrane bound tyrosine kinases, due to their charge.

In 2016, Yuming *et al* developed some Pt(II)- vandetanib conjugates, as per the previously mentioned Pt(II)-erlotinib (**20**–**22**) and Pt(II)-imatinib conjugates (**79**–**81**)[54]. These Pt(II) complexes were based on *cis*platin (**129**), *trans*platin (**130**) and oxalilplatin (**131**), allowing for evaluation of the effect of stereochemistry on pharmacological properties (Fig. 51).

The Pt(II) conjugates retained the same selectivity profile as the free ligand vandetanib and, interestingly, displayed higher potency against HCC827 (containing ΔE746-A750 mutation) than H292 cell line (wild-type), while they showed minimal cytotoxicity towards LLC-PK1 (normal kidney cell line). However, as expected due to the poor conjugation strategy utilised here, conjugates **129** and **131** displayed a ten-fold reduced toxicity against HCC827 cells than vandetanib control (IC_{50}'s against HCC827: Complex **129** = 0.42 ± 0.08 μM, Complex **131** = 0.47 ± 0.01 μM, vandetanib = 0.011 ± 0.002 μM). As in the previously mentioned erlotinib-transplatin conjugate **21**, the vandetanib-transplatin conjugate **130**, exhibited similar activity (IC_{50} = 0.043 ± 0.007 μM) to the vandetanib control.

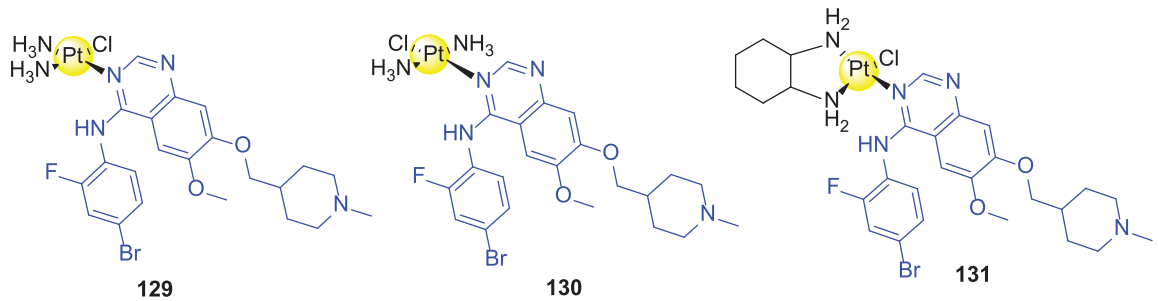

Fig. 51. Structures of the Pt(II)-vandetanib conjugates.

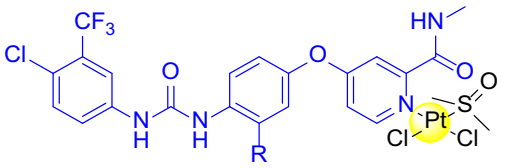

132: R = H, i.e. Sorafenib
133: R = F, i.e. Regorafenib

Fig. 52. Structure of Pt(II) sorafenib/regorafenib Complexes.

However, unlike the erlotinib-transplatin conjugate, the vandetanib-transplatin conjugate is stable in PBS and as such, this activity cannot be explained by the release of free vandetanib, but rather the intact-complex itself. DNA damage was also observed with the conjugates, which were able to form monodentate adducts with guanine base pairs. Unfortunately, no biological assays were conducted against VEGFR/VEGFR over-expressing cell lines.

Most recently, in 2019, Qin *et al.* released a communication detailing the development of Pt(II) sorafenib and regorafenib complexes, **132** and **133**[110]. (Fig. 52).

The complexes were observed to be stable in Tris-HCl buffer after 48 h. The *in vitro* activity was assessed against multiple cancerous cell lines; NCI-H460 (human non-small cell lung cancer NCI-H460 cell line), SK-OV-3 (ovarian cancer cell line), SKOV-3/DDP (cisplatin-resistant SK-OV-3 cell line), T-24 (human bladder cancer cell line), HeLa (cervical cancer cell line), A549/DDP (cisplatin-resistant A549/DDP non-small-cell lung cancer cell line). Unfortunately, the conjugates **132** and **133** were less active than their corresponding free ligands against NCI-H460, SKOV-3, SK-OV-3/DDP, T-24, and HeLa cancer cell lines, but they were at least 50 times more potent against A549/DDP cells (IC_{50} of **132** = 1.18 ± 0.15 μM > IC_{50} of **133** = 0.13 ± 0.03 μM) in contrast to all positive controls (cisplatin, sorafenib, regorafenib, *cis*-Pt(DMSO)$_2$Cl$_2$). In addition, the complexes were less toxic against normal HL-7702 cells than the corresponding free ligands. Flow cytometry indicated that both conjugates ceased the cell cycle in the G2/M and S phase, suggesting apoptosis of the A549/DDP cells. **132** displayed a higher percentage of inducing cell apoptosis (~67%) than **133** (~48%), in agreement with anti-proliferation assays. This is believed to be due to the increased cellular uptake of the regorafenib conjugate, due to the higher lipophilicity provided by the fluorine substituent. Findings, such as and activation of caspase-3/9, an increase in the mitochondrial Ca^{2+} level, ROS generation, and disruption of the mitochondrial membrane potential indicated that both conjugates induced apoptosis via the mitochondrial death pathway.

4.3. Copper

In 2014, Li *et al.*, developed ^{64}Cu-DOTA-Vandetanib conjugates for use as small molecule VEGFR probes in PET/CT[111]. Two different probes were synthesised – one containing one vandetanib (i.e. mono) moiety (**134**) and another containing two vandetanib moieties (**135**) (Fig. 53).

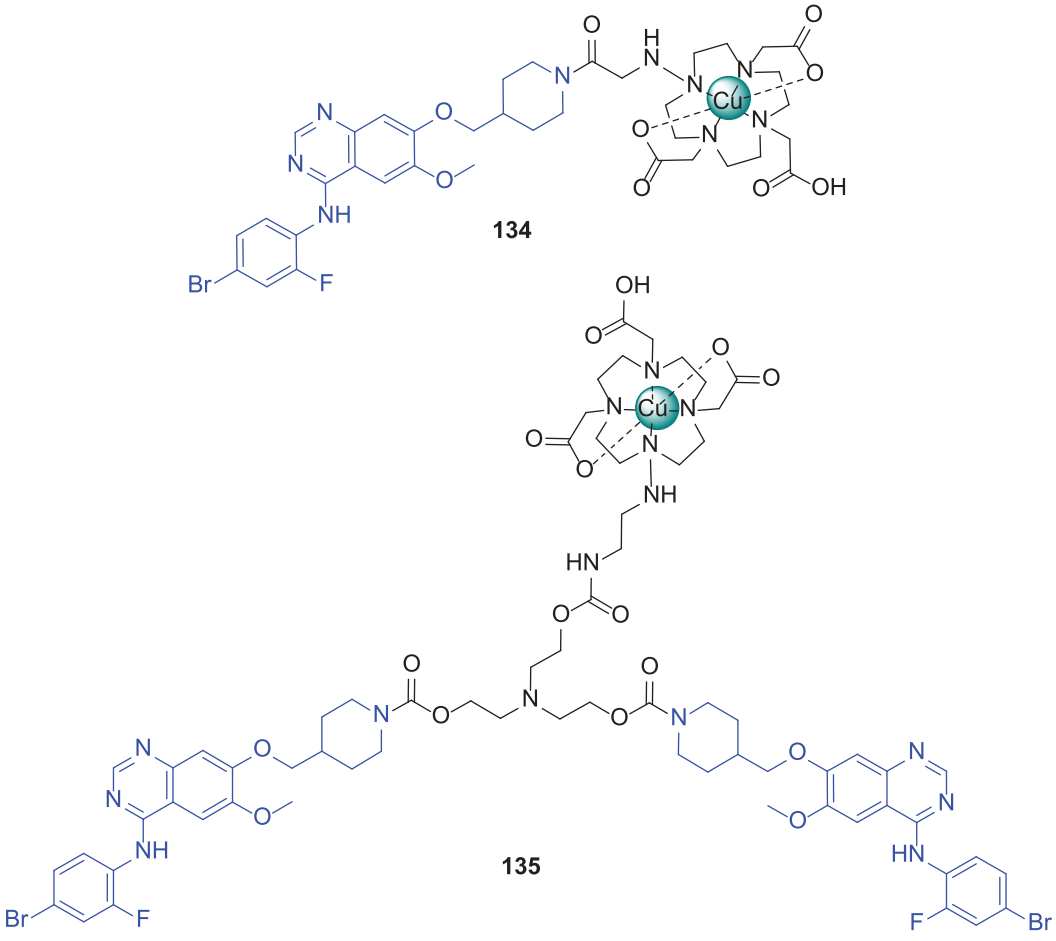

Fig. 53. ^{64}Cu-DOTA-vandetanib mono and bis derivatives.

The conjugates **134** and **135** were observed to be stable after incubation in both DMEM medium and mouse serum after 24 h at 37 °C. Cellular uptake studies indicated that the compounds were internalised by cells with higher degrees of VEGFR2 expression, i.e. in the following order: HUVEC has high expression > U-87 which has a moderate expression > HeLa and MDA-MB-231 both with low expression. It was clear that the bis conjugate **135** had a much higher cellular uptake than the mono conjugate **134**. Cellular VEGFR2 binding assays revealed that **135** had a 100-fold higher binding affinity than **134** (K_d = 0.45 nM vs 44.7 nM respectively against U-87 MG cells). In agreement, IC_{50} were much lower for **135** (IC_{50}: 0.023 nM vs 17.63 nM, respectively). Multiple time-point small-animal PET/CT scans in mice bearing U-87 MG tumours demonstrated that 24 h after injection **135** had a 5-fold higher tumour uptake than **134**. This study clearly indicates a precedence for developing multi-valent metal-TKi conjugates to possibly obtain both increased inhibitory activity and improved pharmacokinetics.

Metal – VEGFR type targeting conjugates prove an effective strategy for circumventing resistance/dose-limiting side effects and/or providing greater on-target metal ion cellular uptake. The previous discussed TKi's are especially suitable for further research due to their ability to strongly inhibit a multitude of other kinases.

5. Conclusion and future perspectives

In conclusion, EGFR, BCR-ABL, PDGFR and VEGFR Kinase Inhibitors – Metal conjugates have proven to provide an effective and promising strategy for circumventing resistance/dose-limiting side effects of the common metal-based drugs (i.e. cisplatin) and/or providing greater on-target metal ion cellular uptake. Preliminary research into metal – TKi conjugates has been focused primarily on imaging/theragnostics, dual-modal and cancer-cell selective conjugates, ULS-targeting systems and bioisostere applications and this area has demonstrated great potential, which may be fulfilled if a number of criteria/developments are entertained. TKi's, where applicable, should preferably be functionalized in the solvent exposed regions of the compounds to retain a strong kinase inhibitory activity. For example, there are little metal functionalised erlotinib conjugates currently in the literature and most have been converted into triazole conjugates (with the use of click chemistry) for more simplistic syntheses but clearly decreasing the inhibition activity. In agreement with this, it has been shown that the pyrrole moiety of sunitinib is crucial to its inhibitory activity and should be retained upon functionalisation. Precedence has been displayed for the inclusion of linkers in functionalised conjugates, to possibly improve cellular uptake and reduce steric constraints that may prevent kinase binding. The choice of metal centre in such conjugates is of course, great importance especially in the context that labile metal centres could lead to undesirable/desirable ligand release. Researchers ideally should develop mono and multi-valent conjugates that may provide greater kinase inhibitory activity as experimentally observed and should attempt to design conjugates utilising various TKi's. For example, while nilotinib has been found to be 30 times more potent than imatinib and can circumvent imatinib-resistance, there are no examples of any nilotinib – metal conjugates in the literature. Finally, further work can be conducted towards both dual-modal conjugates and pro-drug systems, which have shown the most promising results (e.g. the Co(III)-ponatinib hypoxia induced pro-drug system). As mentioned before, our group is highly interested in this area and some current work focuses on developing Pt(IV)-imatinib/nilotinib conjugates while following the above criteria to further demonstrate the potential of this field.

Declaration of Competing Interest

The authors declare that they have no known competing financial interests or personal relationships that could have appeared to influence the work reported in this paper.

Acknowledgements

The author DFB would like to thank the Irish Research Council for funding the research *via* a Government of Ireland Postgraduate Scholarship (GOIPG/2020/55).

References

[1] S.W.J. Gould, M.D. Fielder, A.F. Kelly, M. Morgan, J. Kenny, D.P. Naughton, The antimicrobial properties of copper surfaces against a range of important nosocomial pathogens, Ann. Microbiol. 59 (2009) 151–156, https://doi.org/10.1007/BF03175613.
[2] , Ment. Holist. Heal. Some Int. Perspect. 21 (2019) 23–24.
[3] A.C. Society, American Cancer Society. Cancer Facts & Figures 2020, Am. Cancer Soc. (2020) 1–52. http://www.cancer.org/acs/groups/content/@nho/documents/document/caff2007pwsecuredpdf.pdf.
[4] L.H. Einhorn, Treatment of testicular cancer: A new and improved model, J. Clin. Oncol. 8 (1990) 1777–1781, https://doi.org/10.1200/JCO.1990.8.11.1777.
[5] A.M. Florea, D. Büsselberg, Cisplatin as an anti-tumor drug: Cellular mechanisms of activity, drug resistance and induced side effects, Cancers (Basel). 3 (2011) 1351–1371, https://doi.org/10.3390/cancers3011351.
[6] Z. Molphy, A. Prisecaru, C. Slator, N. Barron, M. McCann, J. Colleran, D. Chandran, N. Gathergood, A. Kellett, Copper phenanthrene oxidative chemical nucleases, Inorg. Chem. 53 (2014) 5392–5404, https://doi.org/10.1021/ic500914j.
[7] S. Leijen, S.A. Burgers, P. Baas, D. Pluim, M. Tibben, E. Van Werkhoven, E. Alessio, G. Sava, J.H. Beijnen, J.H.M. Schellens, Phase I/II study with ruthenium compound NAMI-A and gemcitabine in patients with non-small cell lung cancer after first line therapy, Invest. New Drugs. 33 (2015) 201–214, https://doi.org/10.1007/s10637-014-0179-1.
[8] C.G. Hartinger, M.A. Jakupec, S. Zorbas-Seifried, M. Groessl, A. Egger, W. Berger, H. Zorbas, P.J. Dyson, B.K. Keppler, KP1019, a new redox-active anticancer agent – Preclinical development and results of a clinical phase I study in tumor patients, Chem. Biodivers. 5 (2008) 2140–2155, https://doi.org/10.1002/cbdv.200890195.
[9] H.A. Burris, S. Bakewell, J.C. Bendell, J. Infante, S.F. Jones, D.R. Spigel, G.J. Weiss, R.K. Ramanathan, A. Ogden, D. Von Hoff, Safety and activity of IT-139, a ruthenium-based compound, in patients with advanced solid tumours: A first-in-human, open-label, dose-escalation phase i study with expansion cohort, ESMO Open. 1 (2016), https://doi.org/10.1136/esmoopen-2016-000154.
[10] B. Neuditschko, A.A. Legin, D. Baier, A. Schintlmeister, S. Reipert, M. Wagner, B.K. Keppler, W. Berger, S.M. Meier-Menches, C. Gerner, Interaction with Ribosomal Proteins Accompanies Stress Induction of the Anticancer Metallodrug BOLD-100/KP1339 in the Endoplasmic Reticulum, Angew. Chemie – Int. Ed. 60 (2021) 5063–5068, https://doi.org/10.1002/anie.202015962.
[11] S. Monro, K.L. Colón, H. Yin, J. Roque, P. Konda, S. Gujar, R.P. Thummel, L. Lilge, C.G. Cameron, S.A. McFarland, Transition Metal Complexes and Photodynamic Therapy from a Tumor-Centered Approach: Challenges, Opportunities, and Highlights from the Development of TLD1433, Chem. Rev. 119 (2019) 797–828, https://doi.org/10.1021/acs.chemrev.8b00211.
[12] G. Bononi, D. Iacopini, G. Cicio, S. Di Pietro, C. Granchi, V. Di Bussolo, F. Minutolo, Glycoconjugated Metal Complexes as Cancer Diagnostic and Therapeutic Agents, ChemMedChem. 16 (2021) 30–64, https://doi.org/10.1002/cmdc.202000456.
[13] W. Zhao, V. Ferro, M.V. Baker, Carbohydrate–N-heterocyclic carbene metal complexes: Synthesis, catalysis and biological studies, Coord. Chem. Rev. 339 (2017) 1–16, https://doi.org/10.1016/j.ccr.2017.03.005.
[14] B. Albada, N. Metzler-Nolte, Organometallic-Peptide Bioconjugates: Synthetic Strategies and Medicinal Applications, Chem. Rev. 116 (2016) 11797–11839, https://doi.org/10.1021/acs.chemrev.6b00166.
[15] G. Dirscherl, B. König, The use of solid-phase synthesis techniques for the preparation of peptide-metal complex conjugates, European, J. Org. Chem. (2008) 597–634, https://doi.org/10.1002/ejoc.200700787.
[16] A.G. Weidmann, A.C. Komor, J.K. Barton, Targeted Chemotherapy with Metal Complexes, Comments Inorg. Chem. 34 (2014) 114–123, https://doi.org/10.1080/02603594.2014.890099.
[17] M. Zhang, C.T. Hagan, Y. Min, H. Foley, X. Tian, F. Yang, Y. Mi, K.M. Au, Y. Medik, K. Roche, K. Wagner, Z. Rodgers, A.Z. Wang, Nanoparticle co-delivery of wortmannin and cisplatin synergistically enhances chemoradiotherapy and reverses platinum resistance in ovarian cancer models, Biomaterials. 169 (2018) 1–10, https://doi.org/10.1016/j.biomaterials.2018.03.055.
[18] M.K. Paul, A.K. Mukhopadhyay, Tyrosine kinase – Role and significance in Cancer, Int. J. Med. Sci. 1 (2012) 101–115, https://doi.org/10.7150/ijms.1.101.

[19] C.B. Gambacorti-Passerini, R.H. Gunby, R. Piazza, A. Galietta, R. Rostagno, L. Scapozza, Molecular mechanisms of resistance to imatinib in Philadelphia-chromosome-positive leukaemias, Lancet Oncol. 4 (2003) 75–85, https://doi.org/10.1016/S1470-2045(03)00979-3.

[20] C. Gambacorti-Passerini, L. Antolini, F.X. Mahon, F. Guilhot, M. Deininger, C. Fava, A. Nagler, C.M. Della Casa, E. Morra, E. Abruzzese, A. D'Emilio, F. Stagno, P. Le Coutre, R. Hurtado-Monroy, V. Santini, B. Martino, F. Pane, A. Piccin, P. Giraldo, S. Assouline, M.A. Durosinmi, O. Leeksma, E.M. Pogliani, M. Puttini, E. Jang, J. Reiffers, M.G. Valsecchi, D.W. Kim, Multicenter independent assessment of outcomes in chronic myeloid leukemia patients treated with imatinib, J. Natl. Cancer Inst. 103 (2011) 553–561, https://doi.org/10.1093/jnci/djr060.

[21] M. Talpaz, N.P. Shah, H. Kantarjian, N. Donato, J. Nicoll, R. Paquette, J. Cortes, S. O'Brien, C. Nicaise, E. Bleickardt, A. Blackwood-Chirchir, V. Iyer, T.-T. Chen, F. Huang, A.P. Decillis, C.L. Sawyers, Dasatinib in Imatinib-Resistant Philadelphia Chromosome-Positive Leukemias, N. Engl. J. Med. 365 (2011) 687–696, https://doi.org/10.1056/NEJMoa055229.

[22] M. Kaur, R.K. Loveleen, Inhibition of histone deacetylases, topoisomerases and epidermal growth factor receptor by metal-based anticancer agents: Design & synthetic strategies and their medicinal attributes, Bioorg. Chem. 105 (2020), https://doi.org/10.1016/j.bioorg.2020.104396 104396.

[23] A.T.N. Lam, J. Yoon, E.O. Ganbold, D.K. Singh, D. Kim, K.H. Cho, S.J. Son, J. Choo, S.Y. Lee, S. Kim, S.W. Joo, Adsorption and desorption of tyrosine kinase inhibitor erlotinib on gold nanoparticles, J. Colloid Interface Sci. 425 (2014) 96–101, https://doi.org/10.1016/j.jcis.2014.03.032.

[24] J. Liu, J. Zheng, H. Nie, H. Chen, B. Li, L. Jia, Co-delivery of erlotinib and doxorubicin by MoS2 nanosheets for synergetic photothermal chemotherapy of cancer, Chem. Eng. J. 381 (2020), https://doi.org/10.1016/j.cej.2019.122541 122541.

[25] A.M. Cryer, C. Chan, A. Eftychidou, C. Maksoudian, M. Mahesh, T.D. Tetley, A.C. Spivey, A.J. Thorley, Tyrosine Kinase Inhibitor Gold Nanoconjugates for the Treatment of Non-Small Cell Lung Cancer, ACS Appl. Mater. Interfaces. 11 (2019) 16336–16346, https://doi.org/10.1021/acsami.9b02986.

[26] M. Dörr, E. Meggers, Metal complexes as structural templates for targeting proteins, Curr. Opin. Chem. Biol. 19 (2014) 76–81, https://doi.org/10.1016/j.cbpa.2014.01.005.

[27] A. Haleel, D. Mahendiran, V. Veena, N. Sakthivel, A.K. Rahiman, Antioxidant, DNA interaction, VEGFR2 kinase, topoisomerase i and in vitro cytotoxic activities of heteroleptic copper(II) complexes of tetrazolo[1,5-a]pyrimidines and diimines, Mater. Sci. Eng. C. 68 (2016) 366–382, https://doi.org/10.1016/j.msec.2016.05.120.

[28] G. Pines, W.J. Köstler, Y. Yarden, Oncogenic mutant forms of EGFR: Lessons in signal transduction and targets for cancer therapy, FEBS Lett. 584 (2010) 2699–2706, https://doi.org/10.1016/j.febslet.2010.04.019.

[29] P. Wee, Z. Wang, Epidermal growth factor receptor cell proliferation signaling pathways, Cancers (Basel). 9 (2017) 1–45, https://doi.org/10.3390/cancers9050052.

[30] J. Wang, B. Xu, Targeted therapeutic options and future perspectives for her2-positive breast cancer, Signal Transduct. Target. Ther. 4 (2019), https://doi.org/10.1038/s41392-019-0069-2.

[31] D. Kazandjian, G.M. Blumenthal, W. Yuan, K. He, P. Keegan, R. Pazdur, FDA approval of gefitinib for the treatment of patients with metastatic EGFR mutation-positive non-small cell lung cancer, Clin. Cancer Res. 22 (2016) 1307–1312, https://doi.org/10.1158/1078-0432.CCR-15-2266.

[32] Nachtnebel A, Erlotinib (Tarceva®) for the firstline treatment of patients with locally advanced or metastatic non-small cell lung cancer with EGFR activating mutations, (2012). http://eprints.hta.lbg.ac.at/941/1/DSD_HSO_Nr.22.pdf. Accessed: 2013-05-10. (Archived by WebCite? at http://www.webcitation.org/6GVg0TrmT).

[33] M. Nagasaka, V.W. Zhu, S.M. Lim, M. Greco, F. Wu, S.H.I. Ou, Beyond Osimertinib: The Development of Third-Generation EGFR Tyrosine Kinase Inhibitors For Advanced EGFR+ NSCLC, J. Thorac. Oncol. 16 (2021) 740–763, https://doi.org/10.1016/j.jtho.2020.11.028.

[34] J. He, Z. Huang, L. Han, Y. Gong, C. Xie, Mechanisms and management of 3rd-generation EGFR-TKI resistance in advanced non-small cell lung cancer (Review), Int. J. Oncol. 59 (2021) 1–20, https://doi.org/10.3892/ijo.2021.5270.

[35] S.S. Ramalingam, J. Vansteenkiste, D. Planchard, B.C. Cho, J.E. Gray, Y. Ohe, C. Zhou, T. Reungwetwattana, Y. Cheng, B. Chewaskulyong, R. Shah, M. Cobo, K. H. Lee, P. Cheema, M. Tiseo, T. John, M.-C. Lin, F. Imamura, T. Kurata, A. Todd, R. Hodge, M. Saggese, Y. Rukazenkov, J.-C. Soria, Overall Survival with Osimertinib in Untreated, EGFR -Mutated Advanced NSCLC, N. Engl. J. Med. 382 (2020) 41–50, https://doi.org/10.1056/nejmoa1913662.

[36] H. Cheng, S.K. Nair, B.W. Murray, Recent progress on third generation covalent EGFR inhibitors, Bioorganic Med, Chem. Lett. 26 (2016) 1861–1868, https://doi.org/10.1016/j.bmcl.2016.02.067.

[37] R.H. Berndsen, A. Weiss, U.K. Abdul, T.J. Wong, P. Meraldi, A.W. Griffioen, P.J. Dyson, P. Nowak-Sliwinska, Combination of ruthenium(II)-arene complex [Ru(η6-p-cymene)Cl2 (pta)] (RAPTA-C) and the epidermal growth factor receptor inhibitor erlotinib results in efficient angiostatic and antitumor activity, Sci. Rep. 7 (2017) 1–16, https://doi.org/10.1038/srep43005.

[38] M.N. Lub-De Hooge, J.G.W. Kosterink, P.J. Perik, H. Nijnuis, L. Tran, J. Bart, A.J. H. Suurmeijer, S. De Jong, P.L. Jager, E.G.E. De Vries, Preclinical characterisation of 111In-DTPA-trastuzumab, Br. J. Pharmacol. 143 (2004) 99–106, https://doi.org/10.1038/sj.bjp.0705915.

[39] C. Fernandes, I.C. Santos, I. Santos, H.J. Pietzsch, J.U. Kunstler, W. Kraus, A. Rey, N. Margaritis, A. Bourkoula, A. Chiotellis, M. Paravatou-Petsotas, I. Pirmettis, Rhenium and technetium complexes bearing quinazoline derivatives: Progress towards a 99mTc biomarker for EGFR-TK imaging, Dalt, Trans. (2008) 3215–3225, https://doi.org/10.1039/b802021c.

[40] A.A. Memon, S. Jakobsen, F. Dagnaes-Hansen, B.S. Sorensen, S. Keiding, E. Nexo, Positron emission tomography (PET) imaging with [11C]-labeled erlotinib: A micro-PET study on mice with lung tumor xenografts, Cancer Res. 69 (2009) 873–878, https://doi.org/10.1158/0008-5472.CAN-08-3118.

[41] J.Q. Wang, M. Gao, K.D. Miller, G.W. Sledge, Q.H. Zheng, Synthesis of [11C] Iressa as a new potential PET cancer imaging agent for epidermal growth factor receptor tyrosine kinase, Bioorganic Med, Chem. Lett. 16 (2006) 4102–4106, https://doi.org/10.1016/j.bmcl.2006.04.080.

[42] Y. Seimbille, M.E. Phelps, J. Czernin, D.H.S. Silverman, Fluorine-18 labeling of 6,7-disubstituted anilinoquinazoline derivatives for positron emission tomography (PET) imaging of tyrosine kinase receptors: Synthesis of18F-Iressa and related molecular probes, J. Label. Compd. Radiopharm. 48 (2005) 829–843, https://doi.org/10.1002/jlcr.998.

[43] A. Pal, A. Glekas, M. Doubrovin, J. Balatoni, T. Beresten, D. Maxwell, S. Soghomonyan, A. Shavrin, L. Ageyeva, R. Finn, S.M. Larson, W. Bornmann, J. G. Gelovani, Molecular Imaging of EGFR kinase activity in tumors with 124 I-Labeled small molecular tracer and positron emission tomography, Mol. Imaging Biol. 8 (2006) 262–277, https://doi.org/10.1007/s11307-006-0049-0.

[44] A. Bourkoula, M. Paravatou-Petsotas, A. Papadopoulos, I. Santos, H.J. Pietzsch, E. Livaniou, M. Pelecanou, M. Papadopoulos, I. Pirmettis, Synthesis and characterization of rhenium and technetium-99m tricarbonyl complexes bearing the 4-[3-bromophenyl]quinazoline moiety as a biomarker for EGFR-TK imaging, Eur. J. Med. Chem. 44 (2009) 4021–4027, https://doi.org/10.1016/j.ejmech.2009.04.033.

[45] R. Schibli, R. La Bella, R. Alberto, E. Garcia-Garayoa, K. Ortner, U. Abram, P.A. Schubiger, Influence of the denticity of ligand systems on the in vitro and in vivo behavior of 99mTc(I)-tricarbonyl complexes: A hint for the future functionalization of biomolecules, Bioconjug. Chem. 11 (2000) 345–351, https://doi.org/10.1021/bc990127h.

[46] F.L. Zhang, Q. Huang, K. Zheng, J. Li, J.Y. Liu, J.P. Xue, A novel strategy for targeting photodynamic therapy. Molecular combo of photodynamic agent zinc(II) phthalocyanine and small molecule target-based anticancer drug erlotinib, Chem. Commun. 49 (2013) 9570–9572, https://doi.org/10.1039/c3cc45487h.

[47] F.L. Zhang, Q. Huang, J.Y. Liu, M.D. Huang, J.P. Xue, Molecular-target-based anticancer photosensitizer: Synthesis and in vitro photodynamic activity of erlotinib-zinc(II) phthalocyanine conjugates, ChemMedChem. 10 (2015) 312–320, https://doi.org/10.1002/cmdc.201402373.

[48] R. Garcia, P. Fousková, L. Gano, A. Paulo, P. Campello, É. Tóth, I. Santos, A quinazoline-derivative DOTA-type gallium(III) complex for targeting epidermal growth factor receptors: Synthesis, characterisation and biological studies, J. Biol. Inorg. Chem. 14 (2009) 261–271, https://doi.org/10.1007/s00775-008-0446-8.

[49] G. Bandoli, A. Dolmella, F. Tisato, M. Porchia, F. Refosco, Mononuclear six-coordinated Ga(III) complexes: A comprehensive survey, Coord. Chem. Rev. 253 (2009) 56–77, https://doi.org/10.1016/j.ccr.2007.12.001.

[50] A. Jain, M. Kameswaran, U. Pandey, K. Prabhash, H.D. Sarma, A. Dash, 68Ga labeled Erlotinib: A novel PET probe for imaging EGFR over-expressing tumors, Bioorganic Med, Chem. Lett. 27 (2017) 4552–4557, https://doi.org/10.1016/j.bmcl.2017.08.065.

[51] A. Jain, M. Kameswaran, U. Pandey, R. Sharma, H. Dev Sarma, A. Dash, Synthesis and evaluation of a novel 68Ga-NODAGA-Erlotinib analogue towards PET imaging of Epidermal Growth Factor Receptor over-expressing cancers, Chem. Biol. Lett. 5 (2018) 3–10. http://www.pubs.iscience.in/journal/index.php/cbl/article/view/727.

[52] C. Liolios, A. Shegani, I. Roupa, C. Kiritsis, A. Makarem, M. Paravatou-Petsotas, M. Pelecanou, P. Bouziotis, M. Papadopoulos, K. Kopka, I. Pirmettis, Synthesis, characterization and evaluation of 68Ga labelled monomeric and dimeric quinazoline derivatives of the HBED-CC chelator targeting the epidermal growth factor receptor, Bioorg. Chem. 100 (2020), https://doi.org/10.1016/j.bioorg.2020.103855 103855.

[53] R. Kok, K. Temming, M. Fretz, Organ- and Cell-Type Specific Delivery of Kinase Inhibitors: A Novel Approach in the Development of Targeted Drugs, Curr. Mol. Pharmacol. 1 (2010) 1–12, https://doi.org/10.2174/1874467210801010001.

[54] Y. Wei, D.C. Poon, R. Fei, A.S.M. Lam, S.C.F. Au-Yeung, K.K.W. To, A platinum-based hybrid drug design approach to circumvent acquired resistance to molecular targeted tyrosine kinase inhibitors, Sci. Rep. 6 (2016) 1–12, https://doi.org/10.1038/srep25363.

[55] Y. Zhang, Q. Luo, W. Zheng, Z. Wang, Y. Lin, E. Zhang, S. Lü, J. Xiang, Y. Zhao, F. Wang, Luminescent cyclometallated platinum(II) complexes: Highly promising EGFR/DNA probes and dual-targeting anticancer agents, Inorg. Chem. Front. 5 (2018) 413–424, https://doi.org/10.1039/c7qi00346c.

[56] C. Li, F. Xu, Y. Zhao, W. Zheng, W. Zeng, Q. Luo, Z. Wang, K. Wu, J. Du, F. Wang, Platinum(II) Terpyridine Anticancer Complexes Possessing Multiple Mode of DNA Interaction and EGFR Inhibiting Activity, Front. Chem. 8 (2020) 1–14, https://doi.org/10.3389/fchem.2020.00210.

[57] M. Yang, H. Wu, J. Chu, L.A. Gabriel, Y. Kim, K.S. Anderson, C.M. Furdui, U. Bierbach, Platination of cysteine by an epidermal growth factor receptor kinase-targeted hybrid agent, Chem. Commun. 54 (2018) 7479–7482, https://doi.org/10.1039/c8cc04251a.

[58] M. Yang, Synthetic and Mechanistic Studies of Precious Metal-Modified Tyrosine Kinase Inhibitors, 2017. https://wakespace.lib.wfu.edu/handle/10339/89873.
[59] Y. Zhao, Y. Yang, F. Xu, W. Zheng, Q. Luo, Y. Zhang, F. Jia, F. Wang, Pharmacophore conjugation strategy for multi-targeting metal-based anticancer complexes, 1st ed., Elsevier Inc., 2020. 10.1016/bs.adioch.2019.10.002.
[60] W. Zheng, Q. Luo, Y. Lin, Y. Zhao, X. Wang, Z. Du, X. Hao, Y. Yu, S. Lü, L. Ji, X. Li, L. Yang, F. Wang, Complexation with organometallic ruthenium pharmacophores enhances the ability of 4-anilinoquinazolines inducing apoptosis, Chem. Commun. 49 (2013) 10224–10226, https://doi.org/10.1039/c3cc43000f.
[61] K.H. Gibson, W. Grundy, A.A. Godfrey, J.R. Woodburn, S.E. Ashton, B.J. Curry, L. Scarlett, A.J. Barker, D.S. Brown, Epidermal Growth Factor Receptor Tyrosine Kinase: Structure-Activity Relationship and Anti-tumour activity of Novel Quinazolines, Bioorganic Med, Chem. Lett. 7 (1997) 2723–2728.
[62] Y. Zhang, W. Zheng, Q. Luo, Y. Zhao, E. Zhang, S. Liu, F. Wang, Dual-targeting organometallic ruthenium(ii) anticancer complexes bearing EGFR-inhibiting 4-anilinoquinazoline ligands, Dalt. Trans. 44 (2015) 13100–13111, https://doi.org/10.1039/c5dt01430a.
[63] L. Ji, W. Zheng, Y. Lin, X. Wang, S. Lü, X. Hao, Q. Luo, X. Li, L. Yang, F. Wang, Novel ruthenium complexes ligated with 4-anilinoquinazoline derivatives: Synthesis, characterisation and preliminary evaluation of biological activity, Eur. J. Med. Chem. 77 (2014) 110–120, https://doi.org/10.1016/j.ejmech.2014.02.062.
[64] F. Wang, H. Chen, S. Parsons, I.D.H. Oswald, J.E. Davidson, P.J. Sadler, Kinetics of Aquation and Anation of Ruthenium(II) Arene Anticancer Complexes, Acidity and X-ray Structures of Aqua Adducts, Chem. – A Eur. J. 9 (2003) 5810–5820, https://doi.org/10.1002/chem.200304724.
[65] J. Du, E. Zhang, Y. Zhao, W. Zheng, Y. Zhang, Y. Lin, Z. Wang, Q. Luo, K. Wu, F. Wang, Discovery of a dual-targeting organometallic ruthenium complex with high activity inducing early stage apoptosis of cancer cells, Metallomics. 7 (2015) 1573–1583, https://doi.org/10.1039/c5mt00122f.
[66] J. Du, Y. Kang, Y. Zhao, W. Zheng, Y. Zhang, Y. Lin, Z. Wang, Y. Wang, Q. Luo, K. Wu, F. Wang, Synthesis, Characterization, and in Vitro Antitumor Activity of Ruthenium(II) Polypyridyl Complexes Tethering EGFR-Inhibiting 4-Anilinoquinazolines, Inorg. Chem. 55 (2016) 4595–4605, https://doi.org/10.1021/acs.inorgchem.6b00309.
[67] R. Ilmi, E. Tseriotou, P. Stylianou, Y.A. Christou, I. Ttofi, N. Dietis, C. Pitris, A.D. Odysseos, S.N. Georgiades, A Novel Conjugate of Bis[((4-bromophenyl)amino) quinazoline], a EGFR-TK Ligand, with a Fluorescent Ru(II)-Bipyridine Complex Exhibits Specific Subcellular Localization in Mitochondria, Mol. Pharm. 16 (2019) 4260–4273, https://doi.org/10.1021/acs.molpharmaceut.9b00608.
[68] J. Amin, I. Chuckowree, G.J. Tizzard, S.J. Coles, M. Wang, J.P. Bingham, J.A. Hartley, J. Spencer, Targeting epidermal growth factor receptor with ferrocene-based kinase inhibitors, Organometallics. 32 (2013) 509–513, https://doi.org/10.1021/om300974d.
[69] M. Yang, A.J. Pickard, X. Qiao, M.J. Gueble, C.S. Day, G.L. Kucera, U. Bierbach, Synthesis, reactivity, and biological activity of gold(i) complexes modified with thiourea-functionalized tyrosine kinase inhibitors, Inorg. Chem. 54 (2015) 3316–3324, https://doi.org/10.1021/ic502998a.
[70] E. Ortega, A. Zamora, U. Basu, P. Lippmann, V. Rodríguez, C. Janiak, I. Ott, J. Ruiz, An Erlotinib gold(I) conjugate for combating triple-negative breast cancer, J. Inorg. Biochem. 203 (2020), https://doi.org/10.1016/j.jinorgbio.2019.110910 110910.
[71] C. Karnthaler-Benbakka, D. Groza, K. Kryeziu, V. Pichler, A. Roller, W. Berger, P. Heffeter, C.R. Kowol, Tumor-targeting of EGFR inhibitors by hypoxia-mediated activation, Angew. Chemie – Int. Ed. 53 (2014) 12930–12935, https://doi.org/10.1002/anie.201403936.
[72] M. Mathuber, H. Schueffl, O. Dömötör, C. Karnthaler, É.A. Enyedy, P. Heffeter, B.K. Keppler, C.R. Kowol, Improving the Stability of EGFR Inhibitor Cobalt(III) Prodrugs, Inorg. Chem. 59 (2020) 17794–17810, https://doi.org/10.1021/acs.inorgchem.0c03083.
[73] S.-J. Zhu, P. Zhao, J. Yang, R. Ma, X.-E. Yan, S.-Y. Yang, J.-W. Yang, C.-H. Yun, Structural insights into drug development strategy targeting EGFR T790M/C797S, Oncotarget 9 (17) (2018) 13652–13665.
[74] E. C Besa. Chronic Myelogenous Leukemia. (2021). https://emedicine.medscape.com/article/199425-overview#showall.
[75] O. Hantschel, Structure, Regulation, Signaling, and Targeting of Abl Kinases in Cancer, Genes and Cancer. 3 (2012) 436–446, https://doi.org/10.1177/1947601912458584.
[76] H.M. Kantarjian, F. Giles, N. Gattermann, K. Bhalla, G. Alimena, F. Palandri, G.J. Ossenkoppele, F.E. Nicolini, S.G. O'Brien, M. Litzow, R. Bhatia, F. Cervantes, A. Haque, Y. Shou, D.J. Resta, A. Weitzman, A. Hochhaus, P. Le Coutre, Nilotinib (formerly AMN107), a highly selective BCR-ABL tyrosine kinase inhibitor, is effective in patients with Philadelphia chromosome-positive chronic myelogenous leukemia in chronic phase following imatinib resistance and intolerance, Blood. 110 (2007) 3540–3546, https://doi.org/10.1182/blood-2007-03-080689.
[77] H. Kantarjian, F. Giles, L. Wunderle, K. Bhalla, S. O'Brien, B. Wassmann, C. Tanaka, P. Manley, P. Rae, W. Mietlowski, K. Bochinski, A. Hochhaus, J.D. Griffin, D. Hoelzer, M. Albitar, M. Dugan, J. Cortes, L. Alland, O.G. Ottmann, Nilotinib in Imatinib-Resistant CML and Philadelphia Chromosome-Positive ALL, N. Engl. J. Med. 354 (2006) 2542–2551, https://doi.org/10.1056/nejmoa055104.
[78] G. Tridente. Nilotinib; Adverse Events and Oncotargeted Kinase Inhibitors, (2017). https://www.sciencedirect.com/topics/pharmacology-toxicology-and-pharmaceutical-science/nilotinib.
[79] J. Rossoff, V. Huynh, R.E. Rau, M.E. Macy, M.L. Sulis, K.R. Schultz, M.J. Burke, U. Athale, M.M. O'Brien, J.J. Gregory, I.M. Sluis, F.G. Keller, C.M. Zwaan, M. Suttorp, N. Hijiya, Experience with ponatinib in paediatric patients with leukaemia, Br. J. Haematol. 189 (2) (2020) 363–368.
[80] I. Ott, A. Abraham, P. Schumacher, H. Shorafa, G. Gastl, R. Gust, B. Kircher, Synergistic and additive antiproliferative effects on human leukemia cell lines induced by combining acetylenehexacarbonyldicobalt complexes with the tyrosine kinase inhibitor imatinib, J. Inorg. Biochem. 100 (2006) 1903–1906, https://doi.org/10.1016/j.jinorgbio.2006.06.013.
[81] K. Wozniak, A. Czechowska, J. Blasiak, Cisplatin-evoked DNA fragmentation in normal and cancer cells and its modulation by free radical scavengers and the tyrosine kinase inhibitor STI571, Chem. Biol. Interact. 147 (2004) 309–318, https://doi.org/10.1016/j.cbi.2004.03.001.
[82] P. Zhang, W.Y. Gao, S. Turner, B.S. Ducatman, Gleevec (STI-571) inhibits lung cancer cell growth (A549) and potentiates the cisplatin effect in vitro, Mol. Cancer. 9 (2003) 1–9, https://doi.org/10.1186/1476-4598-2-1.
[83] M. Mayr, K. Becker, N. Schulte, S. Belle, R. Hofheinz, A. Krause, R.M. Schmid, C. Röcken, M.P. Ebert, Phase I study of imatinib, cisplatin and 5-fluoruracil or capecitabine in advanced esophageal and gastric adenocarcinoma, BMC Cancer. 12 (2012), https://doi.org/10.1186/1471-2407-12-587.
[84] Y. Wei, K.K.W. To, S.C.F. Au-Yeung, Synergistic cytotoxicity from combination of imatinib and platinum-based anticancer drugs specifically in Bcr-Abl positive leukemia cells, J. Pharmacol. Sci. 129 (2015) 210–215, https://doi.org/10.1016/j.jphs.2015.10.008.
[85] E.P. Reddy, A.K. Aggarwal, The Ins and Outs of Bcr-Abl Inhibition, Genes and Cancer. 3 (2012) 447–454, https://doi.org/10.1177/1947601912462126.
[86] M.A. Babaei, B. Kamalidehghan, M. Saleem, H.Z. Huri, F. Ahmadipour, Receptor tyrosine kinase (c-Kit) inhibitors: A potential therapeutic target in cancer cells, Drug Des. Devel. Ther. 10 (2016) 2443–2459, https://doi.org/10.2147/DDDT.S89114.
[87] S. Kaulfuß, H. Seemann, R. Kampe, J. Meyer, R. Dressel, B. König, J.-G. Scharf, P. Burfeind, Blockade of the PDGFR family together with SRC leads to diminished proliferation of colorectal cancer cells, Oncotarget 4 (7) (2013) 1037–1049.
[88] R. Roskoski, The role of small molecule platelet-derived growth factor receptor (PDGFR) inhibitors in the treatment of neoplastic disorders, Pharmacol. Res. 129 (2018) 65–83, https://doi.org/10.1016/j.phrs.2018.01.021.
[89] M.E.M. Dolman, K.M.A. Van Dorenmalen, E.H.E. Pieters, M. Lacombe, J. Pato, G. Storm, W.E. Hennink, R.J. Kok, Imatinib-ULS-lysozyme: A proximal tubular cell-targeted conjugate of imatinib for the treatment of renal diseases, J. Control. Release. 157 (2012) 461–468, https://doi.org/10.1016/j.jconrel.2011.08.041.
[90] M. Dalla Via, Discovery of wtRET and V804MRET Inhibitors, From Hit to Lead (2017). http://paduaresearch.cab.unipd.it/10758/.
[91] T.N. Rohrabaugh, A.M. Rohrabaugh, J.J. Kodanko, J.K. White, C. Turro, Photoactivation of imatinib-antibody conjugate using low-energy visible light from Ru(ii)-polypyridyl cages, Chem. Commun. 54 (2018) 5193–5196, https://doi.org/10.1039/c8cc01348a.
[92] A. Cipurković, S. Marić, E. Horozić, S. Hodžić, D. Husejnagić, L. Kolarević, A. Zukić, D. Bjelošević, Complexes of Co (II), Cu (II) and Ni (II) with Antineoplastic Agent Imatinib Mesylate : Synthesis, Characterization and Biological Activity, Am. J. Chem. 9 (2019) 159–164, https://doi.org/10.5923/j.chemistry.20190906.01.
[93] E. Gundogdu, E.S. Demir, E. Özgenç, G. Yeğen, B. Aksu, Applying Quality by Design Principles in the Development and Preparation of a New Radiopharmaceutical: Technetium-99m-Imatinib Mesylate, ACS Omega. 5 (2020) 5297–5305, https://doi.org/10.1021/acsomega.9b04327.
[94] M. Mathuber, M. Gutmann, M. La Franca, P. Vician, A. Laemmerer, P. Moser, B. K. Keppler, W. Berger, C.R. Kowol, Development of a cobalt(iii)-based ponatinib prodrug system, Inorg. Chem. Front. 8 (2021) 2468–2485, https://doi.org/10.1039/d1qi00211b.
[95] D. Beirne, T. Velasco-Torrijos, D. Montagner. Unpublished Results. (n.d.).
[96] T. Takahashi, S. Yamaguchi, K. Chida, M. Shibuya, A single autophosphorylation site on KDR/Flk-1 is essential for VEGF-A-dependent activation of PLC-γ and DNA synthesis in vascular endothelial cells, EMBO J. 20 (2001) 2768–2778, https://doi.org/10.1093/emboj/20.11.2768.
[97] L. Lian, X.L. Li, M.D. Xu, X.M. Li, M.Y. Wu, Y. Zhang, M. Tao, W. Li, X.M. Shen, C. Zhou, M. Jiang, VEGFR2 promotes tumorigenesis and metastasis in a pro-angiogenic-independent way in gastric cancer, BMC Cancer. 19 (2019) 479–489, https://doi.org/10.1186/s12885-019-5322-0.
[98] Stivarga (Regorefanib). (n.d.). https://www.accessdata.fda.gov/drugsatfda_docs/label/2012/203085lbl.pdf.
[99] C. Lawrie, Membrane Trafficking and Endothelial-Cell Dynamics During Angiogenesis, Hematol. – Sci. Pract. (2012), https://doi.org/10.5772/34226.
[100] P. Wu, T.E. Nielsen, M.H. Clausen, FDA-approved small-molecule kinase inhibitors, Trends Pharmacol. Sci. 36 (2015) 422–439, https://doi.org/10.1016/j.tips.2015.04.005.
[101] J. Spencer, A.P. Mendham, A.K. Kotha, S.C.W. Richardson, E.A. Hillard, G. Jaouen, L. Male, M.B. Hursthouse, Structural and biological investigation of ferrocene-substituted 3-methylidene-1,3-dihydro-2H-indol-2-ones, Dalt. Trans. 9226 (2009) 918–921, https://doi.org/10.1039/b816249b.

[102] A.R. Suresh Babu, R. Raghunathan, Synthesis of ferrocenyl monospirooxindolopyrrolidines-a facile [3+2]-cycloaddition of azomethine ylides, Tetrahedron Lett. 49 (2008) 4487–4490, https://doi.org/10.1016/j.tetlet.2008.05.064.
[103] B.V. Silva, N.M. Ribeiro, A.C. Pinto, M.D. Vargas, L.C. Dias, Synthesis of ferrocenyl oxindole compounds with potential anticancer activity, J. Braz. Chem. Soc. 19 (2008) 1244–1247, https://doi.org/10.1590/S0103-50532008000700003.
[104] J. Spencer, J. Amin, S.K. Callear, G.J. Tizzard, S.J. Coles, P. Coxhead, M. Guille, Synthesis and evaluation of metallocene containing methylidene-1,3-dihydro- 2H-indol-2-ones as kinase inhibitors, Metallomics. 3 (2011) 600–608, https://doi.org/10.1039/c1mt00017a.
[105] J. Spencer, J. Amin, P. Coxhead, J. McGeehan, C.J. Richards, G.J. Tizzard, S.J. Coles, J.P. Bingham, J.A. Hartley, L. Feng, E. Meggers, M. Guille, Size does matter. sterically demanding metallocene-substituted 3-methylidene-oxindoles exhibit poor kinase inhibitory action, Organometallics. 30 (2011) 3177–3181, https://doi.org/10.1021/om200278j.
[106] J. Amin, I.S. Chuckowree, M. Wang, G.J. Tizzard, S.J. Coles, J. Spencer, Synthesis of oxindole-based bioorganometallic kinase inhibitors incorporating one or more ferrocene groups, Organometallics. 32 (2013) 5818–5825, https://doi.org/10.1021/om400359m.
[107] S. Sansook, C.A. Ocasio, I.J. Day, G.J. Tizzard, S.J. Coles, O. Fedorov, J.M. Bennett, J.M. Elkins, J. Spencer, Synthesis of kinase inhibitors containing a pentafluorosulfanyl moiety, Org. Biomol. Chem. 15 (2017) 8655–8660, https://doi.org/10.1039/c7ob02289a.
[108] S. Harmsen, M.E.M. Dolman, Z. Nemes, M. Lacombe, B. Szokol, J. Pató, G. Kéri, L. Öfi, G. Storm, W.E. Hennink, R.J. Kok, Development of a cell-selective and intrinsically active multikinase inhibitor bioconjugate, Bioconjug. Chem. 22 (2011) 540–545, https://doi.org/10.1021/bc1005637.
[109] M. Dolman, S. Harmsen, E.H.E. Pieters, R.W. Sparidans, M. Lacombe, B. Szokol, L. Orfi, G. Kéri, G. Storm, W.E. Hennink, R.J. Kok, Targeting of a platinum-bound sunitinib analog to renal proximal tubular cells, Int. J. Nanomedicine. 7 (2012) 417–433.
[110] Q.P. Qin, Z.F. Wang, M.X. Tan, S.L. Wang, B.Q. Zou, D.M. Luo, J.L. Qin, S.H. Zhang, Two novel platinum(II) complexes with sorafenib and regorafenib: Synthesis, structural characterization, and evaluation of in vitro antitumor activity, Inorg. Chem. Commun. 104 (2019) 27–30, https://doi.org/10.1016/j.inoche.2019.03.031.
[111] F. Li, S. Jiang, Y. Zu, D.Y. Lee, Z. Li, A tyrosine kinase inhibitor-based high-affinity PET radiopharmaceutical targets vascular endothelial growth factor receptor, J. Nucl. Med. 55 (2014) 1525–1531, https://doi.org/10.2967/jnumed.114.138925.